



**Politecnico
di Torino**

Politecnico di Torino

Ingegneria chimica e dei processi sostenibili

A.a. 2023/2024

Sessione di Laurea Luglio 2023

Mucus rheology in the airways of patients with severe lung disease

A bibliographic, experimental and computational insight

Relatori:

Daniele Marchisio
Isabelle Seyssiecq

Candidati:

Giovanni Ferrarese
S288665

TABLE of CONTENTS

NOMENCLATURE	5
ACRONYMS.....	6
CONTEXTUALISATION of the THESIS PROJECT	7
GENERAL INTRODUCTION	8
CHAPTER 1:.....	10
LITERATURE REVIEW	10
1.1 INTRODUCTION to RHEOLOGY of VISCOELASTIC SUBSTANCES	10
RHEOLOGICAL BEHAVIOURS:.....	10
1.1.1 ELASTIC BEHAVIOUR.....	10
1.1.2 VISCOUS BEHAVIOUR	10
SHEAR THINNING BEHAVIOUR.....	11
SHEAR THICKENING BEHAVIOUR.....	12
1.1.3 VISCOELASTIC BEHAVIOUR	12
1.1.4 TIXOTROPIC BHEAVIOUR	12
1.2 TYPE of MUCUS, STRUCTURE and BEHAVIOUR	15
1.2.1 MUCUS COMPONENTS	15
MUCINS.....	15
PROTEINS	16
LIPIDS.....	16
NUCLEIC ACIDS and FILAMENTOUS of ACTIN	16
1.2.2 MOLECULAR INTERACTIONS	17
1.2.3 PATHOLOGIES EFFECT on MUCUS STRUCTURE and RHEOLOGY	18
HEALTHY BRONCHIAL MUCUS.....	18
CHRONIC OBSTRUCTIVE BRONCHIAL DISEASE (COPD) BRONCHIAL MUCUS.....	20
CYSTIC FIBROSIS (CF) BRONCHIAL MUCUS	21
ASTHMA (AH) BRONCHIAL MUCUS	22
1.3 RECONSTITUTED MUCUS.....	25
1.3.1 MUCINS.....	25
1.3.2 DNA.....	26
1.3.3 MICRORGANISMS and MUCINS	28
1.3.4 IONS.....	30
1.3.5 PAA	32
1.3.6 ARTIFICIAL SURFACTANT and PROTEINS	32
1.3.7 CHELANTS and NUTRITION for BACTERIAL CULTURES in RECONSTRUCTED MUCUS.....	35

CHAPTER 2:.....	36
MATERIALS AND METHODS.....	36
2.1 RHEOLOGICAL EXPERIMENTS	36
2.1.1 SMALL AMPLITUDE OSCILLATORY SHEAR TEST (SAOS)	37
2.1.2 STEADY STATE FLOW CONDITION TEST at CONTROLLED SHEAR STRESS (CSS)	39
2.1.3 THREE INTERVAL THIXOTROPY TESTS (3ITT)	40
2.2 BRONCHIAL MUCUS RECONSTRUCTION METHOD	41
CHAPTER 3:.....	42
CELLULAR and NASAL REAL BRONCHIAL MUCUS	42
3.1 CELLULAR MUCUS	42
3.2 EXPERIMENTAL PROCEDURE	43
3.3 OPTIMIZATION of RHEOLOGICAL PARAMETERS	44
3.4 RESULTS AND DISCUSSION	46
CHAPTER 4:.....	49
RECONSTRUCTED BRONCHIAL MUCUS.....	49
4.1 DESIGN of EXPERIMENTS (DOE).....	49
4.1.1 DOE 1	51
4.1.2 ASCERTAINMENT EXPERIMENTS	53
4.1.3 DOE 2	53
4.1.4 DOE 3	55
4.2 RESULTS	56
4.2.1 REPEATABILITY	56
4.2.2 DOE1	57
4.2.3 DOE 2	59
4.2.4 DOE 3	64
CHAPTER 5:.....	66
FLUODYNAMIC SIMULATION OF THE LUNG MUCUS	66
5.1 MODEL.....	66
5.1.1 SOLVENT NEWTONIAN TENSOR	67
5.1.2 POLYMER ELASTIC TENSOR.....	68
5.2 TESTS PERFORMED and PARAMETERS STUDIED.....	68
5.3 RESULTS and BIOMEDICAL PURPOSE	69
CONCLUSIONS and FUTURE PROSPECTS.....	71
THANKSGIVING	73
FIGURES.....	75
TABLES.....	78

ANNEXES78
BIBLIOGRAPHY.....79

NOMENCLATURE

A = Surface area [m^2]	α = Womersley number
CV = Variation Coefficient [%]	β = kinematic viscosity ratio
\mathbf{D} = Strain rate tensor [Nm]	β_z = Principal effect coefficient
\mathbf{e}_z = Discrete velocities	β_{zj} = First order interaction coefficient
E_c = Energy of Cohesion [J]	γ = Deformation [%]
f = frequency [s^{-1}]	$\dot{\gamma}$ = Shear rate [s^{-1}]
$f_z(\mathbf{x}, t)$ = Boltzmann equation	δ = Phase lag between stress and strain [rad]
$f_z^{eq}(\mathbf{x}, t)$ = Boltzmann equation at equilibrium	Δ = Difference operator
F = Resultant force [N]	η' = Dynamic o Absolute Viscosity [Pa·s]
\mathbf{F} = Body force vector [N]	η_0 = Ostwald viscoelastic constant [Pa·s]
g_x = Characteristic magnitude of the force [N]	η_{app} = Apparent viscosity [Pa·s]
$G(t)$ = Dynamic Modulus [Pa]	λ_{ss} = Structured fraction in the thixotropic model
$\hat{G}'(\omega)$ = Elastic modulus [Pa]	λ = Relaxation time of the polymer [s]
$\hat{G}''(\omega)$ = Viscous modulus [Pa]	μ_p = Polymer viscosity [m^2s^{-1}]
h = Height between plates [m]	μ_s = Solvent viscosity [m^2s^{-1}]
H = Height of the studied geometry [m]	ν_s = Solvent kinematic viscosity [$ms^{-1}Kg^{-1}$]
i = Imaginary operator	ν_{tot} = Viscoelastic kinematic viscosity [$ms^{-1}Kg^{-1}$]
$K(T)$, K_T or K_{SS} = Consistency index [$Pa \cdot s^n$]	ξ_z = a dimensional force parameter
k_1 = Factor of shear-induced breakdown	τ = Relaxation time in LBM
k_2 = Factor of Brownian build up	τ = Shear stress [Pa]
k_3 = Factor of shear-induced build up	τ_0 = HB Stress constant [Pa]
n = Shear index	τ_f = Flow stress [Pa]
m, p = Linearization parameters	τ_y = Yield Stress [Pa]
p = Number of values	τ_{pk} = Peak Stress [Pa]
Re = Reynolds number	σ = Standard deviation of the parameter
R^2 = Coefficient of determination	σ_p = Polymer elastic stress tensor [Nm]
s = Shift [m]	σ_s = Solvent Newtonian stress tensor [Nm]
t = Time [s]	Σ = Summatory operator
T = Temperature [K]	ϕ = Diameter [m]
T = Torque moment [Nm]	Ω_{coll} = Collision operator
\mathbf{u} or u = Velocity vector [ms^{-1}]	∇ = Nabla operator
u_0 = Velocity at the inlet of the channel [ms^{-1}]	
$U_x(y, t)$ = Womersley flow Velocity [ms^{-1}]	
u, v = Linearization parameters [Pa]	
ω = Angular velocity [$rad \cdot s^{-1}$]	
W_z = Weissenberg number	
x_z = Parameter value	
\bar{x} = Average of the values of a parameter	
Y = Answer of the system	
z = Element index	

ACRONYMS

AA = Amino acids

AMPs = Antimicrobial peptides

AS = Artificial surfactant

CF = Cystic Fibrosis

CMC = Critical micellar concentration

COPB = Chronical Obstructive Bronchi Pneumopathy

CSS = Controlled Shear Stress

DIETHYL_{sol}0.5M = 0.5M aqueous solution of diethylenetriaminepentaacetic acid

DNA= Desossiribonucleic acid

DOE = Design of experiments

DPPCs = Dipalmitoylphosphatidylcholines

DTPA = Diethylenetriaminepentaacetic acid

eDNA = Extracellular DNA

EDTA= Ethylendiaminetetracetic

GFM = Gel-Forming Mucus

HB = Herschel-Buckley Model

HDLs = high-density lipoproteins

LBM = Lattice Boltzmann model

LDLs = Low-density lipoproteins

LVER = Linear Viscoelastic Region

MB = Bronchial Mucus

NETs = Neutrophil extracellular traps

NM = Nasal Mucus

PAA = Polyacrylic acid

PCs = Phospholipids

SAOS = Small Amplitude Oscillatory Shear

ST = Shear-thinning

XG = Xanthan gum

3ITT = Three Interval Thixotropy Tests

CONTEXTUALISATION of the THESIS PROJECT

This thesis was developed as part of a "Proposal Thesis" project of the Politecnico di Torino at the M2P2 research centre of the University of Aix-Marseille. The work required the coordination of two of the six teams of the laboratory: the TED (Dr Isabelle Seyssiecq), which mostly deals with the treatment of waste and waste water (for the experimental part) and the ITC (Pr. Julien Favier), engaged in the study of Instability, Turbulence and Control of fluid dynamic models (for the fluid dynamics part).

In the development of the project, the M2P2 laboratory also works with another Aix-Marseille University laboratory, the Cardio-Vascular and Nutrition Research Centre of La Timone University Hospital in Marseille (C2VN). This medical university laboratory (Dr. Delphine Gras and Pr. Pascal Chanez) provided the actual mucus samples and ensured valuable biomedical support for the study carried out. Finally, the planning of the Design of Experiments required the advice of the Experimental Design Course of the University of Aix Marseille (in the person of Dr. Magalie Claeys).

The effort and combination of the expertise of all these institutions and researchers made it possible to develop a comprehensive interdisciplinary insight into the lung mucus.

GENERAL INTRODUCTION

A global increase of the rate in severe respiratory pathologies has been observed worldwide over the last decades. These pathologies are linked to and/or exacerbated by pollution, global warming and population increase¹⁻³. They can be either acute (such as the one linked to the SARS-Cov-2), or chronic (such as severe Asthma, Chronic Obstructive Bronchi Pneumopathy (COPB) or cystic fibrosis (CF)).

Furthermore, some of these pathologies can be combined. For instance CF superimposed with one of the other pathologies will lead to a more negative prognostic^{4,5}. People have become more and more aware of these problems since 2020 because of the COVID 19 pandemic. In the case of Covid, it has been reported that up to 50% of the patients admitted in intensive care eventually die mostly because of lungs failure linked to bronchial airways saturation⁶. It is therefore undoubted that the treatment of severe respiratory pathologies is a major public health issue and this justifies the intensification of science research in this field^{6,7}.

A large number of available treatments for these diseases rely on the restoration of a normal bronchial airways mucus transportation. This is obtained either by chemical means, consisting in the use of drugs directly reducing the mucus macromolecular network, or by physical ones (mechanical solicitations), using for instance a device generating depression waves to increase mucus transportation⁸.

Considering that severe respiratory diseases are associated with a clearance defect that causes congestion basically linked to a change in the production but also composition and therefore rheology of bronchial mucus, it is then necessary to carry out rheological studies to characterize the behaviour of this material⁹⁻¹¹.

In this context the project undertaken by the experimental and computational research laboratories of the Aix-Marseille University (M2P2) in cooperation with the C2VN (Cardio-Vascular and Nutrition Research Centre of La Timone University Hospital in Marseille) and the ISM2 laboratory (Aix-Marseille University) for the design and interpretation of experimental matrixes, is about the intensification of research in this field to reach two objectives.

- The determination of rheological properties of airway mucus overcoming the problems of small quantity and significant variability (in composition and behavior) of natural samples.
- Provide a fluid-dynamic model for the flow of mucus in lungs, based on a relevant rheological parameter or model and guaranteeing both technical improvements of the air-respiratory machines, and an increase of the efficiency of the therapeutic procedure as a function of the possible pathology.

The present work tries to contribute to both aims, pursuing the following objectives:

Based on an intensive literature review:

- Characterizing the change in bronchial mucus composition for each single pathology and the associated change in rheological behaviour.
- Codifying the chemical composition and a standard operating mode to reconstruct bronchial mucus at laboratory scale (under healthy and sick conditions).

Based on a large experimental measurements campaign:

- Determining the influence but also the interactions between mucus main components (in terms of rheological parameters) in order to adapt the possible treatments to the mucus specificities for a given patient suffering from a given disease at a given state of exacerbation. To reach this goal, we have performed measurements on reconstituted mucus of various compositions in mucus main components (Mucins / DNA / Lipids...). Experimental matrixes have been used in order to minimize the number of experiments to carry out (ISM2 laboratory).

- Determining rheological parameters and/or models that can be used to validate the CFD model, working on the following mucus types:
 - In Vitro real Bronchial Mucus (MB) harvested from cellular cultures (based at the C2VN lab) using epithelia either coming from sane or sick patients. The composition of the main components has varied to cover the range from healthy mucus to sick mucus corresponding to the previously cited pathologies.
 - In Vivo real Nasal Mucus (NM) coming from Asthmatic patients and sampled during medical consultations in Marseille (AP-HM).

CHAPTER 1:

LITERATURE REVIEW

1.1 INTRODUCTION to RHEOLOGY of VISCOELASTIC SUBSTANCES

The rheology is defined as the ability of a material to undergo flow and deformation in response to the application of forces ¹². In this study will be used a Macro-rheological approach, which consists in the measurement of mean macroscopic rheological properties, at the scale of a whole sample of hundreds of μL to characterize the mucus in the airways of patients with or without severe lung disease^{13,14}.

For this reason is interesting to first review the principal rheological behaviours and the parameters linked to them.

RHEOLOGICAL BEHAVIOURS:

1.1.1 ELASTIC BEHAVIOUR

It is defined as the capacity of the material to transmit recoil energy back to the object applying the stress ¹². It is the property of solids materials. Given a force acting on a body, if it is an elastic one, it will regain its original shape and size instantaneously at the removal of applied stress.

This behaviour is described by the Hooke's law that relates the stress and the deformation to the elastic modulus (G') proper of each elastic material:

$$\tau = G' \cdot \gamma \tag{1.1}$$

$$\tau = \frac{F}{A} \tag{1.2}$$

$$\gamma = \frac{\partial s}{h} \tag{1.3}$$

1.1.2 VISCOUS BEHAVIOUR

It is the ability of a body to resist deformation and flow, under the application external forces. As showed in figure 1, given a force acting on a viscous body it will change its shape and it will not regain its original one with the removal of the applied stress¹⁵. This behaviour is regulated by the

Newton's law that relates the shear stress and the local shear velocity with a proportionality constant, η , proper to each viscous material at a given pressure and temperature:

$$\tau = \eta' \cdot \dot{\gamma} \quad (1.4)$$

$$\dot{\gamma} = \frac{\partial u}{\partial y} = \frac{\partial \gamma}{\partial t} \quad (1.5)$$

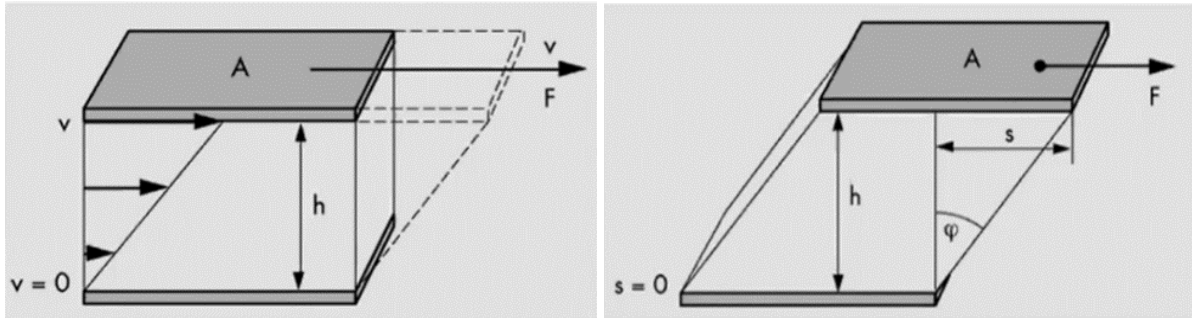


Figure 1 Free body diagram of the system of two planes moving relative to each other at constant speed and force 12.

The ideally viscous materials are also called Newtonian. On the other hand, Non-Newtonian materials that are structurally characterized by the presence of complex structural units, such as long macromolecular chains that lead to particular behaviour in between purely Elastic and Viscous one. The most important Non Newtonian behaviours are:

SHEAR THINNING BEHAVIOUR

It is the behaviour of fluids whose apparent viscosity decreases under increasing shear strain. It is observed in many industrial and everyday fluids such as polymer solutions and molten polymers, as well as complex fluids and suspensions like ketchup, whipped cream, blood, paint, and nail polish. The elastic behaviour is dominant under low stress or strain levels, while increasing levels of them leads to a transition towards viscous domain (flow). Taking the example of aqueous polymeric solutions ST behaviour can be explained by the fact that at rest, high molecular weight polymers are entangled and randomly oriented. However, when undergoing shear under an high enough shear rate, these highly anisotropic polymer chains start to disentangle and align along the direction of flow. In the ST region, the relation between shear stress and the shear rate can be modelled by the Ostwald power law:

$$\tau = K(T) \cdot \dot{\gamma}^n \quad (1.6)$$

$K(T)$ is a constant of the substance at given temperature, represent (for a Bingham fluid) the apparent viscosity of the body without any stresses application (η_0). As this parameter increases, the material will be able to absorb stresses more effectively without giving rise to major laminar slippage.

n is comprised between 0 and 1 for an ST fluid and represents the ability of the substance to decrease its viscosity as the shear rate increases (shear thinning). This parameter can be obtained by the slope plus 1 of Shear rate/Apparent viscosity log-log scaled graph.

$$\ln(\eta_{app}) = (n - 1) \cdot \ln(\dot{\gamma}) + \ln(K(T))$$

(1.7)

n is an indication of the ST behaviour of the substance, the more n tends towards 1, the more the material behaves as a Newtonian viscous element, while when it tends towards 0, the material behaves more like an Hookean elastic element.

SHEAR THICKENING BEHAVIOUR

It is the behaviour of fluids whose apparent viscosity increases under increasing shear strain. It can be observed in several industrial applications, such as liquid bulletproof vests and brake pads. The suspension used to create these products are composed of flocculated dispersed silica nanoparticles in a polyethylene glycol medium that form stronger links under high shear strains. The elastic viscous behaviour is dominant at low stress or strain levels, while the increasing levels leads to a transition towards elastic domain. This phenomenon is regulated by the velocity of the transition from order to disorder of the system and the subsequent particles aggregation and de-aggregation of hydro clusters. Once again the relationship between stress and shear rate is the Ostwald power law with $-1 < n < 0$ ¹⁶:

$$\tau = K(T) \cdot \dot{\gamma}^n \tag{1.8}$$

1.1.3 VISCOELASTIC BEHAVIOUR

This property is characteristic of a material that behaves like rigid elastic material under low stresses but flows as a viscous fluid under high stresses. It is typical of substances containing particles (such as clay) or large molecules (such as polymers) with interactions with one another, creating a weak solid structure, formerly known as a false body. In this case an yield stress τ_y is required to start brakes the weakest structure links so that particles move under viscous forces. In a Viscoelastic material at removed stress the false body returns to the initial configuration without any permanent structural deformation. To explain the relationship between the stress and the shear rate in a viscoelastic substance is commonly used the Herschel-Buckley (HB) model, which adds a threshold shear stress component to the Ostwald equation. This additional parameter τ_0 represents the sollicitation above which the weak solid structure of the material start to change irreversibly shifting form a solid-like to a liquid-like behaviour. It has to be considered that the so called flow stress is not an inherent property of a viscoelastic material since the structural strength material is time and stress dependent ¹³. The HB model is:

$$\tau = \tau_0 + K(T) \cdot \dot{\gamma}^n \tag{1.9}$$

This last rule is particularly relevant because describes all the previous ones as follows:

$\tau = \tau_0 + K(T) \cdot \dot{\gamma}^n$ ($n = 0, K(T) > 0, \tau_0 = 0$)	$\tau = G \cdot \gamma$	Elastic Behaviour
$\tau = \tau_0 + K(T) \cdot \dot{\gamma}^n$ ($n = 1, K(T) > 0, \tau_0 = 0$)	$\tau = K(T) \cdot \dot{\gamma}$	Newtonian Behaviour
$\tau = \tau_0 + K(T) \cdot \dot{\gamma}^n$ ($-1 < n < 0, K(T) > 0, \tau_0 = 0$)	$\tau = K(T) \cdot \dot{\gamma}^n$	Shear Tickening Behaviour
$\tau = \tau_0 + K(T) \cdot \dot{\gamma}^n$ ($0 < n < 1, K(T) > 0, \tau_0 = 0$)	$\tau = K(T) \cdot \dot{\gamma}^n$	Shear Tinning Behaviour
$\tau = \tau_0 + K(T) \cdot \dot{\gamma}^n$ ($n = 1, K(T) > 0, \tau_0 \neq 0$)	$\tau = \tau_0 + K(T) \cdot \dot{\gamma}$	Bingham Behaviour
$\tau = \tau_0 + K(T) \cdot \dot{\gamma}^n$ ($0 < n < 1, K(T) > 0, \tau_0 \neq 0$)	$\tau = \tau_0 + K(T) \cdot \dot{\gamma}^n$	Viscoelastic Behaviour

1.1.4 TIXOTROPIC BHEAVIOUR

It is the behaviour followed by a material that, under a given shear rate variation responds with an instantaneous over stress following the tendency of the imposed $\dot{\gamma}$ variation, switching then

gradually towards a new plateau in the opposite tendency^{17,18}. The thixotropic behaviour occurs if the thixotropic characteristic time is longer than the time scales involved during viscoelastic phenomena (structure relaxation times), but smaller respect to the aging or rejuvenation ones¹³. The difference between shear-thinning and thixotropy is that the first one corresponds to a quite instantaneous reversible structural evolution as a function of strain rate (with a characteristic time small compared to the measurement characteristic time), while the second is related to a slower structural evolution (with a characteristic time of the same order of magnitude as the measurement characteristic time).

A thixotropy model imply the knowledge of a time dependence model of the material rheological behaviour. Among the various attempted approaches there is one proposed by Albert Magnin and all in the "Rheology of bronchial mucus"¹³. This model is based on the Herschel-Bulkley behaviour, and modified to take in account the instantaneous structural state $\lambda(t)$ of the material.

$$\tau(t) = \tau_y + K_T \cdot \dot{\gamma}(t)^n \quad \rightarrow \quad \tau(t) = \tau_y[\lambda(t)] + K_T[\lambda(t)] \cdot \dot{\gamma}(t)^{n[\lambda(t)]} \quad (1.10)$$

The structure evolution is considered based on the equation governing the rate of time evolution for the structural parameter.

$$\frac{\partial \lambda}{\partial t} = -k_1 \dot{\gamma} \lambda + k_2 \dot{\gamma} (1 - \lambda) + k_3 \dot{\gamma} (1 - \lambda) \quad (1.11)$$

Observing the condition of constant structure ($\frac{\partial \lambda}{\partial t} = 0$) under a reference shear rate and correlating the $K(T) = K(T)_{ss}$ observed experimentally from the isostructural curves and fitted with the empirical laws reported below:

$$K(T)_{ss} = \frac{b + c\dot{\gamma}}{1 + a\dot{\gamma}} ; K_{ss} = Const \cdot \lambda_{ss} ; \lambda_{ss} = \frac{1 + \frac{k_3}{k_2} \dot{\gamma}}{1 + \frac{k_1 + k_3}{k_2} \dot{\gamma}} ; \frac{k_3}{k_2} = \frac{c}{b} ; Const = b ; \frac{k_1}{k_2} = a - \frac{c}{b} \quad (1.12)$$

It is possible to find λ_{ss} given K_{ss} , then the parameters u , v , m and p considering a linear relationship between λ_{ss} and the corresponding $\tau_{y_{ss}}$ and n_{ss} taken from the fitting of the HB model by the isostructural curves.

$$\tau_{y_{ss}}(\lambda_{ss}) = u \cdot \lambda_{ss} + v \quad (1.13)$$

$$n_{ss}(\lambda_{ss}) = m \cdot \lambda_{ss} + p \quad (1.14)$$

Assuming then that τ_y , K_T and n evolve instantaneously with the level of structure, the yield stress in a given transitory structural state $\lambda(t)$ under any shear rate $\dot{\gamma}_1(t)$ is equal to the yield stress in the steady structural state $\lambda_{ss}(\dot{\gamma}_2)$ corresponding to the same level of structure so that:

$$\tau(t) = u \cdot \lambda(t) + v + b \cdot \lambda(t) \cdot \dot{\gamma}(t)^{m \cdot \lambda(t) + p} \quad (1.15)$$

In addition solving the structure kinetic differential equation the correlation between $\lambda(t)$, λ_{ss} , k_1 , k_2 , k_3 can be written as follow:

$$\lambda(t) = \lambda_{ss} + (\lambda_{t=t_0} - \lambda_{ss}) \cdot e^{-[(k_1+k_3)\dot{\gamma}(t)+k_2](t-t_0)} \quad (1.16)$$

To satisfy each set of experimental data it is necessary to add a shear rate dependent term to complete the $\tau(t)$ equation. This factor is dependent a residual viscosity $\eta_{\lambda=0}$ of the material under its maximum degree of restructuration ($\lambda(t) = 0$). Its identification is performed by techniques of error minimalization, implemented on software such as "MATLAB R2022a".

$$\tau(t) = u \cdot \lambda(t) + v + b \cdot \lambda(t) \cdot \dot{\gamma}(t)^{m \cdot \lambda(t) + p} + \eta_{\lambda=0} \dot{\gamma}(t) \quad (1.17)$$

1.2 TYPE of MUCUS, STRUCTURE and BEHAVIOUR

The viscoelastic fluid studied in the present work is human airway mucus, a substance secreted by the mucous glands. It is mainly composed of water (90-95%), mucins (2-5%), lipids (1-2%), salts (1%), DNA (0.02%) and other molecules such as cells debris¹³. Particularly we will focus on bronchial mucus, the one involved in the respiratory acts. Mucus ascension from the distal to the proximal airways, through the cilia movement protects the respiratory tract avoiding the development and accumulation of pathogenic bacteria that induce infection and obstruction.

The different mucus components will be classified in this chapter with respect to the effect that they have on the structure and behaviour of the fluid.

1.2.1 MUCUS COMPONENTS

MUCINS

Also called gel-forming mucins GFMs, they are macromolecules specific to the different types of mucus (different organs) and constitute the prevalent solid part of it. In this work, we have focused our attention on mucins' types MUC5AC, MUC5B and MUC2, that are present in the lungs. These bronchial mucins all derive from a same ancestral mosaic structure (figure 2), divided into three distinct regions :

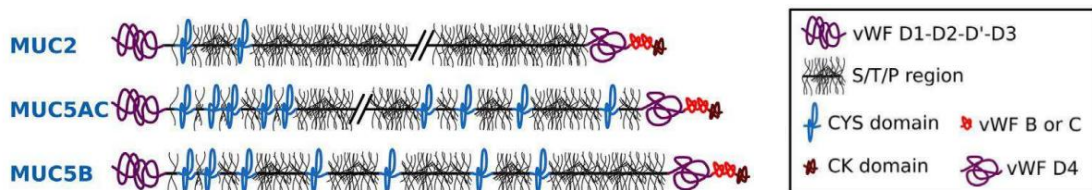


Figure 2 The three most important bronchial mucins structure and sections 19.

Amino- and Carboxy- terminal regions:

The Amino-terminal regions account for one-third of the terminal mucins length and are composed by four von Willebrand factor (vWF) domains (vWD1, vWD2, vWD', vWD3), rich in cysteines (amino acid). All cysteine residues are highly conserved and mostly engaged in the intradomain disulphide bonds in vWD, producing a globular secondary structure.

The carboxy-terminal regions are very different in the domain composition (are present vWB, vWC, vWD4) except for the cystine knot one (CK), a globular structure of 80 amino acid (aa). Both GFM amino- and carboxy- terminal factors include several *N*-glycosylation sites, directly involved, but not fully responsible of the GFMs oligomerization.

Central region:

The GFM central region (S/T/P region) is mainly organized in tandem hydrophilic repeated sequences (TR) reached in amino acids (particularly serine, threonine and proline). The high content of serine and threonine residues results in a dense *O*-glycosylation, that block the access of proteases to the mucin backbone, slowing mucus degradation. Glycan fraction contribute up to 80-90% of the GFMs dry weight and is composed mainly of *N*-acetylglucosamine, *N*-acetyl galactosamine, galactose, fucose, sialic acid and contains

numerous sites for hydrogen bonds, as well as ionic interactions. Human nasal and bronchial GFM's central region is interrupted by hydrophobic "necked domains" (CYS) of 110 aa which possesses cysteine residues (10% dry CYS w/w %) involved in the mucin network and in the intradomain disulphide bonds. MUC5AC, MUC5B, MUC2 contain respectively nine seven and two CYS domains and play a crucial role in the regulation of mucous architecture, relate to the protection against exogenous particles and pathogens ¹⁹.

PROTEINS

They represent approximately 1 % (w/w %) of the healthy mucus, having strongly related structures and protective (innate immunity) functions. The amphipathic and cationic nature of antimicrobial peptides (AMPs) allows electrostatic interactions with mucin carbohydrate side chains and or with multiple microbes, causing aggregation and trapping²⁰. For this reason, protein content in sputum of sick patients have been demonstrated to serve as reliable biomarkers for disease, even before symptomatology. Ionic or hydrophobic interactions are commonly linked to GFM's proteins such as the three peptides (TFF1, TFF2 and TFF3) of the Trefoil Factor Family (TFF), through lectin activity ¹⁹. Other proteins in the mucus such as Transglutamines (TGs) are enzymatically active. They are involved in the post translational modifications of proteins, catalysing a broad range of transamidation reactions (reactions that stabilizes noncovalent assemblies under physiological conditions) in other to mediate cross-link between GFM fibres.

LIPIDS

With 1–2 % (w/w %) by mass, lipids are another essential component of mucus and can be associated in a covalent or non-covalent way, contributing to the hydrophobic interactions. Together with mucins, bronchial surfactant (PS) represents the most relevant constituent of the lung lining fluid. It acts at distal airways as the first renewable barrier against foreign matter while at alveolar air–liquid interface, reducing the surface tension, it facilitates the process of breathing. PS, composed by lipids (approx. 90 % by mass) and proteins (approx. 10 % by mass) ensure open and functional airways, host defence and displacement of foreign material into the mucus layer to be cleared via mucociliary escalation ²¹.

NUCLEIC ACIDS and FILAMENTOUS of ACTIN

Nucleotides chains (in the range of 50 kbp) deriving from extracellular DNA are present in mucus of healthy individuals at 0.028 % (w/w %). The semi flexible conformation of polyelectrolyte polymers like DNA and f-actinis, regulated by the molecular weight and number of counterions in the mucus, has been demonstrated to affect the mucus rheology ²¹.

While listing the principal molecules that constitute the mucus it is interesting to understand what kind of bonding determine GFM's gel.

1.2.2 MOLECULAR INTERACTIONS

In addition to the weak bonds susceptible to even small mechanical stresses that GFM establish with macromolecules in the mucus, the interactions (figure 3) underlying its architecture are:

Disulphide bonds or covalent bonds: The inter and intramolecular, covalent links that join wFDs between them or with CYS or TR glycoprotein subunits. This type of hydrophobic interaction can occur also between CYS or CYS and TR glycoprotein subunits.

Oligosaccharide side chains and hydrogen bonds: The inter-mucins bonds between complementary sugar unit, constituent of the oligosaccharide side chain. Singularly weak and easily broken, if repeated in a wide mucin side they become potentially very important. This type of hydrophobic interaction, as seen before, can occur also between mucins and proteins.

Van der Waals bonds: The inter-mucins bonds that occur between complementary saccharide moieties on neighbouring mucins chains. They are not a real entanglement but are due to the mucins steric dimension.

Ionic bonds: These occurs for the ionization of mucins that contain both positively charged amino acid residues and negatively charged sugar units ^{12,22}.

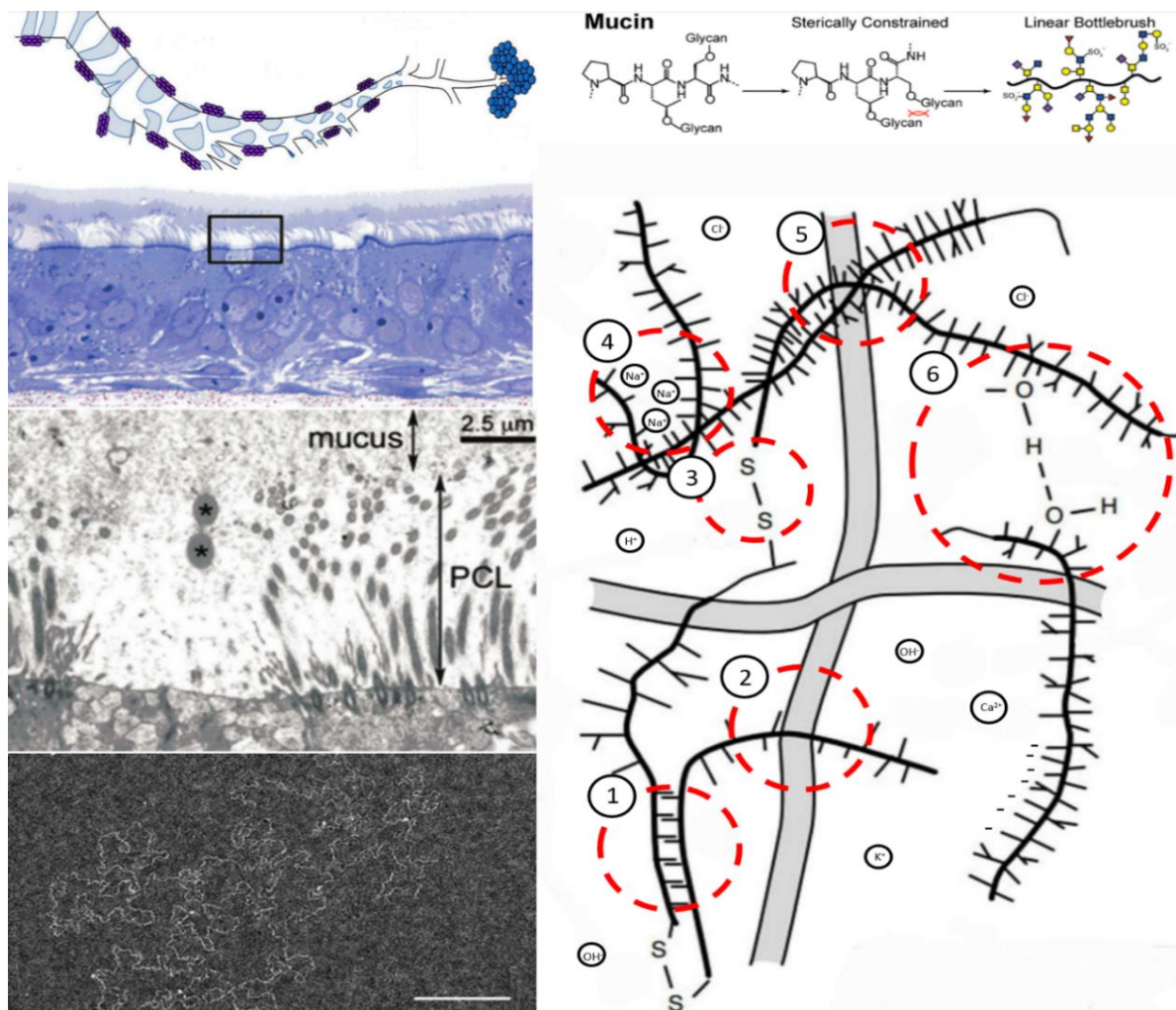


Figure 3 From top to bottom left: Successive enlargements of the surface of the bronchiolar walls ⁵¹, up to the identification of mucus and periciliary layer (PCL) ¹⁹ and observation by electronic microscope of mucins ²¹. From top to bottom right: Molecular components of mucins ²² and pattern of interactions in gel-forming mucins (GFMs) ¹². we distinguish 1. and 5. Van der Waals bonds 2. extra networks of high-molecular-weight 3. Disulphide bonds or covalent bonds 4. Ionic bonds 6. Oligosaccharide side chains and hydrogen bonds.

Referring again to ionic interactions, it is necessary to consider that all the macromolecules listed above are immersed in a physiological solution, whose pH and ions concentration greatly influence the configuration and thus the properties of the GFMs. Principal dissolved salts within the mucus are NaCl and KCl, as well as CaCl₂. The ions that they generate once dissolved in water contribute to the osmotic regulation between mucus and epithelial glands, but also to the neutralization of TRs. Sugar chains present in the S/T/P region are negatively charged. The presence of positive ions allows to modify the configuration of the central mucin section, so that it can have more interactions with similar sections of adjacent mucins. The ions involved in this change are different from the inside of the epithelial glands, where mainly Ca²⁺ ions act by directly connecting two mucins, to the "bulk" of the mucus, where Na⁺ and K⁺ ions simply neutralize the oligosaccharide chains, letting other forces (Van der Waals or hydrogen bonds) determine the structure of the GFMs. During secretion, the exchange between Na⁺ and Ca²⁺ ions promote local hyper-osmolarity within the gel. The result is a configuration constituted by mucins quasi spherical macromolecules about 400 to 600 nm in diameter (with the centre of each molecule being about 70 to 75 nm in distance from its nearest neighbours) whose large coiled structure interpenetrate one to each other, creating entanglements. This structure can swelled, passing from a condensed state to a hydrogel one depending on the solicitation the mucus is submitted to ¹⁹. A similar argument can be made (and will be addressed in detail in future chapters) concerning the concentration of H⁺ ions, i.e. the pH, and the presence of polyelectrolytic macromolecules such as DNA or actin filaments.

1.2.3 PATHOLOGIES EFFECT on MUCUS STRUCTURE and RHEOLOGY

In the interactions displayed upward, no account is taken for the so called **extra networks of high-molecular-weight**, related to the occurrence of airway diseases, characterized by infection and inflammation. The immune reaction that the body has in response to a certain pathology, impact, because of the different production of the mucus components, the health of people affected by bronchial chronic disease. Asthma, Chronic Obstructive Bronchial Disease (COPD) and cystic fibrosis (CF) are the main obstructive airway diseases. In all these diseases, inflammation plays a role in the pathology, causing increased mucus production of mucus and a decrease in its clearance through hypertrophy of glands and metaplasia of epithelia. Cellular necrosis lead to the formation of extracellular bundles of anionic polyelectrolytes in the form of DNA and filamentous (f)-actin fibres. Those two alter the levels of membrane transporters of chloride (Cl⁻) and sodium ions (Na⁺), that are responsible for maintaining fluid balance in airway epithelia. Deficiencies in ion transport and the resulting fluid imbalance lead to insufficient flushing of mucin macromolecules, mucus accumulation and impaired ticker rheology. In addition, static mucus further narrows the airways and promotes bacterial growth and persistent inflammation. Those two phenomena recruit immune cells (innate type such as neutrophils, macrophages and eosinophils, but also leucocytes) to the lung epithelium, leading to an increase in antimicrobial peptide/protein counts in the sputum ^{20,21}.

The following sections will compare the chemical composition and rheological characteristics of the bronchial mucous of healthy subjects and those with respiratory diseases.

HEALTHY BRONCHIAL MUCUS

Chemical composition of the healthy bronchial mucus, found in the literature, is given in the following table, as well as the rheological characteristics associated with it ^{13,20,23-25}.

Table 1 Composition of healthy bronchial mucus

Components	Weight %	1L Mucus Comp. [g]
H ₂ O	98	980
Mucins	0.81	8
Plasma end not plasma Proteins	0.44	4.4
Lipids	0.36	3.6
Salts	0.39	3.9
DNA	-	-
Immune cells and filamentous-actin	-	-
Bacteria	-	-

Table 2 Rheological parameters of healthy bronchial mucus

Rheol. Param.	Values
G' [Pa]	0.1 β ; 0.39 γ ; 0.05 δ ; 14.9 ζ
G'' [Pa]	0.04 β ; 0.36 γ ; 0.02 δ ; 4.3 ζ
G* [Pa]	0.11 β ; 0.53 γ ; 0.05 δ ; 15.50 ζ
tan δ	0.39 β ; 0.93 γ ; 0.4 δ ; 0.29 ζ
τ_f [Pa]	42.42 β ; 1 δ

Given the small quantities of lung mucus taken from time to time (between 10² and 10³ μ L), it is complicated to perform both a chemical and rheological analysis on the same sample. However, It has been possible to proceed, based on the listing of the rheological data found in the literature (see the end of the chapter for the fundamental analytical conditions under which the data were obtained) and make an average chemical composition related to each mucus pathology as follow:

Starting from the healthy mucus average chemical composition has been calculated the dry fraction (5% w/w) ^{13,19}. The so reached weight has been fitted for a solution constituted by 98% w/w of H₂O ²¹. Than has been assumed to describe a solution of 1 g of the healthy mucus with the so reached w/w proportions. It has been assumed to maintain constant the water mass and modify the amount of the other elements applying a multiplication factor (following figure 4) to the upward health mucus composition ²⁶. Actin filaments and DNA has been grouped in DNA, being not distinguished in the literature papers. To determine the last two components, not originally present in the healthy mucus, the DNA mass value of a CF subject has been found into literature and scaled for the other pathologies. Similarly, given the number of bacteria per gram of CF mucus and estimating the weight of a single unit of Pseudomonas Aeruginosa (typical bacteria present in the CF bronchial mucous), it has been possible to scale the bacteria mass contribution for each pathology ^{10,27-29}. The amount of salt, thus ions but also in lipids in all the conditions has been maintained constant with respect to the healthy one since there is not enough data in the literature concerning these aspects. It is important to say that the so constituted chemical compositions have just been a starting point, further subjected to little adjustments, explained in the following chapters, when transferred in the project of the reconstructed mucus.

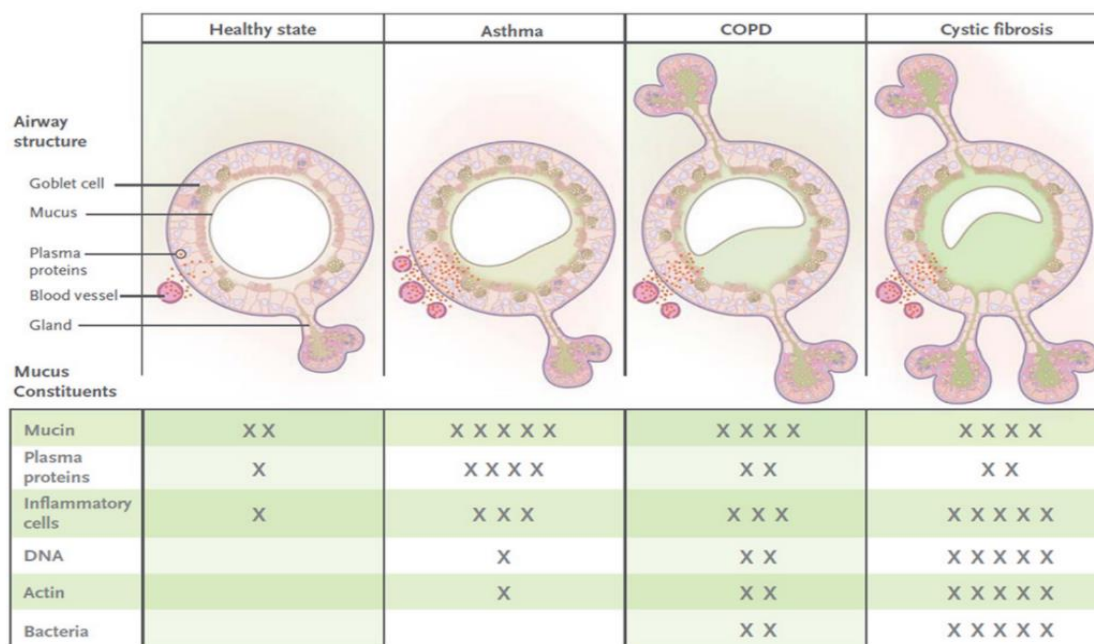


Figure 4 Qualitative table of the change in lung mucus mass composition for different pathologies accompanied by the tracheal sections for each pathology ¹⁰.

CHRONIC OBSTRUCTIVE BRONCHIAL DISEASE (COPD) BRONCHIAL MUCUS

COPD is a respiratory disease often caused by smoking and is characterised by excessive mucus secretion by the glands, that can be eliminated by coughing. Cigarette smoke contains multiple toxins, including particulate matter, oxidative chemicals and organic compounds which potently induces mucin production. This also manifests itself in goblet cell hypertrophy and submucosal gland hyperplasia. Increased mucin production increases the viscoelasticity of COPD sputum, furthermore the decrease of luminal fluids lead to bacterial proliferation, that increases with severity of the disease. The mucoïd sputum of COPD showed higher values than CF and normal sputum for all parameters of viscosity and elasticity ²⁴.

Table 3 Composition of COPD bronchial mucus

Components	Weight %	1L Mucus Comp. [g]
H ₂ O	96.18	965
Mucins	1.59	16
Plasma end not plasma Proteins	0.87	8.8
Lipids	0.36	3.6
Salts	0.39	3.9
DNA	0.01	0.1
Immune cells and filamentous-actin	0.06	0.6
Bacteria	0.54	5.4

Table 4 Rheological parameters of COPD bronchial mucus

Rheol. Param.	Values
G' [Pa]	1.7 β ; 1.4 γ ; 1 δ
G'' [Pa]	0.55 β ; 0.77 γ ; 0.25 δ
G^* [Pa]	1.79 β ; 1.59 γ ; 1.03 δ
$\tan \delta$	0.32 β ; 0.55 γ ; 0.25 δ
τ_f [Pa]	67.88 β ; 10 δ

CYSTIC FIBROSIS (CF) BRONCHIAL MUCUS

Cystic fibrosis is a respiratory disease caused by a mutation in the gene encoding the cystic fibrosis transmembrane conductance regulator, resulting in reduced chloride secretion and increased sodium content. The combination of these factors results in insufficient airway luminal fluid. The collapse of the viscoelastic mucus layer over the cilia of epithelial cells provides a favourable environment for the colonisation of neutrophilic bacteria, which are responsible for increased cross-linking of disulphides in mucin with consequences for mucus rheology. Furthermore, analysis of CF mucus revealed an increase in the solid component, particularly lipids^{21,26}. Biopolymer systems studied here because the abnormal sputum rheology in CF is not due to inherent changes to the mucins but rather to the high load of non mucin polymers present in the infected mucus²⁹.

Table 5 Composition of CF bronchial mucus

Components	Weight %	1L Mucus Comp. [g]
H ₂ O	95.35	965
Mucins	1.58	16
Plasma end not plasma Proteins	0.87	8.8
Lipids	0.36	3.6
Salts	0.38	3.9
DNA	0.02	0.2
Immune cells and filamentous-actin	0.11	1.1
Bacteria	1.33	13.5

Table 6 Rheological parameters of CF bronchial mucus

Rheol. Param.	Values
G' [Pa]	9.6 α ; 3.5 β ; 0.54 γ ; 20 δ
G'' [Pa]	3.9 α ; 0.9 β ; 0.47 γ ; 6 δ
G^* [Pa]	13.31 α ; 3.61 β ; 0.72 γ ; 20.88 δ
$\tan \delta$	0.34 α ; 0.25 β ; 0.87 γ ; 0.3 δ
τ_f [Pa]	148.49 β ; 11 δ

ASTHMA (AH) BRONCHIAL MUCUS

Asthma is a respiratory disease characterised by mucosal metaplasia (i.e. increased production of surface epithelial mucin) and increased numbers of bronchial microlesions. Airway obstruction by mucus plugs can cause localised atelectasis and extensive airway obstruction. Diffuse narrowing of the airways, due to the combination of concentric contraction of smooth muscle and luminal obstruction by mucus, makes asthma uniquely dangerous among airway diseases due to its propensity for sudden exacerbations. Airway mucus in severe asthma has a viscoplastic quality, biochemical analysis shows high concentrations of mucins and plasma proteins, while, biophysical analysis shows a high levels of entanglement density and elastic modulus²⁶.

Table 7 Composition of Asthmatic bronchial mucus

Components	Weight %	1L Mucus Comp. [g]
H ₂ O	95.49	965
Mucins	1.98	20
Plasma end not plasma Proteins	1.74	17.6
Lipids	0.36	3.6
Salts	0.38	3.9
DNA	-	-
Immune cells and filamentous-actin	0.04	0.4
Bacteria	-	-

Table 8 Rheological parameters of CF bronchial mucus

Rheol. Param.	Values
G' [Pa]	0.15 β ; 0.5 δ
G'' [Pa]	0.05 β ; 0.1 δ
G* [Pa]	0.16 β ; 0.51 δ
tan δ	0.33 β ; 0.2 δ
τ_f [Pa]	53.03 β ; 4 δ

In figure 5,6 and 7 a review of the rheological characterization, relevant for this study is reported. The reported red values are those obtained with the most similar analysis with respect to this work, while the grey ones are the average values resulting by the bibliographic researches. This distinction is necessary because, as explained in the following chapter, it is important to compare results gained in the same test and under the same operating conditions. This might be enough to explain the variability of the presented results, (up to three orders of magnitude) but it is not. In addition to the operating conditions, the way in which the lung mucus is extracted must be considered, as it could be contaminated by the mucus in the trachea (which differs in composition) and saliva during expectoration.

The storage time and conditions are also important, given the possible mucosal degradation that may occur depending on these aspects and influencing biochemical and rheological parameters. Another source of variability in results are environmental factors. such as air pollution or even air quality due to geographical location (marine atmosphere or altitude) can deeply affect the mucus composition and therefore physical properties. Lastly, there is the

person's symptomatology, which influences the conditions under which the mucous membrane develops and causes biochemical-structural changes. Perhaps of all the variables related to sampling, this is the least controllable as it is due to the individual's immune response. It is for this reason that in the following chapters, laboratory analyses performed on lung mucus will be introduced, and the characteristics of the sampling methods will be associated with the symptomatology presented by the patient at that time.

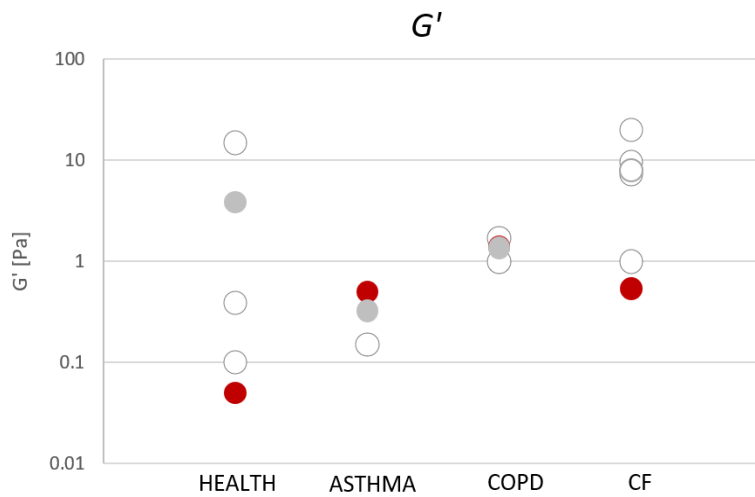


Figure 5 Summary graph of mucus elastic modulus of healthy and asthma, COPD or CF patients. Denoted in grey the mean values and in red the results obtained with the most similar analysis respect the one performed at M2P2 laboratory.

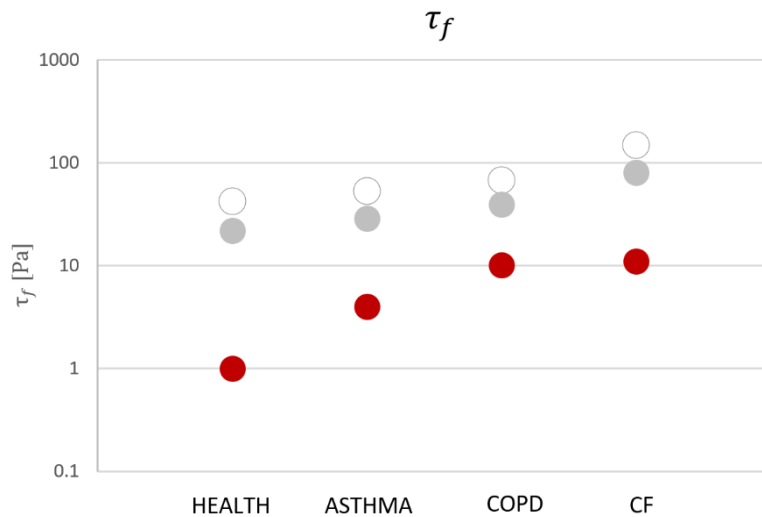


Figure 6 Summary graph of mucus flow point of healthy and asthma, COPD or CF patients. Denoted in grey the mean values and in red the results obtained with the most similar analysis respect the one performed at M2P2 laboratory.

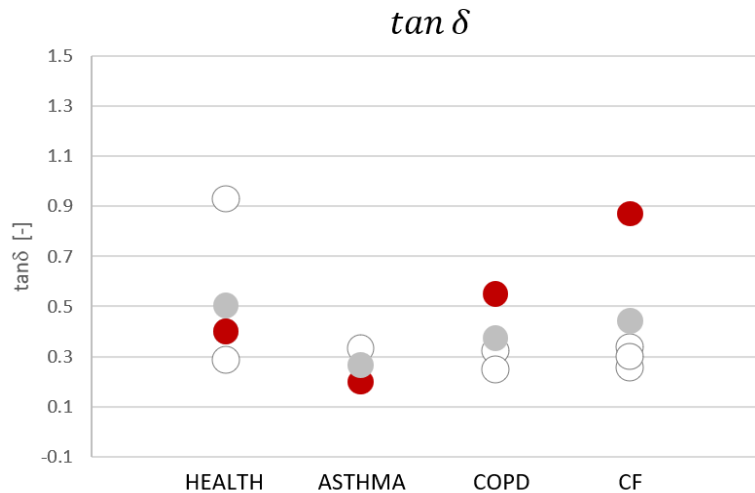


Figure 7 Summary graph of mucus viscoelasticity of healthy and asthma, COPD or CF patients. Denoted in grey the mean values and in red the results obtained with the most similar analysis respect the one performed at M2P2 laboratory.

Summary of analyses evaluated by the bibliography

α. MCR 702 rheometer, parallel plate mode, sandblasted steel plate, temperature of 20 ± 1 °C, , two consecutive measurements: frequency sweep (0.1–100 rad/s, $\gamma = 1\%$) at 5% and 10% strain, followed amplitude sweep (0.1–1000%, $\omega = 1$ -10 rad/s) ²³.

β. Strain-controlled, rotational rheometer, oscillatory mode, rough plane geometries, temperature within the gap is regulated at 37 ± 1 °C, two consecutive measurements frequency sweeps (0.1–5 Hz) at 5% and 10% strain, followed by a strain sweep (0.9–3000%) at 0.6 Hz (each set of measurements typically takes 20 minutes per replicate) ²⁰.

γ. Controlled-stress rheometer, dynamic oscillatory mode, parallel-plate geometry, temperature at 20 ± 1 °C. Two consecutive measurements, torque sweeps (0.1 – 10 Pa) a logarithmic frequency sweeps (0.1–10 Hz) were then performed in triplicate at the determined shear stress and displacement (each set of measurements typically takes 30 minutes per replicate) ²⁴.

δ. Rheometer rheomuco, dynamic oscillatory mode, plate-plate geometry with rough surfaces, temperature at 37 ± 1 °C. An oscillatory (1 Hz) shear sequence is exerted with a strain sweep (0.1–3000%) ²⁵.

ε. Rotational rheometer, dynamic oscillatory mode, 40-mm stainless steel cone-and plate geometry with an angle of 2°, room T, sweeps at a frequency of $\omega_0 = 0.16$ rad/s for strains of $\gamma \in [10^{-4}, 0.5]$, frequency sweeps completed at a strain of $\gamma_0 = 0.01$. The frequency-dependent elastic modulus, G' , and viscous modulus, G'' , were found by performing an oscillatory shear sweep with frequencies of $\omega \in [0.01, 50]$, rad/s. Finally, the shear viscosity was found by completing steady-shear flow sweeps with shear rates of $\dot{\gamma} \in [0.01, 100]$, 1/s ³⁰.

ζ. Anton Paar MCR 702 rheometer, dynamic oscillatory mode, cone-plate geometry (diameter: 25 mm, cone angle: 2°). Low viscosity silicon oil was applied to prevent potential mucus dehydration during the measurement, temperature of 25 °C, strain amplitude (γ) sweep of 0.1–10% strain with a frequency fixed at 1 Hz. Elastic (G') and viscous (G'') moduli were determined by frequency (ω) sweep experiments in a range of 0.5–50 rad/s at $\gamma = 1\%$ ³¹.

1.3 RECONSTITUTED MUCUS

Given the difficulties linked to the sampling of non-contaminated human tracheobronchial samples, most studies on drug and mechanical therapies delivery, linked to the chemical structure formation and the answer to stress solicitations of the bronchial mucus, are performed with alternative mucus sources. Some of these mucus, are formulated based on studies that establish the concentrations of nutrients commonly found in pathological or sane sputum. This formulation of purely synthetic reconstructed mucus is used since 1997 with the first reconstructed sick mucus³², only composed of water, Mucins and DNA. This basic formulation has been further modified either adjusting the Mucins and DNA types and w/w mass percentages or with the addition of specific amino acids, bovine serum albumin (BSA), ions, pH regulators and iron chelators. This latter component being particularly important in the case of studies using reconstructed mucus to grow pathogenic bacteria cultures^{33,34}. The researches carried out for the development of the artificial mucus, by Catherine Taylor Nordgard et al (in 2011), Benedikt C. Huck et al (in 2019) and Mingyang Tan et al. (in 2020) provided a comprehensive overview of the components used in previous studies in the reconstructed mucus. Based on these works, it is possible to highlight the different components structural, biological and rheological function in relation to the characterization of the actual mucus presented in the previous chapters. The three reported articles also provide the basis for the development of a plan of experiments to determine the degree of interaction between components of the reconstructed mucus, correlating them with the change in the rheological parameters of the mucus.

Using the literature developed so far on this subject, this last introduction part of the Chapter 1 will review the major components of reconstructed bronchial mucus evaluating their chemical-structural interactions and rheological influence.

1.3.1 MUCINS

Mucins are macromolecules with the ability to form reticulated structures, that have been already described in the introduction. These molecules are also involved in the biological response to viral and bacterial bronchial infections. The two main mucins present in the airways mucus (MUC5B and MUC5AC) and their relative composition vary depending on the respiratory tract considered. In the distal tracts, including the bronchi and bronchioles, it can be observed that the average mucin composition shows a preponderance of MUC5B over MUC5AC³⁵. In the mucus of patients with CF and COPD MUC5B is still the predominant mucin³⁶⁻³⁸, but an increase in both the total mucin concentration (from 120 to 1200 pmol/mL as reported in figure 8) and in the MUC5AC/MUC5B ratio is generally observed (from 0.1 to 0.45)³⁹⁻⁴¹.

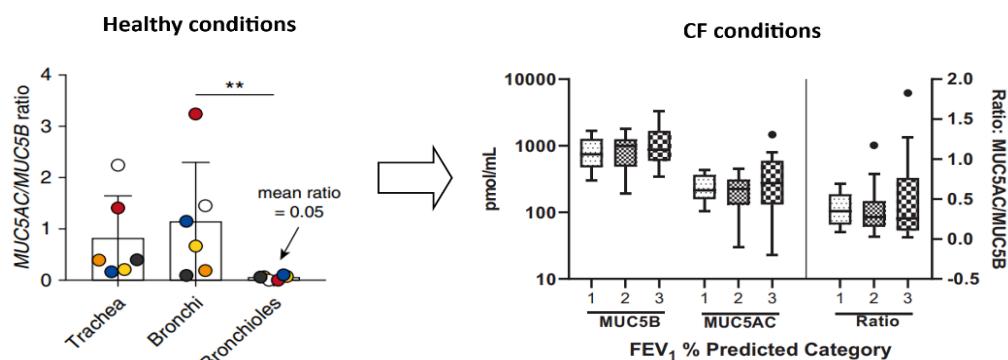


Figure 8 Variation of Mucins fraction in different sections of the air ways in healthy⁴² and CF patients⁶⁰.

This phenomenon is thought to be due to the immune response that increases the MUC5AC production thus forming a more tightly organised and branched networks^{42,43}. This conformation leads to an increased network rigidity caused by a more concentrated cysteine sites with respect to MUC5B²¹, and a more effective binding with hydrophobic surfaces^{44,45}.

Purified mucins used in the reconstruction of bronchial mucus are generally obtained from porcine stomach (preponderant presence of MUC6 and MUC5AC plus little amounts of MUC2) and bovine submaxillary glands (preponderant presence of MUC5B and little amounts of MUC5AC and MUC19). The extraction process of these mucins has been optimised to preserve proper barrier function. However, these processes are not able to guarantee in the reconstruction the reproduction of the same intensity and frequency of binding between the mucins, originally present in the source mucus⁴⁶.

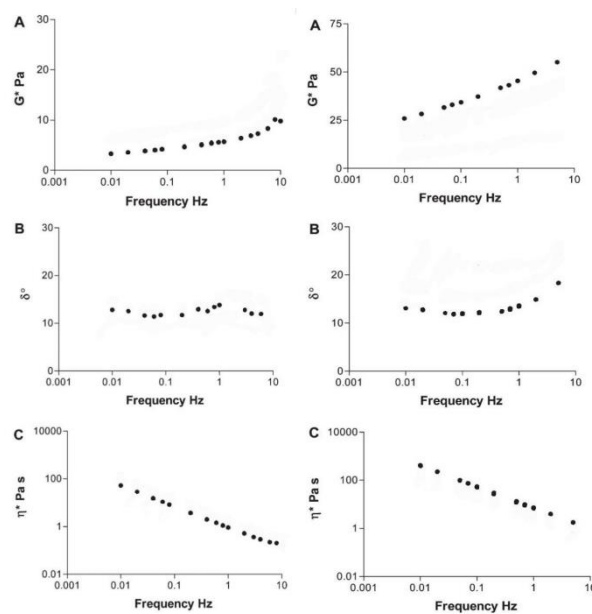


Figure 9 Rheological properties of a mucins aqueous solution (left side) compared to CF real mucus (right side)²⁸.

The behaviour of aqueous mucins solutions compared to sputum of CF patients shows that the rheological properties of the two samples following an oscillatory frequency sweep gives the same ratio between elastic and viscous moduli (δ°). However, both complex modulus and viscosity (G^* and η^*) of real mucus (right of figure 9) is 3 times above that of the aqueous mucins solution (left of figure 9). An explanation can come from the fact that even if mucins are the prevalent component in weight percentage, there are lots of other components with complex interactions leading to an increase of the network strength in real mucus^{29,38}.

1.3.2 DNA

DNA and actin filaments present in real mucus are of two main origins. Firstly, a large amount of genetic material is released into the extracellular fluid following the epithelial cells lysis. Secondly, DNA can come from bacteria, using DNA bridges as a cell-cell interconnection matrix in their biofilms⁴⁷. Higher concentrations of DNA are commonly found in bronchial mucus of people with diseases such as CF and COPD. These pathologies induce a size increase and a rapid death of the

mucus secretion glands. It is a consequence of the severe stress they are subjected to during the disease¹⁰. In addition it has been noticed that human DNA, with a low molecular weight range (0.300-50 kbs), is the most present in pathologic bronchial mucus (nearly 80% of total DNA) with respect to the bacterial one⁴⁸.

To explain the possible increase in mucin connections due to the presence of DNA, two main mechanisms are proposed. The first is based on the electrostatic bonds. It is based on the classification of both DNA and actin strands as anionic polyelectrolytes, covered by a positive layer of counterions dispersed in the mucus bulk. The interactions, both between the S/T/P domains of mucins and bacterial cells, are then classified as electrostatic ones^{49,50}. The second theory sees the DNA as part of a neutrophil extracellular traps (NETs) used by the human organism to capture and neutralize microorganisms and virus. Those traps consist of DNA filaments covered with granule proteins. NETs are supposed to rise the oxidative stress of mucins, increasing the number of disulphide bonds⁵¹ (figure 10).

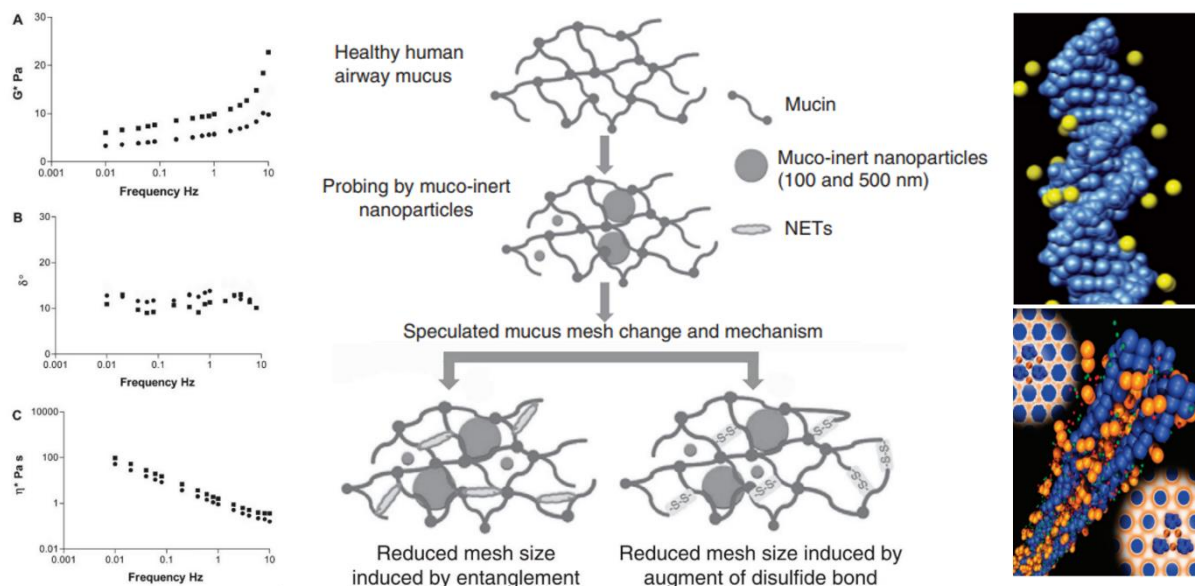


Figure 10 Left side: the comparison between rheological properties of mucins solution (squares) with a mucins-fish sperm DNA one (dots)²⁸. Centre: representation of possible links due to the presence of DNA within the mucins⁴⁹. Right side: from top to bottom DNA and actine filament obtained from molecular dynamics calculations in conjunction with synchrotron X-ray diffraction experiments⁴⁷.

In the reconstructed bronchial mucus DNA is used to mimic the reconstitution of these bonds. Sometimes it is also used as a carbon-rich substrate for the growth of pathogenic bacteria on the synthetic mucus⁵². To simulate the presence of DNA, either human and bacterial one, salmon sperm DNA is generally used. This DNA type described represents properly both extracellular DNA types (eDNA) up listed^{41,47,53,54}. The behaviour of an aqueous mucins solution with (squares of right graphs in figure 10) and without DNA (dots of left graphs in figure 15) has been observed by some authors. They observe a slight increase of both complex modulus and viscosity (G^* and η^*), with a rise in elastic over flow behaviour (δ° squared $>$ δ° dotted) in the presence of DNA. However, values of G^* and η^* are still below in order of magnitude with respect to real CF mucus.

1.3.3 MICRORGANISMS and MUCINS

In reconstructing mucus, particularly the one of patients suffering from CF, it is important to take polymicrobial colonization into account. Bacteria may grow in aggregate form and, depending on the strain, form a biofilm in the mucus environment of the CF lung.

Facultative aerobes can grow in micro-aerated media, in the hypoxic regions of deep mucus and their growth is connected to their adhesion and mobility into the mucus. The most common of the opportunistic bacterial pathogens present on the mucus of CF subjects is *Pseudomonas Aeruginosa*³³. The expression of scourges by this bacteria induces an increase in MUC5AC secretion, causing alteration in mucus viscoelastic properties. The rise of mucins level results in a reduction of mucus humidity, decreasing the mobility of immune cells and thus reducing the effectiveness of bacterial eradication.

In order to study the effect of the presence of pathogenic bacteria on mucus rheology, a biosimilar surrogate for native human mucus has been used in some studies. It is sterilized by thermal or UV treatments and then infected with pathogenic bacteria. Incubated in an environment mimicking bronchial lungs the bacterial culture is then grown to be finally analysed under a chemical and a rheological point of view²¹.

The role of bacteria in artificial sputum is also described by adding several cross-linking or entangling polymers, including PAA (Poly Acrylic Acid), Xanthan Gum, Glutaraldehyde and Alginate²¹. The latter one is a linear polysaccharide produced as a structural component in marine brown algae (Phaeophyceae) and also as a capsular component in some bacteria such as *Azotobacter vineland* and several species of *Pseudomonas*.

Alginate is composed of two sugar monomers (b-D-mannuronate and a-L-guluronate) known as M units and G units³³. The distribution of these monomers is not random within the alginate chain, that can be described as an alternance of regions of repeating G or M or G-M units (G, M and GM blocks). The sequence of these three structures determines the ability of the molecule to form gels with cations (particularly the calcium one), able to bind to G blocks to form intermolecular junction zones³³. Based on experiments, it has been seen that an alginate concentration increase lead to a decrease of $\tan \delta$ and an increase of G^* and η^* (left graphs figure 11)²⁹. This demonstrates that the alginate-alginate electrostatic interactions increase intermolecular long order cross-link density, giving to the solution a more elastic behaviour with respect to the viscous one. Considering that mucins-alginate interactions are electrostatic too, it has been seen that alginate addition in a mucins aqueous solution gives the same trend as increasing alginate concentration in an aqueous solution (left graphs figure 11)^{33,55,56}.

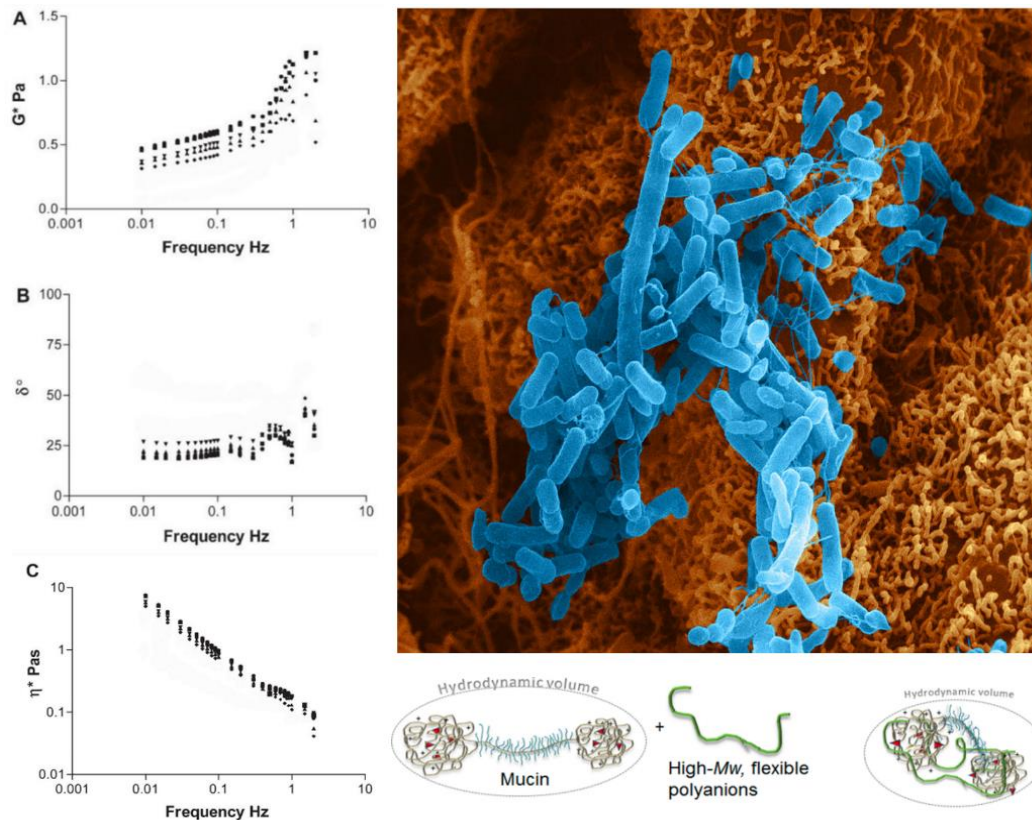


Figure 11 Left side: rheological parameters of a mucins aqueous solution at different alginate concentration (dot) 1.0 mg/mL, (square) 0.8 mg/mL, (triangle) 0.6 mg/mL, (inverted triangle) 0.4 mg/mL and (rhombus) 0.2 mg/mL²⁸. Right side from top to bottom : *Pseudomonas aeruginosa* infection attached to GFMs into the bronchi and model for the interaction between alginate and the double globular comb of mucins⁵⁵.

More recent studies about the effect of bacteria on the rheology of CF sputum have been performed, using mucus reconstructed on the basis of another type of heteropolysaccharide: xanthan gum (GM), (produced by the *Xanthomonas campestris* bacterium)^{31,57}. Starting from a recipe of synthetic CF mucus proposed in previous studies, the conducted experiments showed that with a 0.5% w/w concentration of XG, the behaviour of reconstituted sample is quite similar to an average CF real mucus (figure 12).

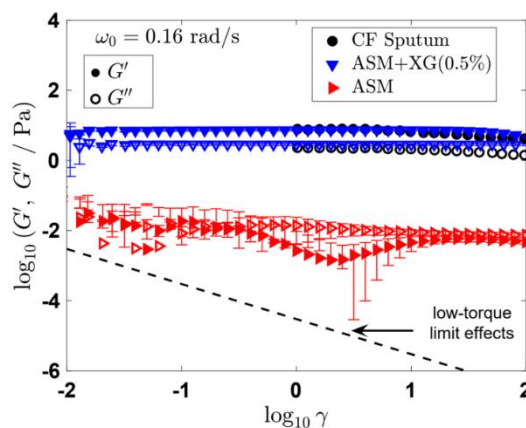


Figure 12 Rheological properties comparison between reconstructed mucus with 0.5% w/w of Xanthan gum (blue) and a real CF sample²⁹.

1.3.4 IONS

As briefly mentioned in the introduction, ions are involved in the regulation of the intermembrane transducer, balancing not only the pH but also mucus water content. The dysfunction of the cystic fibrosis transmembrane conductance regulator (CFTR) is the basis of CF. The origin of this disease is therefore due to an accumulation of Na^+ ions in the epithelial cells and a decrease of Cl^- in the mucus which as a consequence becomes dehydrated (73, 40). The mis-regulation of Cl^- and the subsequent dehydration of mucus are also associated to an increased expression of ATP12 which is an energetic molecule, responsible for the epithelial cells-mucus ions regulation by their interchange of H^+ and K^+ ions over the KB channel⁵⁸ (figure 13).

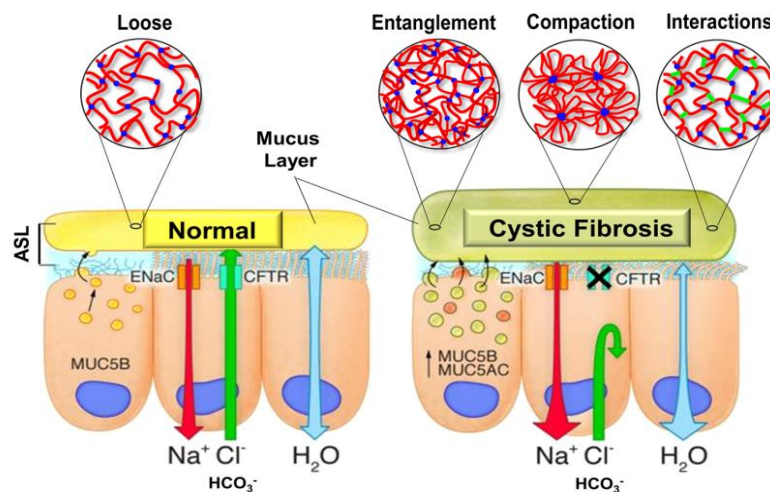


Figure 13 Model of normal vs CF airway mucus layer illustrating changes within the mucus network (polymer entanglement, mucin compaction, and/or changes in molecular interactions) in response to altered ionic fluxes³⁷.

Another effect of the rise in monovalent cations concentration is the screening of electrostatic interactions that reduces the degree of repulsion between sugar side chains, allowing stronger associations between mucin molecules (schematically indicated by the increased size of the yellow triangles on figure 14). Furthermore, it has to be taken into account that salt monovalent cations form the so-called salt bridges. These links increase the folded configuration of the non-carboxylate globular part of mucins, decreasing the binding in these mucin sections. The increase of H^+ ions (so the acidification of the sample) does not seem to be at the origin to those bridges. On the contrary an acidic condition induces a reduction of the number and strength of the saline bridges, decreasing the folded configuration of the globular, non-carboxylate part of the mucins. It increases the number of either disulphide bonds (light blue dots in figure 14) and hydrophobic interactions (yellow triangles in figure 14)⁵⁹.

Under a rheological point of view, the folded configurations of the side chains of the mucins are responsible for the decrease in both viscosity and elasticity of the salted-mucin (MUC5AC) solutions as well as pathological and non-pathological real mucus under low pH range^{20,60} (figure 14). In other words, under near neutral pH, salt bridges are already formed and the addition of cations increases the elasticity and viscosity of the mucus. This behaviour is still observed for increasing acidity. In this case, however, the increase in H^+ produces an anionic mucins stabilization, effectively decreasing the effect of cation addition on both viscosity and elasticity. Under low pH levels, the great oxidative stress to which mucins are subjected increases the formation of disulphide bonds, rising both the

elasticity and viscosity of the mucus. Under these conditions cations addition has an opposite effect, reforming the salt bridges that are basically unbonded under these low pH values (figure 14). In the aforementioned pathological conditions (especially CF), pH levels close to neutral, or slightly acidic are generally observed ⁶¹. This is linked (in the transition from healthy to CF-affected mucus) to a decrease in the degree of mucus viscoelasticity as the salt concentration increases.

Within the reconstructed mucus, ionic presence is produced through the addition of salts such as NaCl and KCl. On the other hand, pH adjustment, is implemented through the addition of bases such as Trizma base. It is good to consider that pH correction, as it will be discussed below, is also critical for the dissolution and binding efficiency of other components of the reconstructed mucus ⁶².

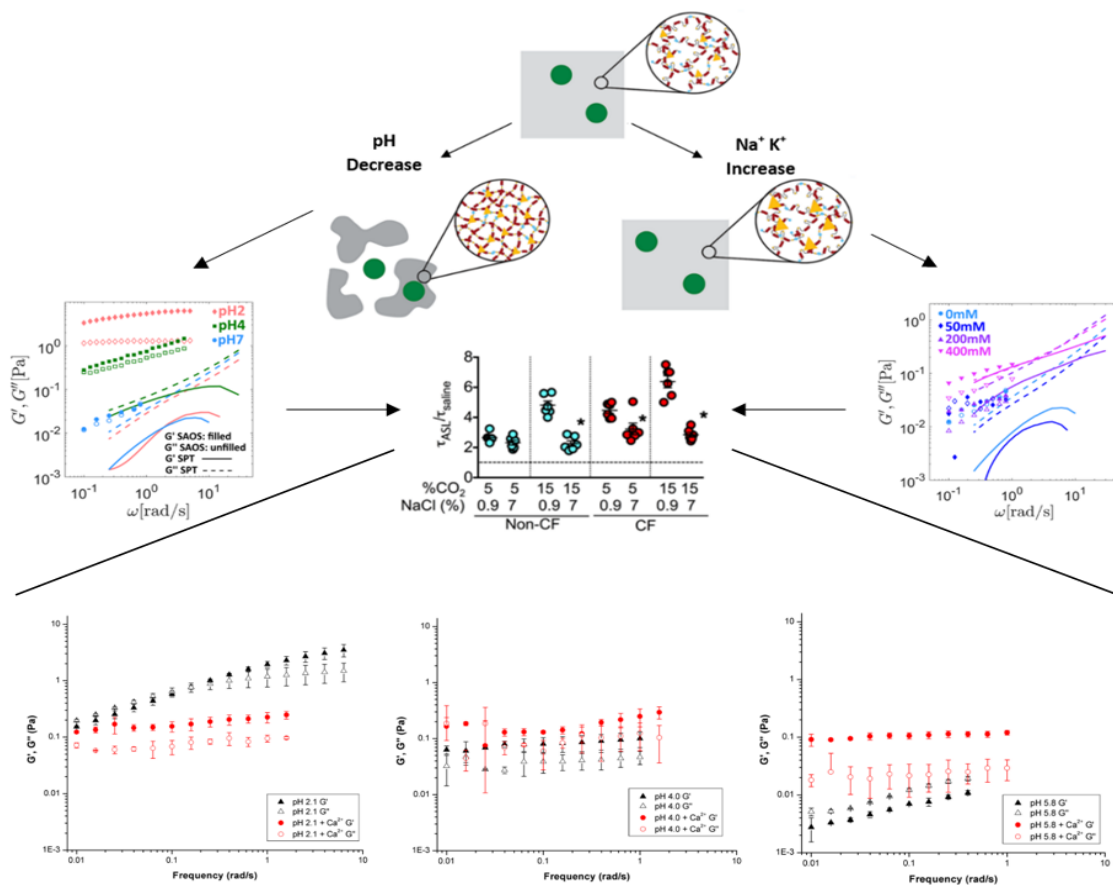


Figure 14 From top to bottom: Schematic illustration of the proposed effects of the various environmental modifications on the supramolecular structure of the mucin network. The mesoscopic porous structure of the mucin gels is represented by the grey regions. Left side: Description of acidification effect on the structure (increase in disulphide bonds (light blue dots) and hydrophobic interactions (yellow triangles) number) and rheology (increase of elasticity and decrease in viscoelasticity) of the mucus. Right side: Description of cations increase effect on the structure (decrease of repulsion degree between sugar side chains and increasing of folded configuration of the mucins non-carboxylate globular part) and rheology (increase of elasticity and decrease in viscoelasticity) of the mucus ⁴³. Centre: Combined effect of increasing environment acidity and salt concentration of a non-CF and CF cultured airway epithelia (middle) ⁵⁶ and in an aqueous mucins solution (bottom) ²¹.

1.3.5 PAA

The results of the rheological investigation of rehydrated mucin demonstrate the efficiency loss of inter mucins bonds due to their extraction procedure⁴⁶. In order to re-establish hydrogen bonds^{63,64} between the CYS domains of mucins, polyacrylic acid (PAA) can be used. At rheological level, this allows increasing the elasticity and viscosity of the reconstructed mucus³¹. The type of PAA used, as well as the presence of amino acids such as cysteine (naturally present in lung mucus) is of fundamental importance for the rheology of the reconstructed mucus. Indeed, with the correct PAA, not only hydrogen bonding, but also thiolation processes can occur with the formation of disulphide bonds^{65,66}.

Before using PAA, however, numerous precautions have to be employed. The ability of PAA to develop bonds is related to the change in pH of the solution in which it is dispersed. In order to have the maximum yield for such a polymer, it is notably necessary to have pH neutrality. A particular focus is also, adopted in the choice of the base used for neutralization. Experimentally it has been observed that for such neutralization triethanolamine works very well. However, given its high cost and structural affinity to Trizma base, the latter one is used as a PAA stabilizer. During the mucus reconstruction PAA is added after divalent cations because they are supposed to cause the shielding of the polymer charges and a subsequent recoiling of the PAA macromolecules on themselves. In the coiled form, PAA molecules cannot easily diffuse and interact with another hydrogel components (such as mucins)⁶². In this way, the addition of PAA would have no effect on the reconstructed mucus.

1.3.6 ARTIFICIAL SURFACTANT and PROTEINS

As seen in the introduction, lipids play a key role in the uptake and adsorption of gases and macromolecules within the mucus. Lipids present in the lung mucus are almost entirely recognized as part of the surfactants of the mucus itself. Thus, 92 % of these surfactants are lipids. Among them, DPPCs (dipalmitoylphosphatidylcholines) are the most abundant (41%). Owing to their low critical micellar concentration (CMC) and their ability to reduce the surface tension of the alveolar mucus (which decreases from 70 to 20 mN/m) they play a fundamental role in the respiratory act. In fact, DPPCs are the main components in the classical model for lung surfactant compression. This model is based on the selective exclusion of poorly compressible compounds from the gas-liquid interface, through the so-called squeeze-out process (corrected by lipid segregation theory and three-dimensional exclusion when examined at the nanoscale). This method allows, therefore, to obtain in alternating steps both a smaller superficial bulk (during exhalation) and a more efficient $O_2 - CO_2$ gas exchange (in inspiration). Squeeze-out consists of two sequential phases. Initially, the diffusion of aggregated surfactants causes them to approach the air-water interface. In a second step, due to the presence of unsaturated phospholipids (PCs), insertion and uncoating of the active material (DPPC) on the interfacial film (liquid-gas) surface occurs.

The protein component of lung mucus surfactants (8% of all lung surfactants) can be divided into two families, hydrophobic and hydrophilic. The hydrophobic one encloses SP-A and SP-D, while the hydrophilic includes SP-B and SP-C. The latter two greatly increase interfacial adsorption by inducing aggregation, fusion and lysis of phospholipid vesicles. These phenomena ensure the stability of the film in the process of surfactant rediffusion during the continuous respiratory cycles of compression-expansion.

Among the above-mentioned proteins, SP-C is the only one that has been found exclusively in lung tissues. Low levels or lack of this protein trade to the formation of severe lung disease. SP-A, on the

other hand, has the ability to bind to a wide variety of microorganisms, such as viruses, bacteria, and fungi, as well as environmental allergens and inorganic substrates. Together with SP-B, during squeeze-out, it rearranges particles from an "onion-shaped" configuration into "network-like" structures of tubular myelin, which then diffuse along the aqueous alveolar subphase ⁶⁷ (figure 15).

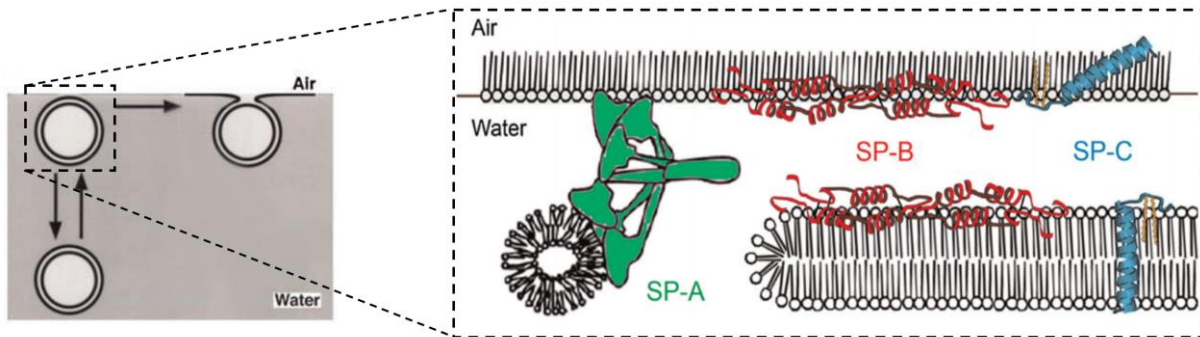


Figure 15 Structure, coupling and function of the main components of the surfactant fraction of the lung mucus ⁶⁷.

In the reconstructed lung mucus, egg yolk is used to simulate both the protein and lipid parts. Its net composition is of 62% lipid and 38% protein. Egg yolk is an emulsifying agent consisting in a granular fraction dispersed in a plasmid substrate (most susceptible to thermal degradation between 55 and 76°). The granular suspension consists in a non soluble high-density lipoproteins (HDLs) and phosphovitins, connected by phosphoric calcium bridges. These linkages make the suspended phase very compact and also provide good chelating capacity. The addition of salts, which by dissociation give monovalent ions, increases the solubility of this fraction. This is due to the ionic substitution process between calcium ions and monovalent cations that weakens the phosphoric calcium bridges. The plasma fraction of egg yolk is mainly composed of levitins and soluble low-density lipoproteins (LDLs) (Figure 16).

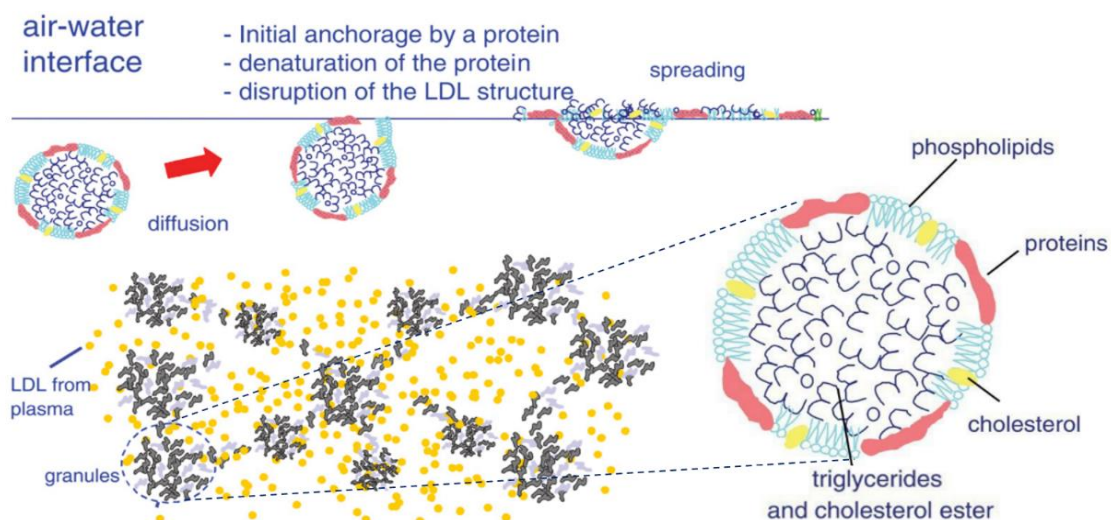


Figure 16 Structure, coupling and function of the main components of the surfactant fraction of Egg Yolk ⁷⁰.

The latter molecules are formed by a core of triglycerides and cholesterol, covered by a mono film of protein and phospholipids (crucial for the structure of LDLs because of their hydrophobic binding

forces). Their high solubility is affected by the ionic concentration and pH to which they are subjected. LDLs act as carriers for surfactant components (proteins and phospholipids) that are not soluble in water. Such lipoproteins underlie a process analogous to squeeze-out (of mucus surfactant) on the surface of the egg yolk. This phenomenon is initiated by the proteins located on the surface of LDL, which, once they reach the liquid-air interface, anchor themselves to it. This anchoring causes protein unfolding, which leads to destabilization of the outer layer of the LDL that opens. Neutral lipids, phospholipids and proteins are then released from the lipoprotein core and can diffuse to the interface. Surface tension is decreased by the flocculating action of phosphovitins. These phosphoglycoproteins have two hydrophobic ends and a highly electronegative central part. Their conformation allows them to take a globular configuration under low pressures and elongated ones under high pressures, decreasing the surface tension of the solution in both cases ⁶⁸ .

The main problems with the use of egg yolk in the reconstruction are due to the degradability of its chemical rheological characteristics. These occur during its storage or during heat treatments, possibly compromising its usability in reconstruction ^{69,70}. In addition, although egg yolk exhibits surface mechanical similarity with lung ones, it does not possess elemental chemical correspondence with either surfactant and protein component of lung mucus (exposed in the above paragraph of this Chapter) ⁷¹. By mean however, egg yolk can be used as a good substitute for average protein and lipid components in the reconstructed mucus. However, this does not grant the rheological and interactional compression of the two aforementioned fractions (lipid and protein) in relation to the occurrence of respiratory disease. This is due to two main reasons. Firstly, the two components have opposite effects at the rheological level: proteins increases mucus viscosity, while lipids decreases it ²⁷. Secondly, the relative importance of these two components in pathological mucus varies independently (figure 17)^{72,73}. This is due to the fact that most of the protein component is related not to surfactant function but to an immune one and so their quantities and typologies varies respect the different pathologies and patience. Hence the need to find a distinct surrogate for each fraction.

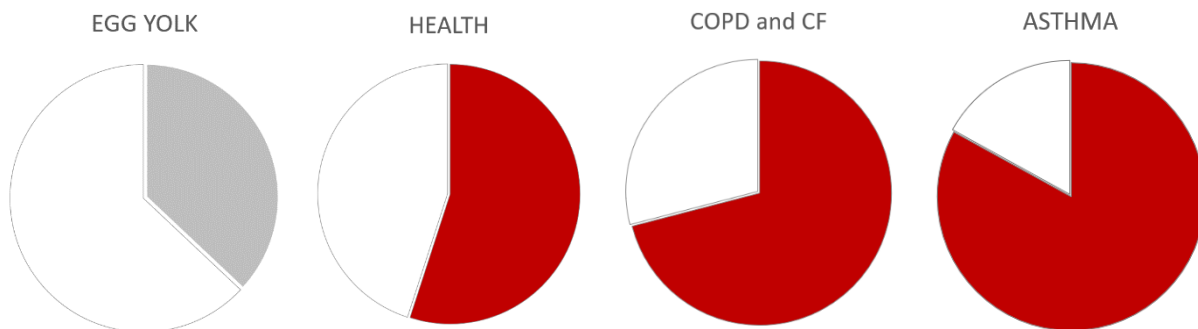


Figure 17 Lipids - proteins qualitative repartition in Egg Yolk (respectively grey and white) and in the mucus of people affected by the principal Bronchial pathologies (in this case red for proteins).

In recent years, numerous studies have been carried out not only on the variation of lipid levels but also on their composition in different diseases such as CF ^{72,74}. These studies reveal a decrease in the level of the surfactant components in the diseased mucus. In addition, the researches carried out have enabled the development of engineered solutions of artificial surfactants (such as CHF5633), having compositions and elements very close to the real ones ^{67,75-77}. Similar compounds are used for the treatment of CF patients, to restore the correct level of surfactants in the airways, facilitating expectoration ⁶⁷. Such components, unlike egg yolk, are very expensive and must be handled with the utmost care because of their rapid thermal degradability.

Concerning now the protein fraction, this component of the lung mucus consists of two main parts, free amino acids and proteins. The second group is in turn divided into three macro groups: the immune modulators, the substances that contribute to host defence, and the antimicrobial peptides (AMPs) ⁷⁸. These latter encapsulate a dozen different proteins (including SP-D and SP-A) ^{21,79}. Since, the protein component is submitted to high variations (as it is related to a subjective immune response), it is generally simulated by the use of egg yolk in reconstructed mucus. To consider the protein part individually (although AA and protein give different interactions with the mucus) it is generally reduced to the free amino acid component alone (for simplicity purposes) ⁸⁰. Several studies on real and reconstructed samples have reported the modification of this fraction as a contributor to the occurrence of bacterial populations on the mucus ^{32,81}. Researches conducted on the composition of amino acids in the lung mucus has reported the presence of all key amino acids. Therefore, initially the AA component of the mucus was simulated by a generic pool of amino acids. More recent analyses have led to the suggestion of a new component, Hydrolysed Casein (Casamino acids) ^{82,83}. This compound is found to possess all the key amino acids. In addition it contains casein, and some peptides present (in small amounts) in the actual lung mucus of sick and non-sick subjects ^{84,85}.

1.3.7 CHELANTS and NUTRITION for BACTERIAL CULTURES in RECONSTRUCTED MUCUS

As seen above substances such as eDNA, actine filaments and AA are used as carbon sources by viral bacterial populations that can grow on the mucus of subjects with lung diseases. In reconstructed mucus, the same sources (casein hydrolyzed, egg yolk, and DNA) can be used ^{33,77}. Microbial growth has also been observed to accelerate in the presence of Fe^{3+} in the mucus. The presence of these ions may be due to particular characteristics of the inner environment of pathological subjects ⁸⁶. In order to make such ions (insoluble in water) available even within the reconstructed mucus, chelating agents such as egg yolk, ethylenediaminetetracetic (EDTA) or diethylenetriaminepentaacetic acid (DTPA) are used ^{62,63,86}. The function of these chelators, however, is not only limited to the transport of iron ions but also to the stabilization of the reconstructed mucus, preventing the phenomenon of proteolysis. Among the above-mentioned chelators there is also a 0.5 molar aqueous solution of diethylenetriaminepentaacetic acid, which is chemically very similar to DTPA ³¹.

CHAPTER 2:

MATERIALS AND METHODS

2.1 RHEOLOGICAL EXPERIMENTS

Macro rheological experiments are conducted with a calibrated (as reported in Annex 1) precision rheometer⁸⁷. The one used in this study, reported in figure 19, is an "Anton Paar MCR (Modular compact Rheometer) 302", coupled with the analysis software "Rheocompass".



Figure 18 Rheometer with the following details: 1. Coupling of the upper plate 2. Detail of the coupling for maximum efficiency of motor-upper plate coupling 3. Different types of upper plates 4. 6 Atm Pressurized motor for maximum precision and wider range of an

This is an air bearing rheometer whose rotational shaft floats locked inside a 6 Atm pressurized chamber. The air pressured greatly reduces friction due to rubbing with the engine block and allows to measure torque momentum as small as 0.5 nN·m or amplitude angles of $5 \cdot 10^{-8}$ rad. The geometry of the rheometer consists of a moving part (upper plate) that shear the sample and a stationary part (lower plate). The material to analyse is deposited in the lower plate that is thermally regulated by a Peltier effect. A small quantity of deionised water is placed around the sample (in a well) to avoid its drying during the measurements, while the sample is kept under two half cups placed around the lower plate ("anti-evaporation cover"). Concerning the small quantities of available samples, a plate-cone or plate-plate blast-sanded upper geometries are used (CP25-1/S or PP25-1/S with $\phi = 25\text{mm}$). With the CP geometry it is possible to analyse samples as small as 100 μL . The chosen geometry and the operating conditions, in particular P and T values, can have a big impact on the rheological characterization of a sample. For this reason those parameters both in literature and for the measurements done in this work are specified.

In order to perform the macro-rheological characterization of a viscoelastic sample at fixed P and T, the following tests are commonly used: SAOS, CSS and 3ITT tests.

2.1.1 SMALL AMPLITUDE OSCILLATORY SHEAR TEST (SAOS)

This test involves a series of dynamic shear experiments that manage to investigate the viscoelastic properties of the material in its "unbroken state". Through this experiment is possible to gain parameters such as the time necessary to reach structural equilibrium inside the sample (equilibrate time) under a certain stress (τ) or quantify both the viscous (through G'') and the elastic behaviour (through G') of a body subjected to a certain deformation. Those last two parameters can be obtained imposing to the upper plate an oscillating stress amplitude (or strain) sweeps at constant frequency, or at frequency sweep at constant stress amplitude^{13,88}.

The first case uses a constant frequency sinusoidal stress, sweeping the maximum amplitude of γ and registering the corresponding T (torque moment used by the rheometer to apply a shear stress). γ and τ (obtained by the definition of $T = r \cdot (\tau A)$, $F = \tau A$) are sinusoidal, thus functions of the imposed f , and are shifted by a δ angle, given a deformation (or stress) step ramp forcing function, measuring the stress (or the deformation) and the difference between the two phases it is possible to obtain the dynamic modulus G , as:

$$G(t) = \tau(t)/\gamma(t) \tag{2.1}$$

$$\tau(t) = \tau_{max} \cdot \sin(\omega t) \tag{2.218}$$

$$\gamma(t) = \gamma_{max} \cdot \sin(\omega t + \delta) \tag{2.319}$$

$$G = \frac{\tau_{max}}{\gamma_{max}} \tag{2.420}$$

As consequence G is a time function and takes a constant value only in the case of perfectly viscous ($\delta = 90^\circ$) and perfectly elastic ($\delta = 0^\circ$) materials, while for a viscoelastic or viscoplastic material it changes ($0^\circ < \delta < 90^\circ$) at different τ_{max} (or γ_{max})⁸⁹.

Considering then the $G(t)$ Fourier transformation is also possible to obtain:

$$\hat{G}(\omega) = \hat{G}'(\omega) + i \cdot \hat{G}''(\omega) \quad (2.521)$$

$$\hat{G}'(\omega) = \hat{G}(\omega) \cdot \cos \delta \quad (2.622)$$

$$\hat{G}''(\omega) = \hat{G}(\omega) \cdot \sin \delta \quad (2.723)$$

$$|\hat{G}(\omega)| = \sqrt{\hat{G}'(\omega)^2 + \hat{G}''(\omega)^2} \quad (2.824)$$

$$\tan \delta = \frac{\hat{G}''(\omega)}{\hat{G}'(\omega)} \quad (2.925)$$

$$\omega = 2\pi f \quad (2.1026)$$

$\hat{G}'(\omega)$ quantifies the amount of force given leading to an elastic deformation, while $\hat{G}''(\omega)$ is the force given to the body and dissipated by friction during the plastic deformation.

Following the previous relationships, a SAOS γ sweep test allows to observe the evaluation of G and δ at increasing γ or τ values, monitoring the shifting of the substance from a completely elastic behaviour ($G' \gg G''$) to a completely viscous one ($G' \ll G''$) with a log-log graph:

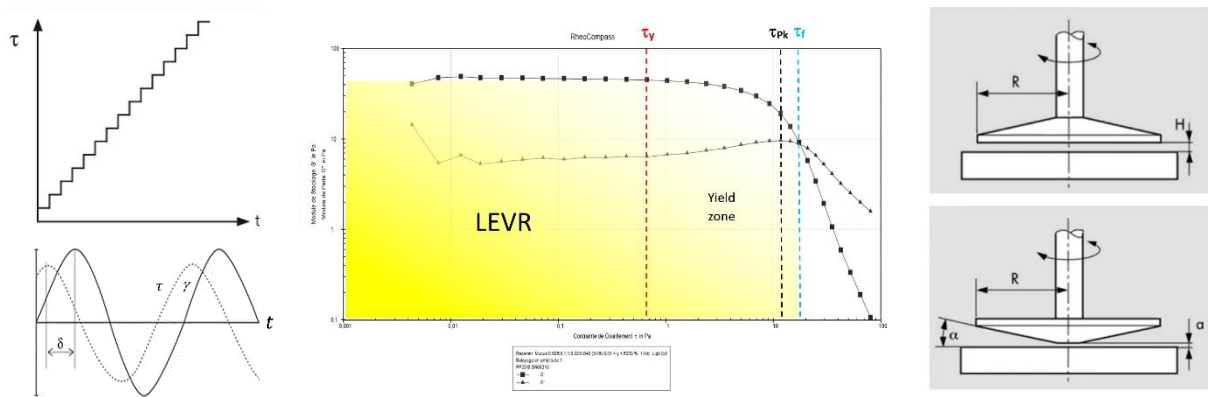


Figure 19 Response of a viscoelastic sample to an oscillating step forcing function (left) at the end of SAOS analysis (middle) performed by Anton Paar MCR 302 Rheometer coupled with Rheocompass software. Detail of the geometry and operation of the conical and plate top plate under oscillation (right) ⁸⁸.

As shown in figure 19 under low values of τ , there is a linear viscoelastic region (LEVR), a plateau interval in which stress and strain remain proportional. This is the elastic region ($G' \gg G''$ and $\tan \delta \cong \text{const.}$) in which applied stresses are not sufficient to cause structural evolutions (yielding). When τ exceeds the yield stress (τ_y), the structural units composing the material begin to evolve in terms of configuration. This region (the yield zone) begins by the G' curve deviation with respect to the linearity the initial plateau and ends when G'' overcome G' (actual flow of the substance). In the yield zone (limited by stress values τ_y and τ_f) the substance has a viscoelastic-solid behaviour so, if the stress application is removed, the material returns to its initial structure configuration ⁹⁰. On the base of τ_y and the corresponding deformation, called critical deformation γ_c , the energy of cohesion E_c of the 3D network can be estimated (equation number 2.11). This energy can be used in a quantitative manner as a measure of the extent of intermolecular and intramolecular interactions of the polymeric internal structure ¹³.

$$E_c = \frac{1}{2} \tau_y \gamma_c$$

(2.1127)

Increasing the applied stress τ the interaction between the sample components structural units can stretched until a certain stress level where they are completely broken, leading to a new structural state. The transition from a perfectly elastic to a perfectly viscous behaviour starts slowly, then is accelerated by the increase of energy dissipated when the interactions between structural units are broken (collapse of the internal structure). At τ_{pk} , the strongest interaction are broken and after a brief tangential disposition (respect the given τ) of the body structural units, the samples becomes more viscous than elastic (see figure 20). The transition between a viscoelastic solid like behaviour to a viscous like one is given by the flow point (τ_f), identified as the moduli crossover stress ($G'(\tau_f) = G''(\tau_f)$, $\tan \delta = 1$). Above this value the material starts to flow as a liquid for critical microstructural breakdowns⁹⁰. For even increased values of τ , there is a new plateau at which this time the substance is considered completely viscous ($G'' > G'$)¹³.

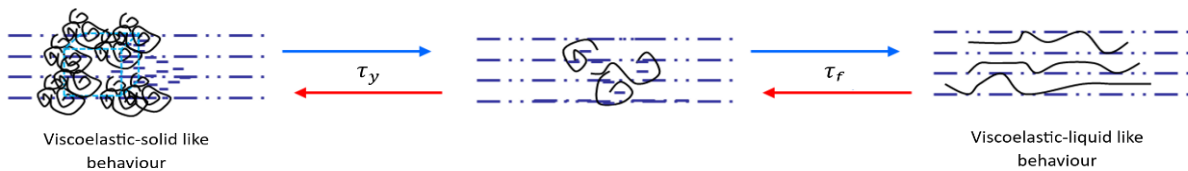


Figure 20 Transformation of the internal structure of a viscoelastic sample at the shear stress increase.

Talking about stress frequency sweeps at constant amplitude test, it is based on the same principle of the previous one but at constant γ_0 or τ_0 values and sweep f . Calculating G and δ , so G' , G'' and $\tan \delta$ this analysis allows to evaluate either the short-term (for $f \gg$), then the long-term behaviours (for $f \ll$) of the sample. This test for a weak gels has to be conducted under a frequency limit due to the resonant effect emerging from the coupling of material elasticity and instrumental inertia.

2.1.2 STEADY STATE FLOW CONDITION TEST at CONTROLLED SHEAR STRESS (CSS)

This test allows to probe the plasticity and the shear-thinning behaviour of a sample under flow conditions, accounting for the breakdown of the inner structure network of the structural units and its subsequent flow. The sample is solicited by a rotational shear stress ramp forcing function, avoiding in this way that the inertial forces inside the false body affect the detected shear rate value. Generally both SAOS and CCS test switch from a τ step to the following one with a steady state sensing method (optimum at $5 < \tau < 10^2$ Pa) that checks a maximum equilibration time or a precision condition. The first one set a certain time interval over which the stress change automatically while the second is fulfilled when the measured parameter was n times within the chosen tolerance.

Alternatively to this method there would be another one (optimum at $10^{-4} < \tau < 5$ Pa) that assumes to use a defined equilibration time over which, for a set time, are collected values, than averaged to replace a single answer at the new equilibrium. For this method it is necessary to know the equilibration time at different stresses (available through literature or a peak hold test)⁸⁸.

SAOS and CSS performed in the present work weep τ values between 10^{-2} and 10^2 Pa. A steady state sensing method (maximum equilibration time 180 s, sample period = 10 s, 3 consecutive data within a 5% tolerance) has been used.

For the CSS test, for geometry is associated a parameter to relate the torque developed (T) under an apparent viscosity varying apparent viscosity (η_{app}) (see equation 2.12). Starting from this equation (Valid for as ex. for a CP25-1/S configuration, $\alpha = 1^\circ$) plus the relationships previously presented it is possible to identify η_{app} and $\dot{\gamma}$ given τ and ω ⁹¹:

$$T = \frac{2}{3} \pi r^3 \frac{\eta_{app} \omega}{\alpha} \quad (2.1228)$$

$$\eta_{app} = \frac{3}{2} \frac{\alpha \tau}{\omega} \rightarrow \dot{\gamma} = \frac{2}{3} \frac{\omega}{\alpha} \quad (2.1329)$$

Through the log graph of the shear stress as a function of shear rate, also called flow curve (figure 21), given by the CCS test, it is possible to determine the HB parameters, and determine the consistency index ($K(T)$), shear thinning or thickening index (n) and the yield stress (τ_0) of the sample¹³.

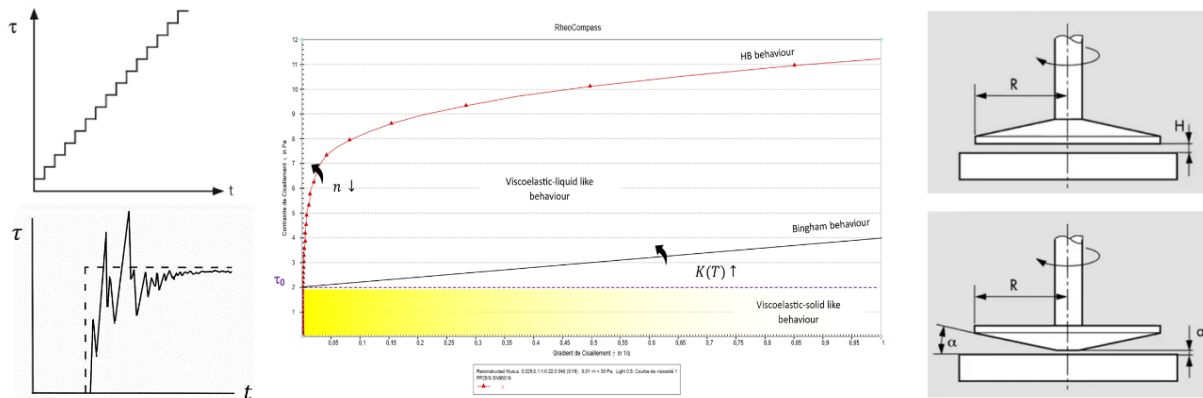


Figure 21 Response of a viscoelastic sample to a rotational step forcing function (left) at the end of CCS analysis (middle) performed by Anton Paar MCR 302 Rheometer coupled with Rheocompass software. Detail of the geometry and operation of the conical and plate top plate under rotation (right)⁸⁸.

The flow curve (FC) presented in figure 5 allows to determine the yield stress (τ_0) at which the substance switch from a viscoelastic-solid like to a viscoelastic-liquid like behaviour. This value is supposed to correspond to a stress value in between would have been placed between τ_{pk} and τ_f in a SAOS graph and can give identical order of magnitudes. At least the effective determination of τ_0 is particularly tricky because there is not a single method to decide when a sample passes from a linear to a power behaviour. The method used in the present work for the τ_0 evaluation is based on the major degree of linearity given by a determined data set and will be better explained in the following section. The roughness of this test is so structural disruptive that generally it can be performed just one or at least two time before to change sample.

2.1.3 THREE INTERVAL THIXOTROPY TESTS (3ITT)

This test has the objective to study the thixotropic behaviour of a substance monitoring the apparent (complex) viscosity and G at different shear stress. It proceeds with the same modality of a CCS test but with a square wave stress forcing function. This type of analyse can be more or less disruptive, in fact can be performed alternating an oscillatory and rotational or just oscillatory step^{13,88}. It allows to use more time the same sample, that is an advantage in shortage of materials. An important

parameter that is gained with this method is the thixotropic recovery time that is the time necessary to reconstitute the 80% of the initial structure of the sample after the end of the sollicitation. As showed in figure 22 the test start with a constant shear stress conditions within the LVE range. Depending on the initial τ this interval gives a complete disrupted or perfectly linked structure reference. In a second interval the shear is decreased, in the first case or increased in the second one, so that the body comes to the opposite configuration. The last step allowed to achieve again the initial condition. In the first case, reported in figure 22, the recovery time is detected between the first and second intervals, or while between the second and the third in the second case.

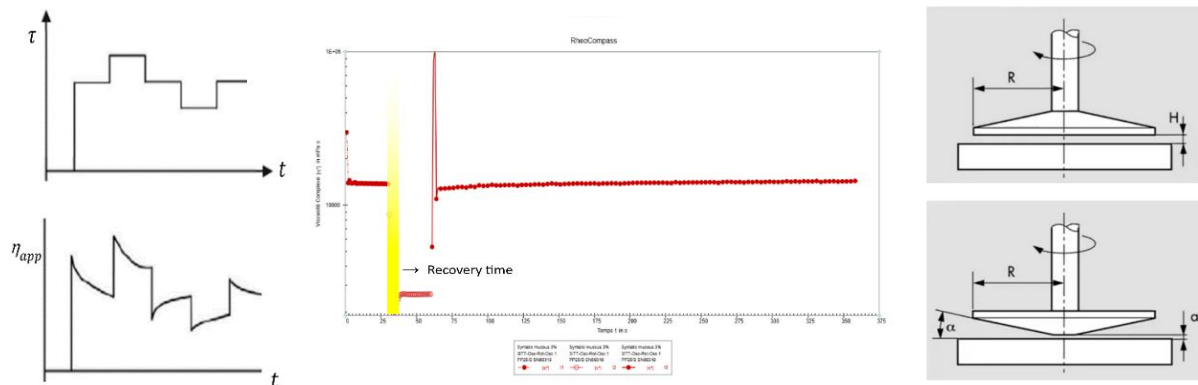


Figure 22 Response of a thixotropic sample to a three step forcing function (left) at the end of 3ITT analysis (middle) performed by Anton Paar MCR 302 Rheometer coupled with Rheocompass software. Detail of the geometry and operation of the conical and plate top plate top plate under rotation (right)⁸⁸.

2.2 BRONCHIAL MUCUS RECONSTRUCTION METHOD

The reconstruction of the synthetic mucus took place at room T and P of 1 Atm. The experimental procedure, explained in detail in Annexes 6, 7 and 8, has been carried out with the support of excel spreadsheets. This allowed to achieve the target compositions more precisely, while reducing the amount of material used thanks to a cascade operating method. This also reduced the time for each reconstruction, while guaranteeing equally high standards of macroscopic homogeneity of the products obtained. Finally, the use of the excel support file allowed the traceability of the dosages carried out in order to refine the methodology for subsequent reconstructions. A reconstruction process (leading to the development of 1 to 4 samples) takes on average 1 to 3 days. Replication of the lung mucus consisted in the water solubilisation of the components reported in the appendices, reaching volumes of 10 or 20 mL (for the mother solutions). During reconstruction step the stirring time and the pH neutrality were crucial. Mixing was implemented at 2 speeds (800 and 250 rpm) with a magnetic stirrer integrated in a induction heater. Dosing of the components was implemented with micropipettes of 5000, 1000, 100 and 10 μ L. The solid fractions were weighed using a 0.0001 g precision balance.

CHAPTER 3:

CELLULAR and NASAL REAL BRONCHIAL MUCUS

As seen in the introduction, rheological data on healthy patients are very variable and complex to interpret due to the many parameters that can determine them. Part of the research work carried out by the M2P2 laboratory is to perform rheological analyses on real samples provided by C2VN. This would ensure a homogeneity of experimental tests (typologies and conditions) applied to real and reconstructed samples, so as to have a one-to-one comparison with them. The following paragraphs will therefore present the activity of analysing real samples, carried out in parallel with the synthetic lung mucus research and reconstruction procedures.

The real mucus analysed were of two types, the nasal mucus of subjects suffering from asthma and the cellular bronchial mucus of patients affected by asthma too or smokers (classified as COPD patients). The results of the rheological analyses carried out on the 23 nasal mucus samples of asthmatic subjects are discussed a part (Annex 3) because the focus of this thesis is mainly the lung mucus, which is structurally different from the nasal one.

3.1 CELLULAR MUCUS

Cellular mucus is produced by lung cells from deceased individuals who have decided to donate their organs to science or from sick patients receiving these organs. The cells thus (bronchial epithelia) are cultivated in the C2VN laboratory. The mucus secreted by these cells is collected by staff for rheological analysis in the M2P2 laboratory. Unlike nasal mucus, which a collection date and an analysis date can be identified, as the cell culture is limited in size, sampling of cellular mucus takes up to a month and a half. For this reason, the samples analysed will be composed of a more or less recent set of mucus, thus undergoing an ageing process. However, the quality of the mucus obtained in this way is particularly good, due to the fact that, unlike classic sputum, it is not contaminated by saliva or other types of mucus during its sampling. It should be remembered, in fact, that the main mechanical processes of expectoration do not allow the purely bronchial fraction to be sampled (since it has to go up part or sometimes all of the airways).

The samples analysed were from donors or receivers both sexes aged between 25 and 71 years: they were classified as healthy (3 subjects), asthmatic (1 subject) and smokers (7 subjects). The smokers are assumed to be suffering from COPD.

3.2 EXPERIMENTAL PROCEDURE

The tests performed were the SAOS and CSS, described in Chapter 2. Due to the availability of the samples to be analysed, 3ITT analyses were not carried out, precluding a thixotropic evaluation of the samples (likely the subject of future studies). The duration of each performed test was approximately 5-10 min. for SAOS and 20-25 min. for CSS. To get an idea of the duration of the complete analysis of a sample, to these values, a time of 15 min. must be added between the two tests, in order to wait the reconstruction of the inner mucus entanglements. It should also be noted that the same interval was applied in case of single test repetition. At the end of each test, in order to avoid contamination between different samples, both the upper and lower plates, the half-covers and the glass protection completing the insulating box were sterilised. In addition, the deionised water in the well was changed. The sterilisation consisted of three sequential cleaning steps (in order distilled water, ethanol and distilled water) before drying. A complete analysis therefore lasted an average of one hour.

The SAOS was performed by imposing a logarithmic step γ ramp (0.01 and 5000%) of 30 pt. at constant frequency ($f = 1$ Hz). Based on the τ_f evaluation, the CSS of the same sample was carried out by imposing a 200 pt. logarithmic step shear ramp around the flow point. The variable stress range within which this was done was 0.0005 and 250 Pa.

All tests carried out in this study were conducted at 32°C (air temperature inside the airway) and a pressure of 1 Atm. The sandblasted superior plate used was CP25-1/S, with an α of 1° and distance to the inferior plate $a = 0.05$ mm (figure 23). Note that most of the time, the amount of samples to be analysed was very small (between 100 and 200 μ L). A small, flat, sharp spatula was used for extraction from the collection vial. This was also necessary due to the sticky characteristic of the mucus itself.



Figure 23 Photos of the analysis procedure. From left to right: Sample placement on the lower plate and loading of deionized water into the channel. Clamping of the moisture-controlled ambient through half covers and upper dish. Flashing of the upper dish to the analysis.

The analysis of the rheological data obtained in the laboratory (in the intervals and under the operating conditions reported, see figure 24) was carried out using the MATLAB R2022a calculator (see Annex 2) and the excel spreadsheet. The importance of this step is fundamental in order not to

add a further degree of uncertainty to the multitude of variables which contribute to the chemical, structural and rheological characteristics of the analysed samples.

3.3 OPTIMIZATION of RHEOLOGICAL PARAMETERS

The articles examined and the experimental evidence shows that, to a first approximation, the mucus is a viscoelastic fluid, thus modelled concerning its flow behaviour agree with the HB's law. The analysis carried out and presented below is for the calculation of the parameters appearing in the HB model (n , k and τ_0) as well as G' , G'' , τ_f and τ_y , for all the analysed samples.

The experimental data, SAOS ($G'(\tau)$, $G''(\tau)$, oscillatory τ) and FC (rotational $\tau(\dot{\gamma})$ and $\dot{\gamma}$) are loaded into ".txt" files and passed to a MATLAB R2022a programme that has been written during the Thesis project. Concerning the τ_0 determination, given a first value τ_0 (graphically evaluated by the user) and a neighbourhood of it, the step 1 of the programme works calculating time by time the line interpolating the previous $\tau(\dot{\gamma})$ values and some of the successive values at the beginning of the neighbourhood (gradually increased until it coincides with the totality of the neighbourhood itself). This first method has been renamed the "tan based method" as it is based on the maximisation of the value of the angular coefficient to guarantee the maximum verticality of the FC initial section of the analysed sample. Having thus obtained an initial estimate of τ_0 , to further refine it, while determining a first approximation of k and n , a second method is used. It consists of a loop that use the linearized form of the HB model and the τ_0 obtained during step 1. This method extrapolates by linear interpolation of $\Delta\tau(\dot{\gamma})$, n and k (with $\Delta\tau(\dot{\gamma}) = \tau(\dot{\gamma}) - \tau_0$). It uses the HB model to calculate a τ_0 for each $\tau(\dot{\gamma})$ prior for the current τ_0 . These values are then averaged to provide a new starting value for τ_0 . The criteria for stopping this loop are the occurrence of a non-zero imaginary part for n and K or a deviation of the new τ_0 (from the previous step) by a value less than the given tolerance (0.1 Pa). The determination of τ_0 is of relevance to the calculation of the other two parameters for the HB model. In addition, there is no unambiguously recognised method for its identification, and it is clearly not possible to rely on subjective judgement. These considerations led to the need of steps which gradually refine the result (figure 24).

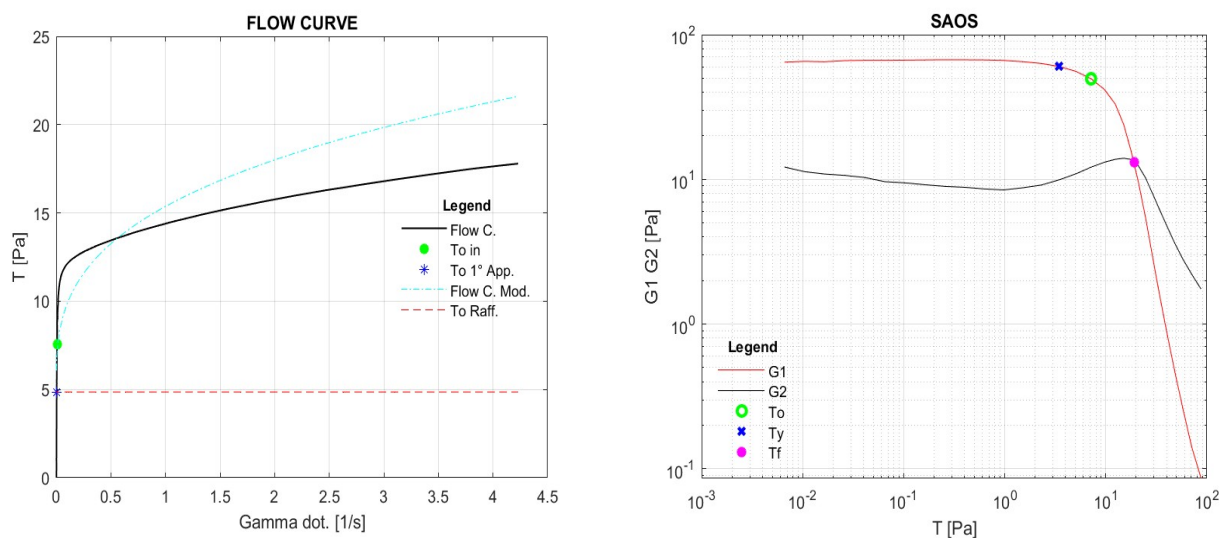


Figure 24 Graphical output of the MATLAB R2022a programme used for data analysis. The FLOW CURVE graph shows the flow curve (black line), τ_0 entered by the driver (green dot), τ_0 approximated with the "tan method" (blue asterisk), τ_0 level refined with the second model (red dashed line) and the first approximation of the HB model for the CSS developed with τ_0 , K and n calculated in it (light blue dashed and dotted). The SAOS curve shows the elastic modulus (red line), the viscous modulus (black line), the yield stress (blue cross), the flow point (pink dot) and the τ_0 refined by the CSS analysis (green empty dot).

Once τ_0 , n and k are obtained from the MATLAB R2022a program, the optimization of these last two parameters was implemented using the excel spreadsheet. To do that, identified the most accurate τ_0 (as shown above), the $\Delta\tau(\dot{\gamma})$ ($\Delta\tau_1(\dot{\gamma})$) was recalculated for the τ values following it. In this way the formulation of the HB model has been reduced to that of a simple viscoelastic material with liquid behaviour. This low has in fact been used to identify a second value ($\Delta\tau_2(\dot{\gamma})$) for each shear rate value subsequent to the flow one. The standard deviation between the $\Delta\tau$'s was then calculated and minimized. Doing this, as shown in figure 25, n and k are set as variables, which at the end of the minimization were returned as optimized. For the optimization procedure of n and k to be undertaken, the following test was applied in order to be more certain of the goodness of the initial value of τ_0 (given by the MATLAB R2022a program):

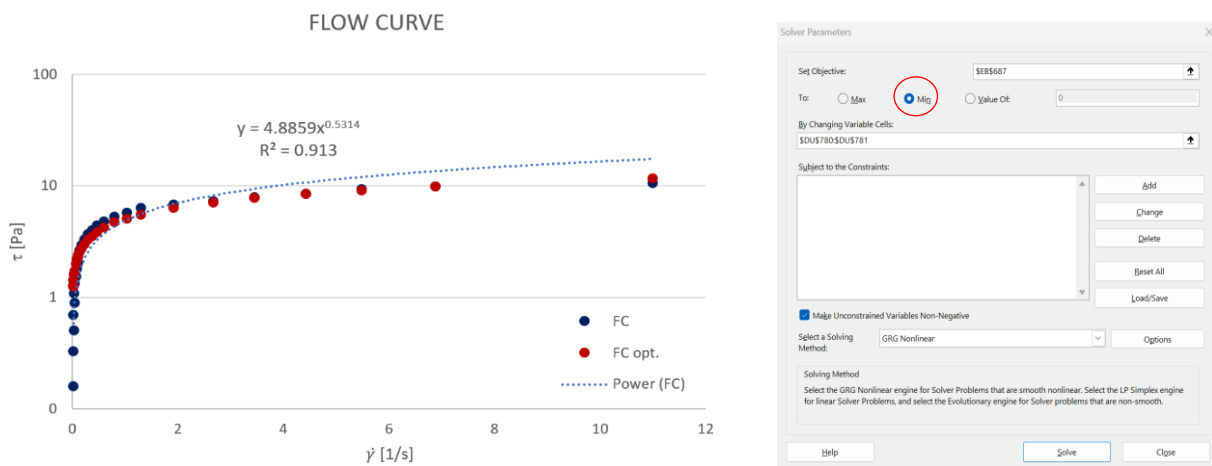


Figure 25 Graphical output of the excel spreadsheet for optimising the data parameters K and n . Highlighted are the coefficient of determination (R^2) and the error minimisation option used in the solver.

$\Delta\tau_1(\dot{\gamma})$ was plotted and modelled through a power law by the excel program. The latter automatically provided a value of n , k and the Coefficient of determination (R^2) for the used law. R^2 is used in statistics to determine the variation of the results predicted by a model compared to the experimental ones. Through the evaluation of R^2 it has therefore been possible to determine from time to time whether, with the assumed τ_0 , a fairly reliable model can be developed ($R^2 > 0.7$). For the modeling of the results of the real and reconstructed bronchial mucus, analysed in this work, the test thus carried out has always given a positive result.

Based on SAOS measurements the MATLAB R2022a program previously described also allows to obtain τ_f by evaluating the intersection of the two straight lines given by the two pairs of coordinates (one for G' and one for G'') at the change of sign of $(G' - G'')$. The program also identifies the τ_y value starting from an average value of G' in the LEVR. The Yield stress is then identified with the first τ which deviates (negatively) from the reference G' value by more than 5%. The procedure implemented in the MATLAB R2022a program was the same. For the first approximation of the G' the first 3 values were taken after the stabilization interval (generally the first 6 experimental data of the SAOS). Once τ_y was obtained, a more accurate estimate of G' was given by averaging all the elastic moduli associated with τ prior to the Yield stress. G'' is calculated using a method similar to the one to evaluate G' , from which G^* and $\tan \delta$ are easily derived, as mentioned in formula 2.8 and 2.9.

3.4 RESULTS and DISCUSSION

The experimental results obtained and reported here show how the pathological conditions have an effect on the elasticity and resistance to flow of the mucus. In particular, it is observed that the mean value (shown in grey) of the elastic component (G') increases both in subjects suffering from asthma (+ 96%) and in those suffering from COPD (+ 57%). The same trend occurs for τ_y , which shows an increase of 93% for asthmatic and 50% for COPD mucus (figure 26).

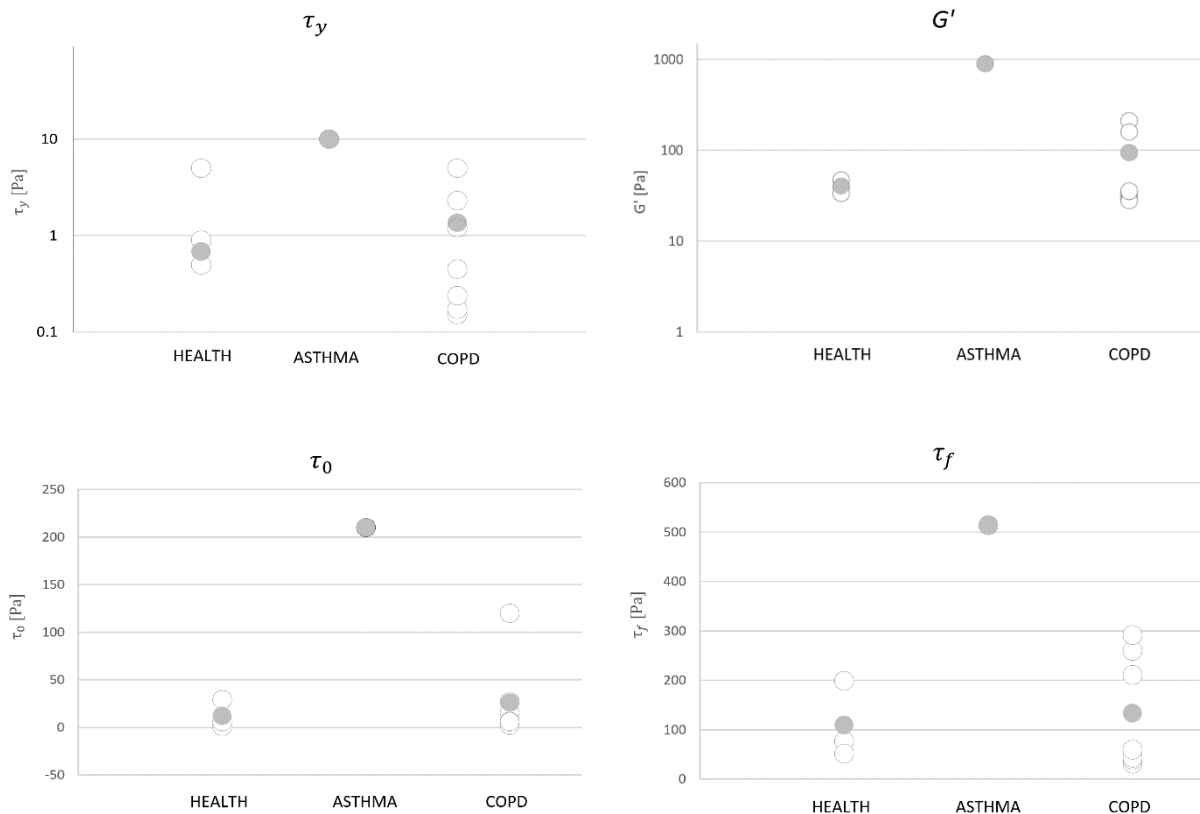


Figure 26 Increased mean values (grey dots) of elastic and viscolastic parameters (τ_y , τ_f , τ_0 and G') gained by the SAOS analysis for the bronchial cellular mucous cell of subjects with smoker (COPD) and asthma.

Comparing the SAOS results with those developed from the data collected in the CSS test, it can be seen that the HB modelling method works correctly. In particular, it can be observed that the trend followed by τ_f is the same as that followed by τ_0 . The order of magnitude between the two, can be attributed to the different method of analysis performed. The increase in shear thinning is notable by the rise in k , which has its maximum for the mucus by cells of asthmatic subjects. The latter, in addition, appears (by the no little variation) to decrease shear thinning, increasing the n value by 7% respect to the healthy condition. The opposite, albeit slightly (decrease in n by 2% compared to the healthy condition), occurs for the lung mucus of subjects with COPD. This phenomena, shown in figure 27, demonstrates an increase in the viscoelasticity of this mucus.

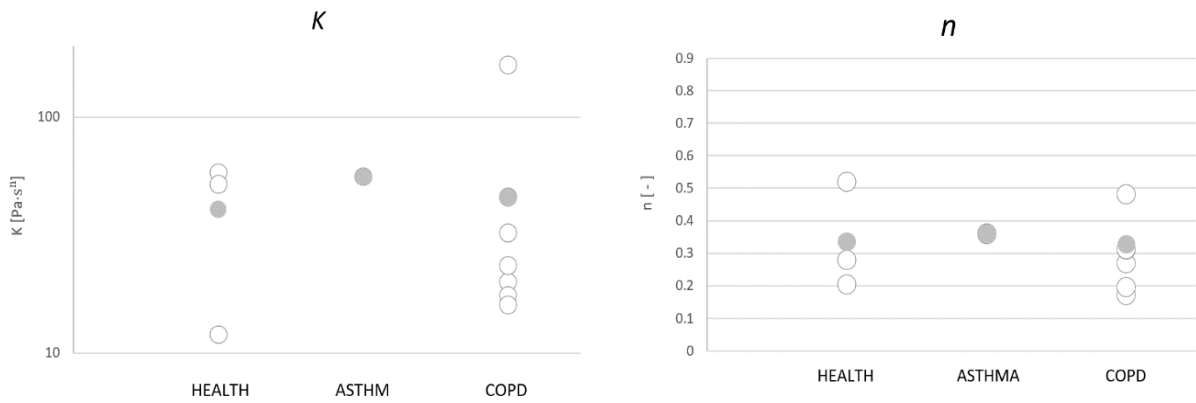


Figure 27 Different trend of increase and decrease of the mean value of shear thinning parameters (k and n) gained by the optimization of HB parameters for the bronchial cellular mucous cell of smoker subjects(COPD) and asthmatic one.

In addition the pathological condition increases the mean variance (defined as below) of the results of both tests. This can be attributed to the different levels of immune response developed by the individual and can easily be observed when comparing healthy and "COPD" subjects. It can also be seen that the mean variance of the parameters developed by the CSS test is particularly high. This phenomenon is presumably due to the complicated determination of τ_0 , during the fitting of the flow curve. It shows that despite the three refining grades adopted in the analysis of these data, τ_0 still remains an important source of uncertainty for the unambiguous identification of the HB model rheological parameters (figure 28).

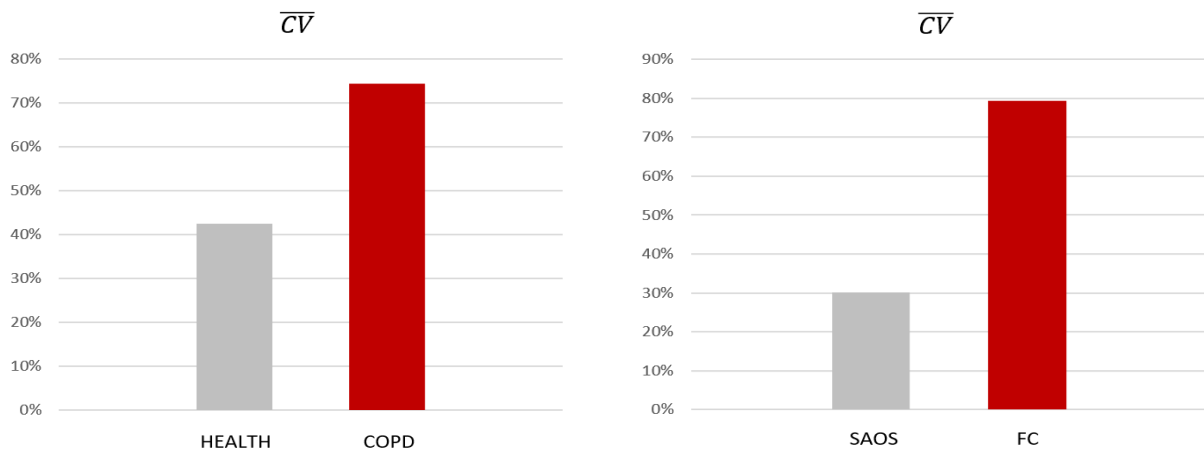


Figure 28 Increased variability in the results obtained when switching from the lung mucus of a healthy to a diseased subject (left) and from SAOS analysis to HB model fitting (right).

As previously mentioned \overline{CV} has been defined by the average of the relative variation coefficients (CV) of each examined parameter.

$$\sigma = \sqrt{\frac{\sum(x_z - \bar{x})^2}{p}} \quad (3.1)$$

$$CV = \frac{\sigma}{\bar{x}} \cdot 100$$

(3.2)

Ultimately, the results obtained and displayed in figure 29 show a degree and ratio of viscoelasticity ($\tan \delta$) between healthy and diseased subjects that is very similar to the data found in the bibliography.

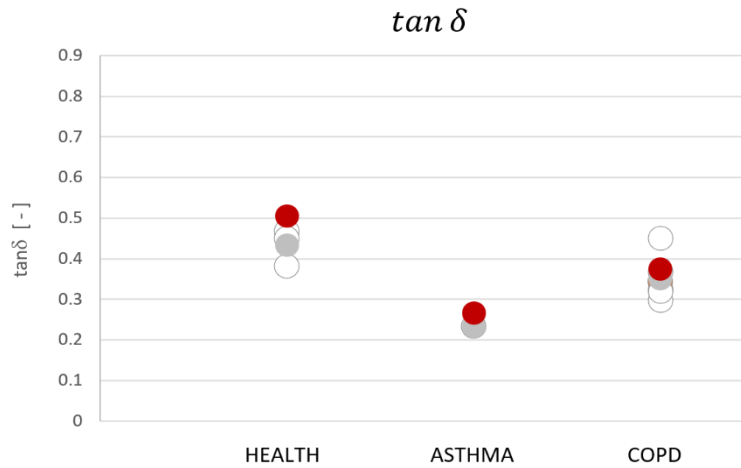


Figure 29 Similarity of the mean value (grey dots) of the degree and level of viscoelasticity of healthy, smoker (COPD) and asthmatic cellular lungs mucus, compared to what is reported in the literature (red dots).

These latter values, together with those obtained from the experimental analysis of the cellular mucus, are now represented here in the table and will provide a useful range for evaluating the experimental evidence of the reconstructed mucus.

Table 9 Summary table resulting from the combination of the rheological parameter data found in the bibliography and the analysis of the cell samples analysed at M2P2 laboratory. Reported the average value and the interval for each parameter by parenthesis.

Pathology	τ_0 [Pa]	K [Pa s]	n [-]	G' [Pa]	τ_f [Pa]	τ_y [Pa]	$\tan \delta$ [-]
Health	12 (1 - 29)	40 (12 - 58)	0.33 (0.20 - 0.52)	19 (0.05 - 47)	74 (1 - 199)	0.68 (0.5 - 0.9)	0.47 (0.29 - 0.93)
Asthma	210 (-)	56 (-)	0.36 (-)	300 (0.05 - 900)	190 (4 - 514)	10 (-)	0.25 (0.2 - 0.33)
COPD	26 (2 - 120)	46 (16 - 166)	0.32 (0.17 - 0.55)	66 (1 - 211)	113 (10 - 292)	1.3 (0.15 - 2.3)	0.35 (0.25 - 0.55)
CF	Not av. (-)	Not av. (-)	Not av. (-)	6 (0.54 - 20)	80 (11 - 148)	Not av. (-)	0.34 (0.25 - 0.87)
Tot.	39 (1 - 210)	45 (12 - 166)	0.33 (0.17 - 0.55)	67 (0.05 - 900)	111 (1 - 292)	1.96 (0.15 - 10)	0.38 (0.2 - 0.93)

CHAPTER 4:

RECONSTRUCTED BRONCHIAL MUCUS

After reviewing the bibliographic results regarding the components of the lung mucus (real and reconstructed) and their chemical rheological properties, a plan of experiments was developed. In this way, it was possible to further verify and investigate the influence and degree of interaction between the different components of the mucus. In the following sections, the methodology and software used for the development of the adopted rheological experience plans will be introduced.

4.1 DESIGN of EXPERIMENTS (DOE)

DOEs are developed in various fields to obtain reliable information to take decisions and or make assumptions with the lowest possible degree of error. DOEs are necessary because the information the research provides is obtained within an experimental setting with different sources of error (human and mechanical). In this context, the goodness of the information found is not related to the quantity of experiments performed but to the quality of them. In addition, to obtain optimal information, the scientific field, must be relevant to the field of study, have good reproducibility and be obtained with good accuracy⁹².

Gathering information for the description of a problem to be solved or (as in the case) the description of a phenomenon, involves a series of steps before the experimental stage. The first is undoubtedly the identification of the objective to be achieved. The second is to draw a list of the responses (or parameters) that need to be measured. Finally, it is essential to define the factors that can be modified as well as their range of variation. Once these points are fixed, the experimental strategy to be adopted can be decided. The 4 main adoptable strategies (reported below) have different purposes and fields of applicability:

- **Exploratory research:** This is used to define the experimental field, make sure that the phenomenon to be studied is controllable and choose the parameters values that will be used as answers, check their repeatability. This type of research is implemented when the problem being treated is almost new and previous results about it are very scarce.
- **Factor screening:** This is used to identify among a set of potentially influencing factors, those that are effectively significant in the given experimental field. This screening can be done if the state of the art on the subject is sufficiently developed.

- **Quantitative factor studies:** This is used to study the selected factors in more details, assessing any interactions among them. The use of this method can be implemented starting from a rather advanced experimental and cognitive experience.
- **Optimization:** Having dealt with the previous steps, this method aims at describing in a n dimensions space the investigated experimental parameters. The influence domain of the model that is generated is of degree n, where n is the number of factors used as inputs to the system.

The Interactional model generated by an optimization process is of the type ⁹³ :

$$Y = \sum_{z=1}^n \beta_z + \sum_{z=1}^n \left(\sum_{j=z+1}^n \beta_{zj} x_{zj} \right) + \varepsilon \tag{4.1}$$

The β_z weight (or of the interaction of two factors β_{zj} weight) in the studied phenomenon is the average deviation between the maximum and minimum effect that this factor (or interaction of factors) induces on the analyzed parameters. In order to determine these weights, it is possible to use software such as AZURAD (used in this work). Once the weights have been calculated, the software verifies their goodness-of-fit by calculating the residual (mean square deviation) between the experimental results and those generated (given the same input) by the model developed for each parameter investigated. From the evaluation of the residual, it is then possible to understand whether the interactions highlighted by the software are reliable or not.

Within the biochemical-pharmaceutical field, the goal is to study the influence of the proportions of certain components (mucous constituents) on the manifestations of a physicochemical phenomenon (rheological properties). Before arriving at an optimized study of the system, it is possible to start by a quantitative study of the factors. To do that, an experimental matrix, generated by special software (such as AZURAD), is preliminarily established.

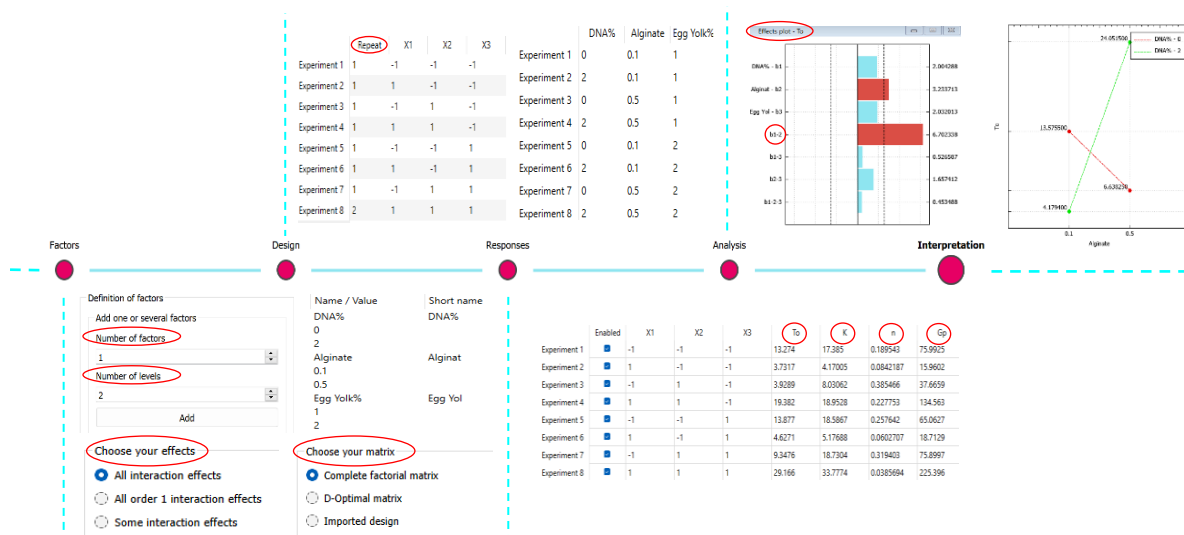


Figure 30 AZURAD Loop steps of a DOE for three factors (DNA, Alginate and Egg Yolk), two level complete factorial matrix and evaluation of effects and interactions plot for one of the four parameters considered (τ_0 , k , n , G').

The input parameters, generally required, are the study factors with their range of variation, the level of the model, the order of interaction to be considered and the type of experimental design to be applied. This latter parameter allows optimizing the number of experiments to be carried out. In the context of biochemical research, DOE are very useful allowing the saving of both time and resources while minimizing wastes. Among the most widely used matrices is the "Fractionary factorial matrix" (of size $2^{(n-1)} \times n$). The prediction of the design depends on the fact that (without taking into account the possible interactions) it can be supplemented with additional rows (experiments) to provide a Complete factorial design. Such a matrix (of size $2^n \times n$) identifies the number and type of experiments to be performed, in order to obtain (through the calculated weights) an optimized interactional complete model of the phenomenon (figure 30)⁹⁴.

After experimentally confirming the literature results on aqueous mucin solution (figure 31)²⁹, 3 different DOEs were developed, each with different purposes, components, operating ranges, and factors. The intensive laboratory activity sustained during the 3 months of experimentation resulted in the reconstruction and analysis of more than 60 bronchial mucus. The purposes and criteria that enabled the definition of each DOE will be explained below, while the experimental procedures (which are also equally important and different from each other) will be elaborated on in the appendices (Annex 6, Annex 7, Annex 8).

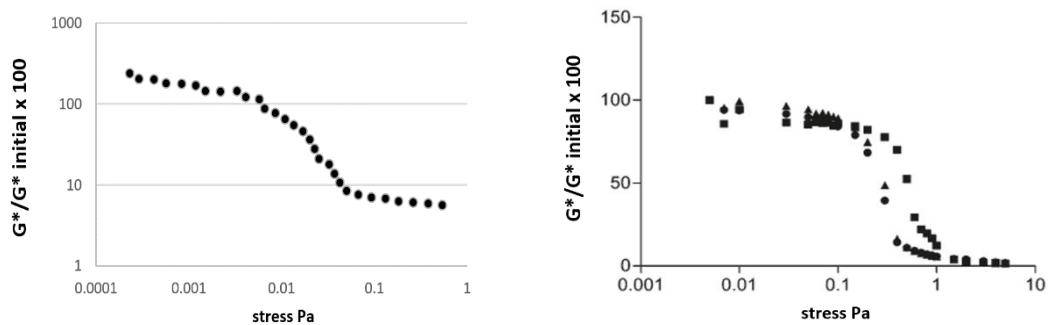


Figure 31 SAOS test comparison for two w/w equal percentage mucins aqueous solutions performed at M2P2 laboratory (left) and reported by literature (right)²⁸.

4.1.1 DOE 1

The first DOE served as an initial screening of the factors supposed to be relevant (DNA, Protein, Lipid, Mucin, Bacteria). In addition, since reconstructed lung mucus (using real components) has never been developed within the M2P2 laboratory, it served as a training ground.

The composition of the reconstructed mucus for the first DOE was produced using compositions found in the bibliography, both from reconstructed mucus (catalogued in detail in Annex 4) and real mucus.

The concentration of components at constant composition for the reconstructed (NaCl, KCl, General amino acids and DIETHYL_{sol0.5M}) was obtained as an average of the values found in the literature. The choice to use DIETHYL_{sol0.5M}, instead of DTPA (since they have similar structure and function), was due to the fact that source³⁰ identified DIETHYL_{sol0.5M} as the best composition developed for reconstructed bronchial mucus so far³³. The AA portion is derived from the laboratory-estimated amounts for proper bacterial population development, in agreement with experimental evidence of bacteria increase in CF subjects⁸¹. The total mucin fraction was calculated based on an average value with respect to 2 reference articles^{30,95}. The % of each mucin was obtained from the average ratio

between MUC5AC (Porcine stomach mucins) and MUC5B (Bovine submaxillary gland mucus) found in real mucus and pathological mucus^{21,36,37,39,41}. Regarding the PAA fraction its concentration (0.9% w/v of the total reconstructed) is based on one study supposed to be the best reconstructed pulmonary mucus developed till 2022³⁰. Trizma base is a of varying composition, but an indicative mass fraction (0.21% w/w) was provided and estimated by a previous study³². However, this value, related to pH stabilization, was changed from time to time in order to obtain the desired pH target (6.8), representative of the lung mucus of sick patients.

The 3 factors considered for this screening were DNA (Fish sperm DNA), the combined fraction of protein and lipid (Egg yolk), and bacterial presence (Alginic acid). Starting with DNA, the lower extreme of its compositional range was considered equal to 0 (same mucus). The upper extreme was, however, difficult to identify. Values reported in the literature for both real samples (from pathological subjects) and reconstructions range by three orders of magnitude (between 0.01 and 10% w/w). The maximum reference value chosen was therefore the result of an average among all the values found (2.45% w/w), the approximation to 2% w/w applied can be traced considering that accounted data are more concentrated between 0.1 and 1% w/w^{10,30,31,54,96,97}. The lipid and protein fractions were merged (given the use of egg yolk). Again, both the lower and upper values turn out to be an average between the sums of the lipid and protein fractions of real^{33,97} and reconstructed^{30,31} lung mucus, combined with the estimates initially reported in the introduction. Finally, the presence of a possible bacterial population was simulated through the addition of alginate. Its range of concentration was estimated based on two reference articles for reconstructed mucus and was found to be consistent with the estimates made in Chapter 1^{29,30}. The aqueous fraction was established as the complement to 100% of the composition thus developed (table 10).

It should be specified that the use of egg yolk in this first DOE is attributable to the need for to gain good experimental awareness before using expensive components such as artificial surfactants. For what said the DOE design has been developed with Four, 2-level factors. In addition, both the first and the second order interactions have been considered, using a Complete Factor Matrix. The entire DOE was repeated twice to check for repeatability.

Table 10 Composition of reconstructed mucus in DOE 1

Components	Weight %
H ₂ O	VAR
NaCl	0.53
KCl	0.23
Generical AA	0.53
DIETHYsol0.15M	1.18
PAA	0.85
MUC5AC	0.16
MUC5B	0.37
Trizma base	1.02 - 1.8
DNA	0 - 2
Alginate	0.1 - 0.5
Egg Yolk	1 - 2

4.1.2 ASSESSMENT EXPERIMENTS

At the end of the first DOE, some experiments were performed to test the necessity to effectively add the chelating agent. These experiments aimed to verify the utility of this component at the structural level. There are indeed some articles that subjected a reconstructed mucus formulated with PAA plus a chelating agent to short-term thermal treatments (100°C for 15 min.) that is used to sterilized the mucus before bacterial growth^{50,82} arise some questions about the utility on a purely structural point of view of this chelating agent in the reconstructed pulmonary mucus.

For this reason, three experiments were developed, using the composition proposed by the first DOE, without the Alginate and Egg yolk. The concentration of DIETHYL_{sol0.5M} either took the value of 0 or 1.18%. At the 1.18% concentration, the reconstructed sample was then subjected or not to an identical heat treatment in a controlled environment and continuous stirring (800 rpm). Analysis of the three samples (reported in figure 32) (without DIETHYL_{sol0.5M} nor heating) / (with DIETHYL_{sol0.5M} no heating) / (with DIETHYL_{sol0.5M} plus heating) showed no real differences of the obtained rheological structures. For this reason this component was deleted of the components list in the next DOE.

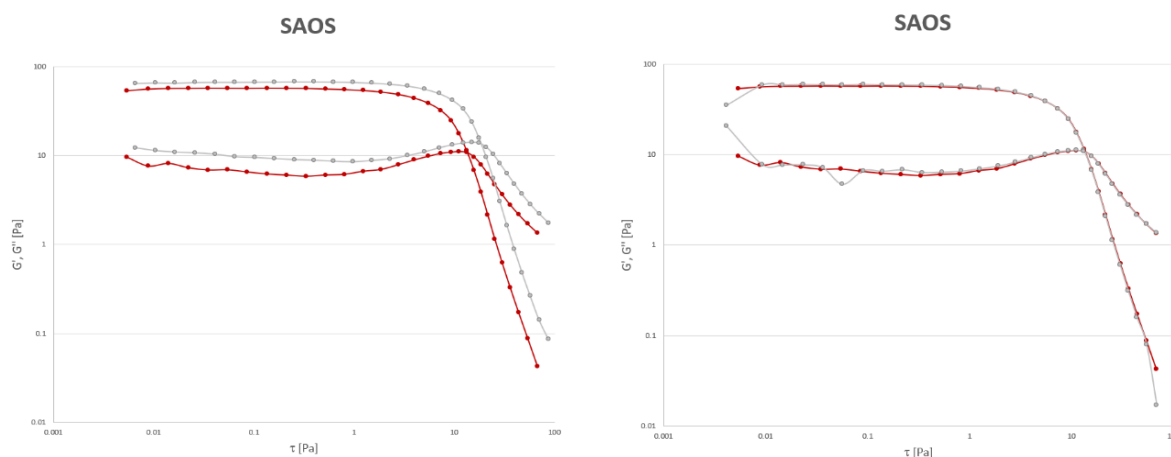


Figure 32 SAOS test comparison of reconstructed mucus with (red) and without (grey) DIETHYL_{sol0.5M} (left) or with (red) and without (grey) thermal treatment at high DIETHYL_{sol0.5M} concentrations (1.18 w/w %).

4.1.3 DOE 2

A second DOE was developed to carry out a quantitative study about the influence of the factors that are supposed to be relevant for the rheological properties (DNA, MUC5AC, MUC5B, Artificial surfactant and Alginate).

Starting from the mucus composition developed in DOE 1, DOE 2 was conservative towards some components while modified others. The results collected between DOE 1 and 2 during the side experiments) led to the deletion of DIETHYL_{sol0.5M} in the constant fraction of the reconstructed mucus. In the composition of the DOE 2, the salts and PAA concentrations remained almost unchanged compared to DOE 1. The generic amino acids were re-replaced by hydrolysed casein, at the same mass fraction. Since there are 5 factors in this DOE a fractional matrix has been used instead of a complete matrix. In addition to DNA and Alginate, already used in DOE 1, the 2 main types of mucins (from Porcine stomach and Submaxillar gland) were added. Concerning the lipoprotein fraction we used instead artificial surfactants (AS) containing mainly mostly lipids.

Its composition was based on the one of CHF5633 found in the literature⁷⁵. Thus, the w/w repartition of the AS used in this work is: DPPC 49.15% , PC 49.15% , SP-A 1.02% , SP-C 0.34% , SP-D

0.34%. The absence of SP-B is due to the lack of availability of the product in the market. So, taken CHF5633, its overall protein fraction (sum of SP-B and SP-C) was evaluated. The composition of the protein component of the real lung surfactants was then considered. Then weighted the amount of protein present in CHF5633 with the latter mass fraction (replacing SP-B with a 1% increase in SP-C and SP-D) the w/w fraction of the AS used in the present work was obtained. For the minimum and maximum ranges, the same method used for DOE 1 was adopted but, considering only the lipid component instead of combining it with the protein one^{33,67,75}. The upper and lower extremes of the AS range were conservatively approximated by excess and defect, respectively. To establish, however, the mucin fractions, a more in-depth investigation was developed. The articles consulted revealed a mucin range between 0.14 and 5%^{21,27,60}. In different articles, CF and asthma patients had a percentage of mucins increased to up to 200 % compared to sane mucus. The interesting point about pathological mucus was that the ratio between the 2 mucins could change a lot with disease from 0.1 to 0.45 (MUC5AC/MUC5B)^{21,36,37,39,41}. Therefore, the ranges and mucin composition were calculated by considering the values cited in this reference publication³¹ as the reference value for healthy mucus. A multiplicative factor of 3 was then applied to obtain the amount of total mucins in the mucus of diseased subjects. The individual quantities of each mucin were then derived applying the above-mentioned ratios for either sane or pathological mucus. The determination of the application range for DNA followed the same assumptions made previously. However, the upper extreme was raised, given the lack of definitive results for this factor, approximating by excess the value calculated in DOE 1. To conclude, the operational range of Alginate was not changed compared to the first DOE.

The composition of the reconstructed mucus for the second DOE was produced following the same method as in DOE 1. Five, 2-level factors were used to identify the experimental Fractional Factor matrix, exploring first-order interactions. Due to time constraints, it was only possible to double 3/4 of these experiments for repeatability purposes (table 11).

Table 11 Composition of reconstructed mucus in DOE 2

Components	Weight %
H ₂ O	VAR
NaCl	0.53
KCl	0.23
Casein Hydrolysed	0.53
PAA	0.85
Trizma base	1.19 - 2.18
MUC5AC	0.048 - 1.03
MUC5B	0.22 - 0.65
DNA	0.025 - 3
Alginate	0.1 - 0.5
AS	1 - 2

4.1.4 DOE 3

The quantitative study carried out in DOE 2 required further bibliographic clarification to interpret the results. These considerations led to the realization of a final DOE. DOE3 is developed to investigate the influence of the type of DNA (fish sperm DNA or low molecular weight salmon sperm DNA) and their actual interaction between the mucins (MUC5B and MUC5AC). The experience gained from previous DOEs led to a modification of the reconstruction procedure (see Annex 8).

In other to study the interactions between the three components (DNA and mucins), the constant part of the reconstructed mucus was also simplified. Firstly, as the interaction of the lipid component (AS) has already been verified, the lipidic fraction used here was Egg yolk emulsion (no preparation). The fraction of this latter was deduced from the reference article used for bronchial mucus reconstruction (0.58%)³¹. The amino acid component, which is useful in both real and reconstructed mucus for bacterial proliferation, was eliminated too as bacteria presence is not simulated in the mucus of this third DOE. The saline composition remained unchanged from DOE 2. As the effect of Alginate (also a by-product of bacterial activity) on the reconstructed mucus rheology had also already been tested, it was also removed from the composition. This allowed to better evaluate the Mucins- Mucins and DNA-Mucins interactions. It was necessary to use Trizmabase for pH balancing (especially in the compositions with a high concentration of DNA, where the Trizmabase fraction reached 0.6% w/w). Finally, in the constant composition fraction of DOE 3's mucus, PAA (used to enhance viscoelasticity to real mucus levels) was replaced by another polymer, Actigum (Food texturizer composed of Xantham gum and scleroglucan previously used for synthetic mucus solutions)¹³. This change was due to a lack of detailed precisions about the PAA molecules used in previous experiments. The PAA used for the reconstruction, as reported in the bibliography, must have a cys-configuration⁶³. Without it, its effect is greatly decreased. Since we did not know whether the PAA used had such configuration, we preferred to use a binder whose effectiveness was better known. The Actigum concentration chosen was 0.7% w/w. The value was chosen based on the fact that aqueous solutions (at 0.75% w/w) of this branched polymer have elasticity (G') close to the ones of healthy real lung mucus^{13,30}. The three factors examined in this DOE were thus mucins (in the ratios and compositions set out in DOE 2) and DNA (low molecular one compared to the one used in DOE2). Indeed, DNA molecules extracted from salmon sperm is shorter than the DNA of generic fish sperm. In this way, it is supposed to better mimic the presence of small DNA stands into the mucus, in particular due to the action of RhdNase, an enzyme belonging to the immune response during lungs infections that breaks eDNA macromolecules into smaller segments^{34,53,54,61}.

The identification of the experimental matrix required three, 2-level factors, that allowed to explore first-order interactions with a Complete Factor Matrix. To conclude, due to a lack of time, the repetition of the DOE3 have not taken place (table 12).

Table 12 Composition of reconstructed mucus in DOE 2

Components	Weight %
H ₂ O	VAR
NaCl	0.53
KCl	0.23
Xantan gum	0.75
Egg Yolk	0.58
Trizma base	0.21 - 0.6
MUC5AC	0.048 - 1.03
MUC5B	0.22 - 0.65
DNA	0.025 - 3

4.2 RESULTS

The following sections will display and comment the results obtained during the three DOEs.

4.2.1 REPEATABILITY

Before proceeding to a punctual analysis of each DOE, it is necessary to make some preliminary considerations about the validity of the results obtained. One of the most important problems in current experimental research is reproducibility. That arises when the phenomenon being studied is not well understood and/or the experimental operational methodology (or data analysis) is unsuited to the experiment being performed.

Therefore, by mastering the phenomenon, tightening the operating methods and developing an accurate method of analysing the results, it is possible to increase the experimental reproducibility, defnyed for a set of p data repeated m times is defined as follows⁹⁸ :

$$S_R = \sqrt{\text{Variance}} \quad (4.2)$$

$$\text{Variance} = \frac{\sum_{z=1}^p \sigma_i}{p} \quad (4.3)$$

$$\sigma_i = \sqrt{\frac{\sum_{j=1}^m (x_j - \bar{x})^2}{m}} \quad (4.4)$$

The reproducibility limit (R), calculated as follows, then allows us to quantify the limits within which 95% of the measurements should fall⁹⁹.

$$R = S_R \cdot 1.96 \cdot \sqrt{2} \quad (4.5)$$

Looking at the R values obtained between the two DOEs for which it was possible to assess reproducibility (DOE 1 and DOE 2), it can be seen that it falls from the first (grey bars figure 34) to the second (white bars figure 33). Through experimental procedure improvements (explained in Annex 6 and 7), associated to the use of the excel file introduced in Chapter 2 and a deeper understanding of experimental phenomenology, it was possible to reduce the reproducibility limit by an order of magnitude for almost all the variables studied (except n).

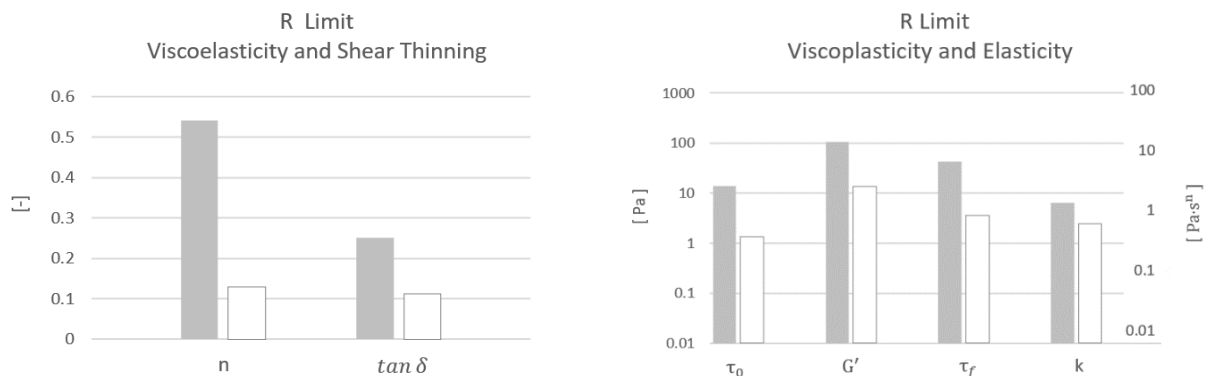


Figure 33 R limit Comparison for the most important rheological parameters of DOE 1 (grey) and 2 (white).

4.2.2 DOE1

The first DOE was designed with the intention of verifying the respective influences of DNA, Egg yolk and Alginate as well as their possible interactions. An analysis of the results shows that the average elasticity (G'), viscoelasticity ($\tan\delta$) and viscoplasticity (τ_f) values obtained from this DOE 1 fall within the range (of the representative parameters for which has been possible to identify a range compressive of CF Asthma and COPD) defined by the literature and presented in Chapter 3. It means that the reconstructed mucus performed during this DOE is thus a fair representation (on a rheological point of view) of real bronchial mucus (figure 34).

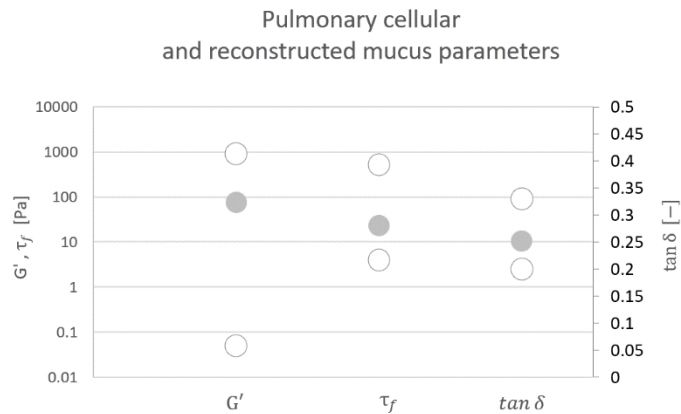


Figure 34 Comparison of the representative parameters for which has been possible to identify a range compressive of CF asthma and COPD gained by chapter 3 (white) and the DOE 1 ones (grey dots).

The study of parameters weight and interactions showed the joined effect of DNA and Alginate on the elasticity (G'), viscoelasticity ($\tan\delta$) and shear-thinning (k) of the reconstructed mucus. The inter-relational diagrams below show the corresponding weight for each factor or interaction. Significant results are marked in red. A factor may therefore individually give rise to an effect on a considered variable and/or interact with another. A single effect of a factor occurs when it has a relevant weight but no relevant interaction weights. For example, the effect of alginate on τ_0 cannot be considered individually, but only in interaction with DNA. As shown therefore by the interaction diagrams (figure 35), the simultaneous presence of DNA and alginate (b_{12} weight) increases the shear-thinning (k) and viscoplasticity (τ_0), decreasing the viscoelasticity of the reconstructed lung mucus ($\tan \delta$).

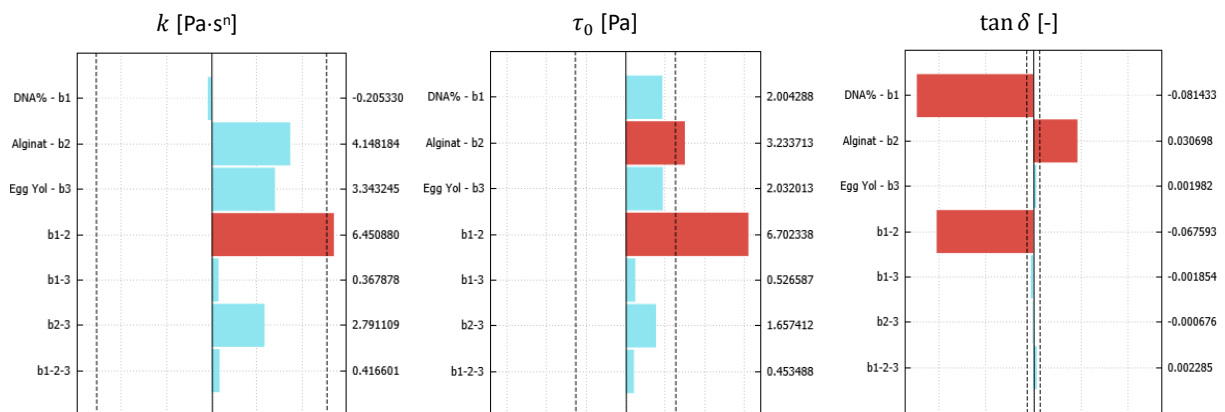


Figure 35 Effect plot of k , τ_0 and $\tan \delta$ for the DOE 1.

This result is consistent with what is stated in the literature describing the Alginate as molecules forming bonds between the mucin lattice, and interacting with other long macromolecules such as fish sperm DNA, thickening the GFM. This is even better understood from the diagram developed for the Alginate-DNA interaction (figure 36), where can see how, by increasing the DNA concentration, under high concentrations of Alginate (dashed line in green), is obtained an increases of τ_0 and k and decrease of \tan (figure 36).

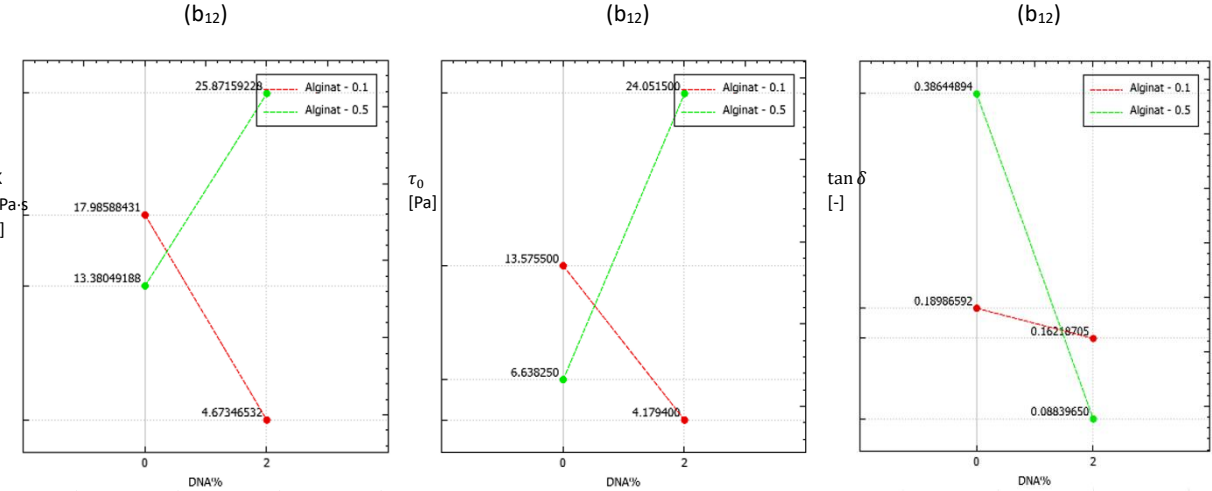


Figure 36 Interaction plot for k , τ_0 and $\tan \delta$ for the DOE 1

The Egg yolk did not appear to give rise to any relevant effects, either alone or in interaction with the other two components (DNA and Alginate). In addition, the elasticity (G'') and the second parameter of shear thinning (n) of the mucus was not influenced by any factor (see figure 44).

In this DOE, the consistency of the results obtained is evidenced by the mean square deviation between the actual experimental values (from which the software obtained the interaction weights) and those returned by the model (processed by the AZURAD integer software) on the basis of the input concentrations provided. By the linearity of the graphs (figure 37) below, an almost perfect correspondence can be, in addition, observed between the values reported experimentally (x-axis) and those processed by the model (y-axis).

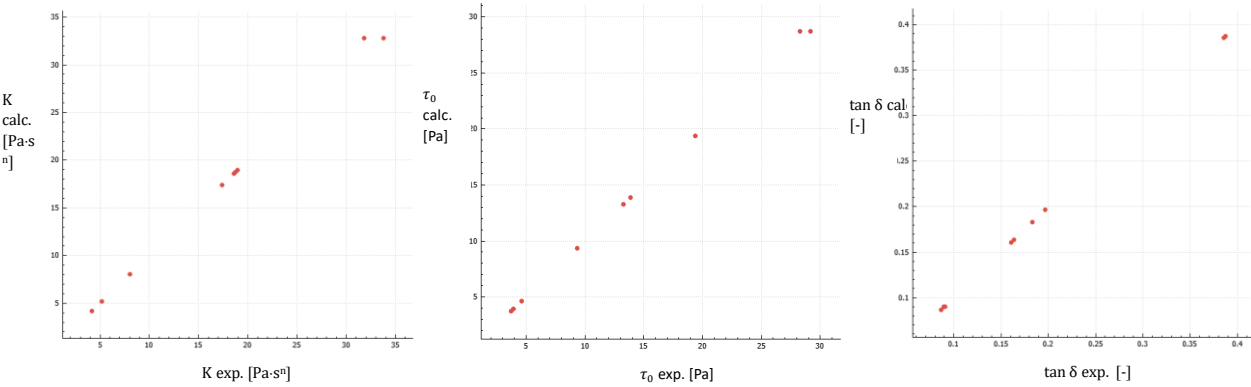


Figure 37 Graphs between the values reported experimentally (x-axis) and those processed by the interactional model (y-axis) for k , τ_0 and $\tan \delta$ for the DOE 1.

4.2.3 DOE 2

The second DOE was designed to determine the respective influences of DNA, AS, Alginate MUC5B and MUC5AC as well as their possible. Again, analysis of the results obtained shows that the average elasticity and viscoelasticity values are within the range (of the representative parameters for which has been possible to identify a range compressive of CF Asthma and COPD) defined by the literature and presented in Chapter 3. This allows the developed solutions to be likened to a real bronchial mucus. Compared to DOE1 (grey dots in figure 38), however, it is observed a decrease in mean reconstructed elasticity (G') and an increase by contrary of the viscoelasticity ($\tan \delta$) (red dots in figure 38) even remaining in the same order of magnitude.

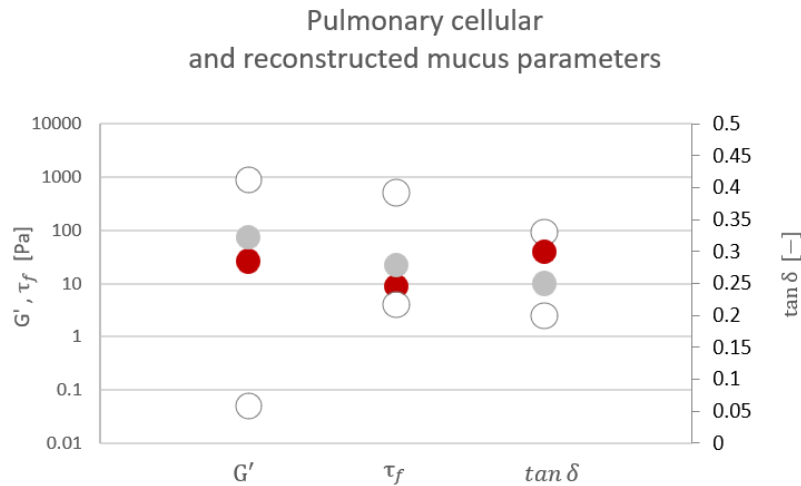


Figure 38 Comparison of the representative parameters for which has been possible to identify a range compressive of CF Asthma and COPD gained by chapter 3 (white), the DOE 1 (grey dots) and the DOE 2 ones (red dots).

The most relevant parameter giving rise to the more important rheological changes, influencing almost all the rheological parameters, is the Alginate concentration. As shown in the inter-comparison diagram (figure 39) Alginic acid, taken individually, increases the elastic modulus more than the viscous one. This therefore makes the substance more viscoelastic. The same effect was observed in DOE 1, and even then, the interaction of the Alginate with other components led to an increase in the viscoelasticity of the solution (see weight $b_{25} \tan \delta$ DOE2 and $b_{12} \tan \delta$ DOE1).

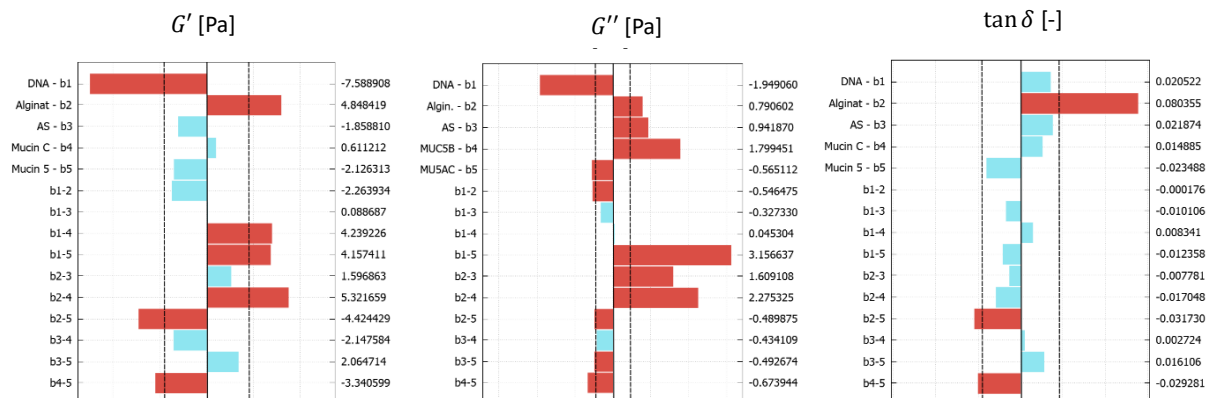


Figure 39 Effect plot of G' , G'' and $\tan \delta$ for the DOE 2.

A decrease in the elasticity, viscoplasticity and shear-thinning of the reconstructed mucus can also be attributed to the interaction effect of the mucin MUC5AC with Alginate and MUC5B (see b_{25} and b_{45} interaction of k , τ_0 , τ_f , G' in figure 40). This may be due to the conformation of MUC5AC. In fact, it is shorter than MUC5B and thus provides less surface area for the formation of inter-mucin and mucins-macromolecules bonds. In addition, the decrease in elasticity, viscoplasticity and shear-thinning, following the addition of MUC5AC seems to be consistent with the increase in its production in CF subjects. In the lung mucus of CF sufferers, the ratio of MUC5B and MUC5AC increases, in fact, from 0.1 to 0.45. The increased production of MUC5AC mucin therefore appears to be a defensive system put in place by the body to facilitate the flow of mucus into the airways. If we pay closer attention to the b_{45} and b_{25} interactions on the variables (k , τ_0 , τ_f and $\tan \delta$), we can observe that within the mucin from porcine stomach (used to simulate MUC5AC mucin), there are other type of them such as MUC6 and MUC2 that are not present in the lung mucus and that can affect the structure and rheology of reconstructed mucus.

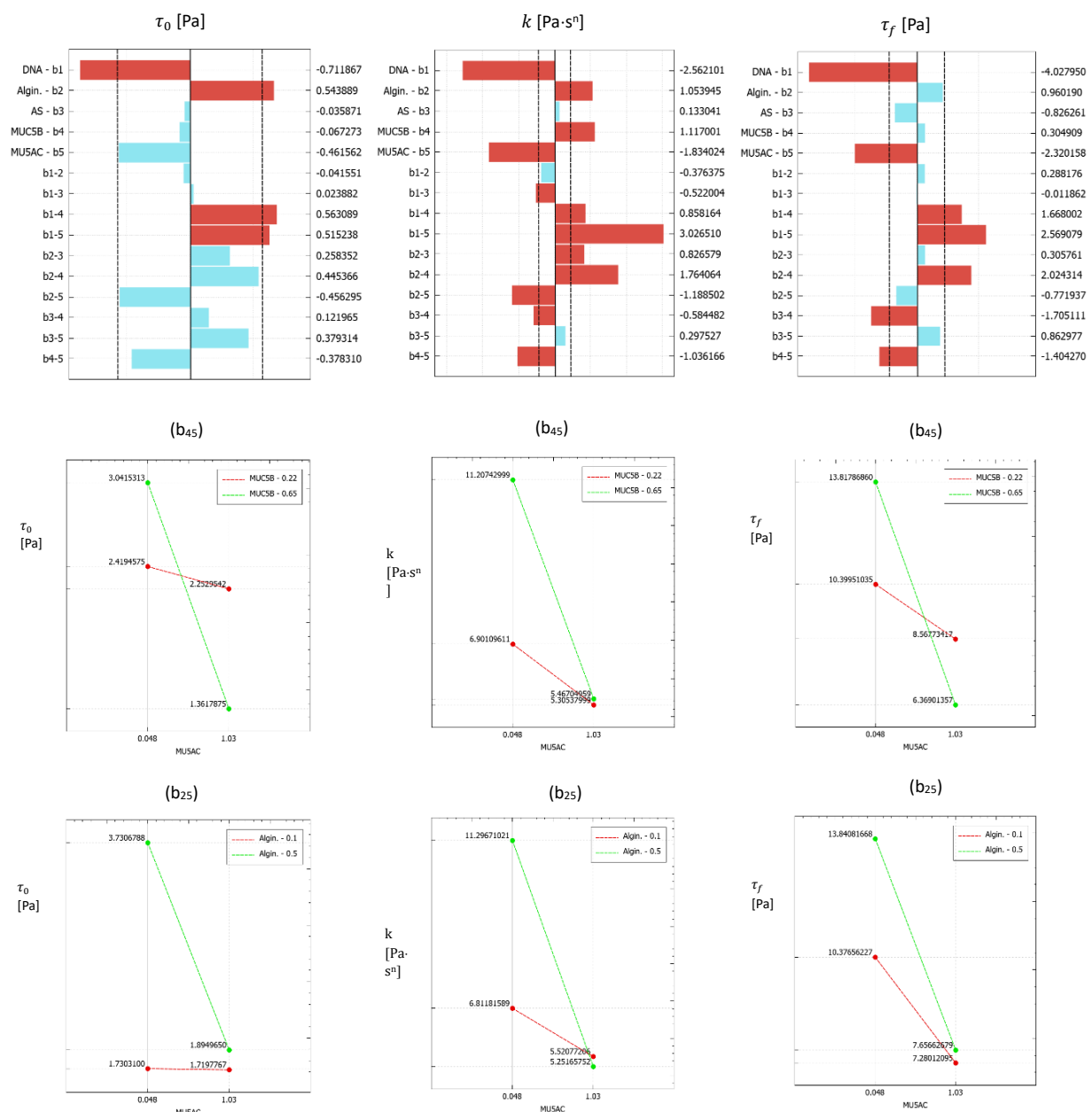


Figure 40 Effect and b_{45} (MUC5AC-Alginate), b_{25} (MUC5AC- MUCB) interaction plot of k , τ_0 , τ_f for the DOE 2.

Finally, the viscoplasticity and shear thinning of the lung mucus is decreased by the interaction of AS with Alginate (see as most representative interaction b_{23} k in figure 42). It so induce an increase of the viscosity (see G'' b_{23} of $\tan \delta$ in figure 41 and 42). This phenomenon is due to the increased mobility of this macromolecule caused by the presence of AS. The lipidic fraction can bind to Alginate molecules, decreasing the formation of stable bonds between Alginic acid and mucins. This phenomenon, although of a negligible amount, also occurs (at low levels) with MUC5B (see weight b_{34} k , τ_f figure 41 and 42) and MUC5AC (see weight b_{13} k , τ_f in figure 41 and 42). At high concentrations of those macromolecules, the effect is reversed, decreasing in intensity. This response is attributed to an increase in the complexity of the GFMs, which also incorporates the protein component of AS, leading to an opposite effect. It is important, to remember that SP-A, SP-D and SP-C are the components responsible of the increased mobility of macromolecules in the bronchial mucus.

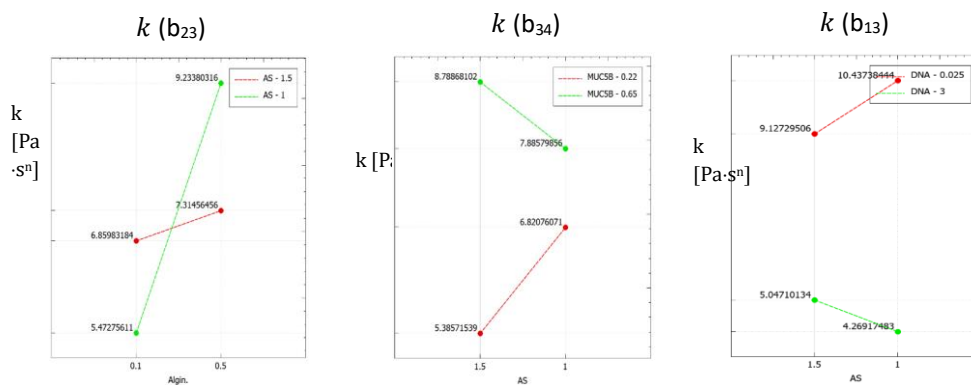


Figure 41 Representative b_{23} (Alginate-AS), b_{34} (AS - MUCB) and b_{13} (DNA-AS) interaction plot of k (but also τ_f) for the DOE 2.

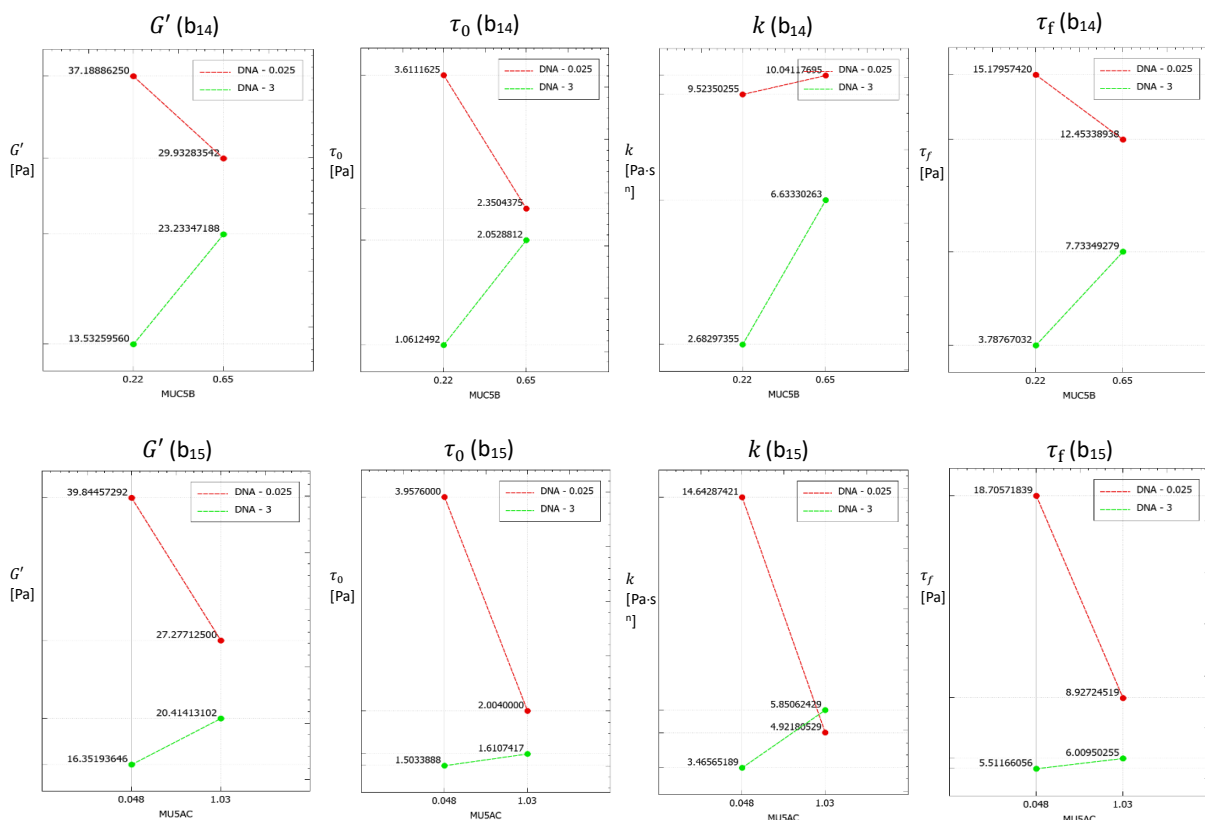


Figure 42 b_{14} (DNA - MUC5B) and b_{15} (DNA - MUC5AC) interaction plot of G' , k , τ_f and τ_0 for the DOE 2.

Thanks to this DOE, it was then possible to observe the interaction between DNA and mucins (see b_{14} and b_{15} of G' , τ_0 , τ_f and k in figure 43). As seen in the bibliography, this leads to an increase in the elasticity, viscoplasticity and shear-thinning of the mucus due to the increase in electrostatic interactions and the formation of NETs that rise the GFMs complexity.

Although DNA interactions are positive, the single effect of Deoxyribonucleic Acid strongly lowers the viscoplasticity and shear-thinning of the reconstructed mucus (see effect b_1 of τ_0 , k , τ_f). This is then accompanied by an almost negligible increase in viscoelasticity (see $b_1 \tan \delta$ effect). A phenomenon probably due to the conformation of the fish sperm DNA. It has a longer chain length than the DNA of salmon sperm, which is normally used in mucus reconstruction. The increased chain length makes it more difficult for cations in the mucus to neutralise it. This decreases the constructive interaction between DNA molecules and leads to less stiffness of the mucus. A similar explanation, added to the considerations about mucins made previously, can help to understand the mucus viscosity increase at increasing MUC5AC for high DNA level (figure 43).

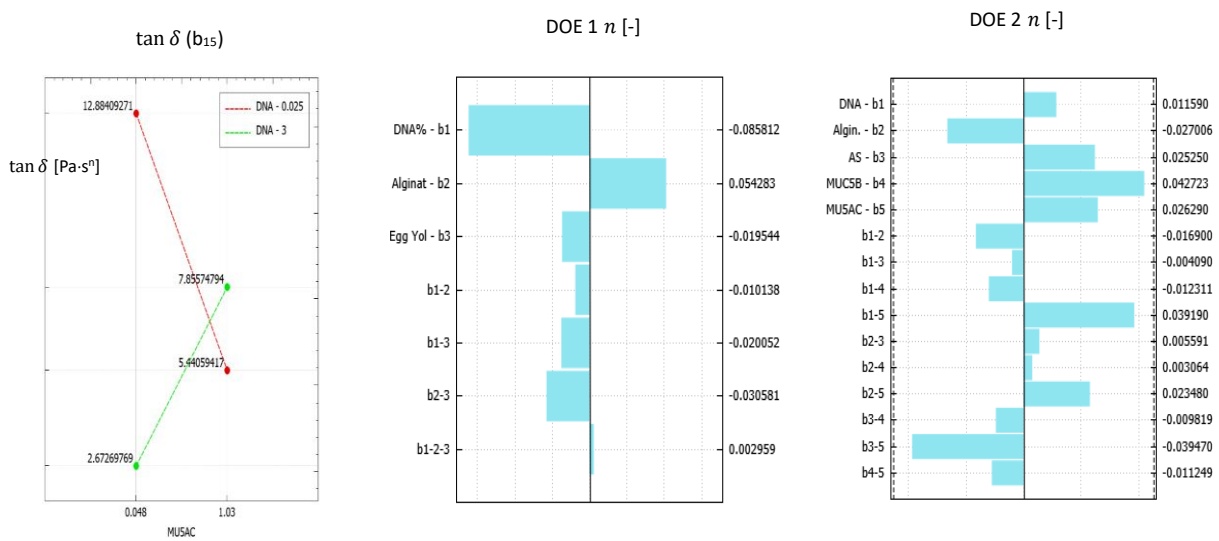


Figure 43 From left to right: b_{15} (DNA - MUC5AC) interaction plot of G'' for the DOE 2, effect plot of n for the DOE 1, effect plot of n for the DOE 2.

Finally, neither DOE 2 has revealed relevant weight for the second shear-thinning parameter (n) (figure 44), but was helpful in defining the type of mucin which Alginate binds to increase mucus elasticity. As demonstrated by the b_{24} (see the interactional diagram of k , τ_f and G' in figure 45). The combined increase in Alginate and MUC5B leads to a considerable increase in mucus elasticity, viscoplasticity and shear-thinning, well simulating the binding effect of the extracellular polymers secreted by bacterial populations within the mucin network.

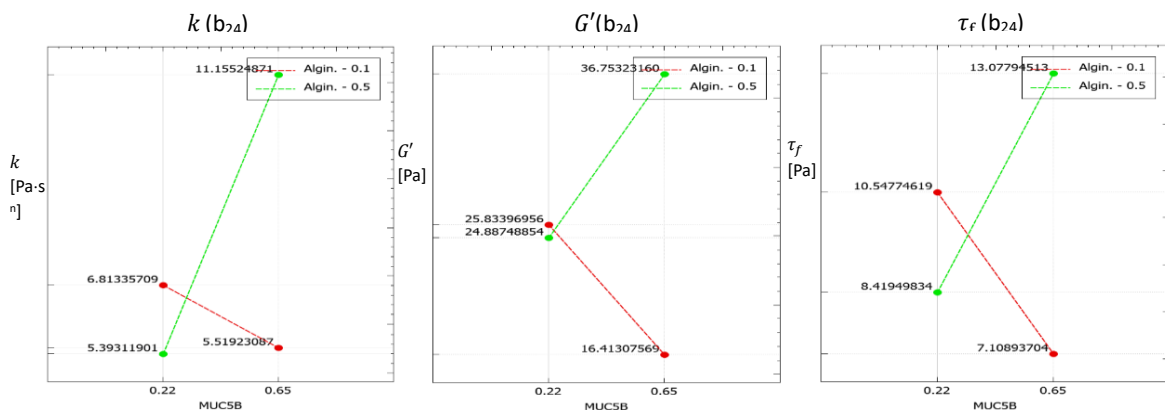


Figure 44 b_{24} (Alginate - MUC5B) interaction plot of G' , k , τ_f and τ_0 for the DOE 2.

The consistency of the information reported in this DOE is given by the fact that the reported interactions follow the same trend (see relevant weights) for all elastic parameters examined, both of the SAOS (G' , and τ_f) and CSS (τ_0 and k) tests. This also verifies the reliability of the programme used for analysing the FC data. However, it should be noted that the mean square deviation between the actual experimental values and those returned by the model based on the input concentrations provided are on average higher than those of DOE1. This phenomenon can also be observed from the wider dispersion of the points describing the correlation line and is due to the increase in the factors studied (figure 45).

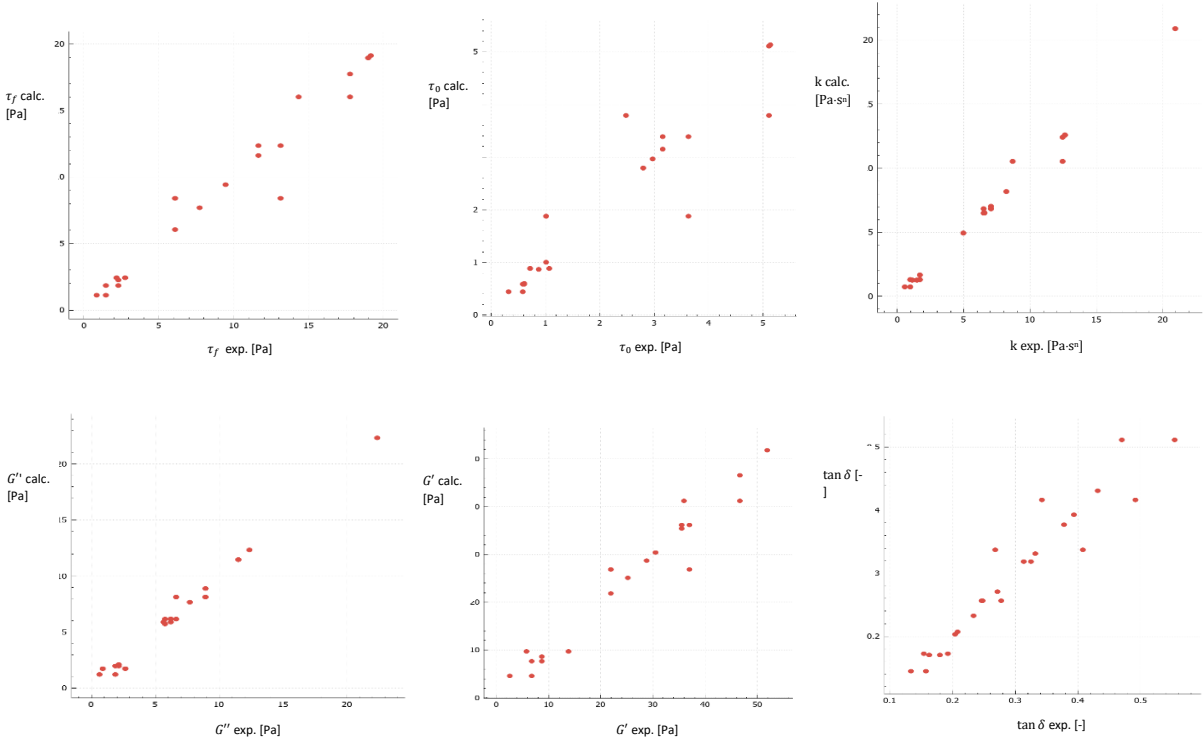


Figure 45 Graphs between the values reported experimentally (x-axis) and those processed by the interactional model (y-axis) for G' , G'' , k , τ_0 , τ_f and $\tan \delta$ for the DOE 2.

4.2.4 DOE 3

The third DOE was designed to determine the respective influences of DNA and mucins. Again, the average values of elasticity, viscoplasticity and viscoelasticity fall within the range defined by the literature and presented in Chapter 2. The developed solutions are thus a fair representation (on a rheological point of view) of real bronchial mucus. The use of Xantan-gum instead of PAA in the specified proportions resulted in an average elastic modulus and flow point similar to those of DOE 2 and the reference article considered¹³. The lowering of these factors (red dots in figure 46) may be due to the absence of the AA component and the proteins present in the AS. Viscoelasticity, on the other hand, seems to be the parameter most similar to DOE 2 despite the great difference between the two basic compositions.

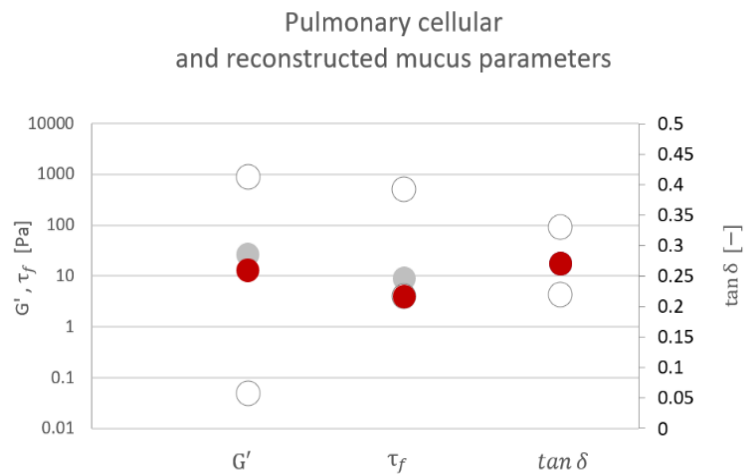


Figure 46 Comparison of the representative parameters for which has been possible to identify a range compressive of CF asthma and COPD gained by chapter 3 (white dots), the DOE 2 (grey dots) and the DOE 3 ones (red dots).

Since the experiments conducted could not be repeated the third DOE cannot be evaluated following the relevance of the weights resulting from the experiments. Therefore, it is only possible to perform a qualitative analysis on the collected data.

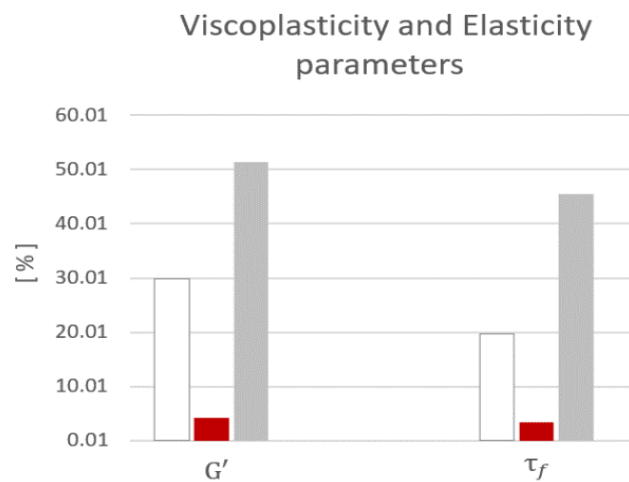


Figure 47 Percentage increase in Elasticity (G') and viscoplasticity of reconstructed mucus at Salmon sperm DNA increase at constant mucins level (white bars), at increased level of MUC5AC (red bars) and at increased level of MUC5B (grey bars).

This analysis demonstrates that the use of low-molecular DNA produces an increase in the elastic and viscoplastic properties of the mucus even individually. This can be deduced observing of the percentage increase in τ_f and G' parameters at increasing DNA levels and constant mucin composition (figure white bars). In addition, it was noted that the viscoplasticity and elasticity of the mucus are not only implemented by the addition of DNA, but this increase explodes when coupled with that of MUC5B at constant MUC5AC (grey bars). Conversely, the increase in DNA (at low concentrations of MUC5B) when coupled with that of the mucin MUC5AC, leads to a reduction in the percentage increase in τ_f and G' (see red bars in figure 47). These results are in agreement with DOE 2 and so valorises the conclusion made previously.

CHAPTER 5:

FLUODODYNAMIC SIMULATION of the LUNG MUCUS

By parallel to the work carried out on the analysis of the rheological behaviour of real and reconstructed mucus of people affected by bronchial disease, the flow of a viscoelastic fluid with shear-thinning was numerically simulated by Amir Hosein Nosrat Kharazmi et al. in another team in the M2P2 laboratory.

In the following paragraphs, the model and the main results obtained with it will be presented. Finally, it will be explained how the information in the previous chapters can be coupled with it to develop more effective therapies in the biomedical field.

5.1 MODEL

A two-dimensional geometry (figure 48) was used to describe the fluid flow within a channel under the action of an oscillating force (formula 5.1) ¹⁰⁰.

$$F_x = g_x(\xi_1 + \xi_2 \cos(\omega t)) \quad (5.1)$$

The law chosen to describe the velocity developed along the section of this channel at a time t is the one adopted by Womersley (formula 5.2) to analytically solve the momentum equation of a Newtonian fluid at low velocities (always parallel to the base of the channel).

$$U_x(y, t) = Real \left\{ \frac{g_x}{i\omega} e^{i\omega t} \left(1 - \frac{\cosh\left(\frac{1}{\sqrt{2}}(\alpha + ai) \frac{2y}{H}\right)}{\cosh\left(\frac{1}{\sqrt{2}}(\alpha + ai)\right)} \right) \right\} \quad (5.2)$$

$$\alpha = \frac{H}{2} \sqrt{\frac{\bar{\omega}}{\nu}} \quad (5.3)$$

$$Re = \frac{\rho u_0 H}{\mu} \quad (5.4)$$

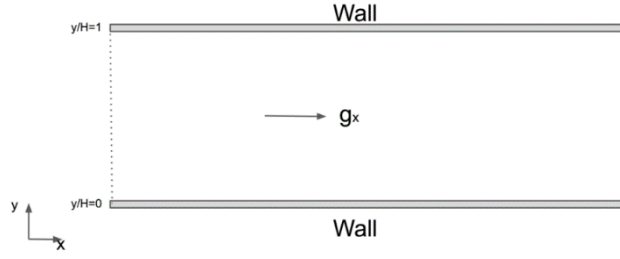


Figure 48 Geometry of CFD simulations

The stress tensor of the viscoelastic fluid (σ_{total}) was divided into a polymeric elastic (σ_p) and solvent Newtonian (σ_s) part, using the Oldroyd-B model (formula 5.5), derived from the kinetic theory of concentrated polymer solutions (formula).

$$\sigma_{total} = \sigma_s + \sigma_p \quad (5.5)$$

5.1.1 SOLVENT NEWTONIAN TENSOR

σ_s represents the component of the fluid stress tensor due to the Newtonian solvent and is defined as:

$$\sigma_s = 2\mu_s \mathbf{D} \quad (5.6)$$

$$\mathbf{D} = \frac{1}{2}((\nabla \mathbf{u}) + (\nabla \mathbf{u})^T) \quad (5.7)$$

The macroscopic velocities (formula 5.8) appearing in this tensor are derived from the resolution of the Boltzmann lattice model (LBM) (formula 5.9), which is a discretization of the Boltzmann equation.

$$\rho \mathbf{u} = \sum_{i=0}^8 f_z \mathbf{e}_z + \frac{\Delta t}{2} \mathbf{F} \quad (5.8)$$

$$f_z(\mathbf{x} + \mathbf{e}_z, t + 1) - f_z(\mathbf{x}, t) = \Omega_z(\mathbf{x}, t) + S_z(\mathbf{x}, t) \quad (5.9)$$

This equation describes the macroscopic dynamics of a Newtonian fluid system and is composed by a collisional (between elements of the system) (formula 5.10) and external forces (formula 5.11) part ¹⁰¹.

$$\Omega_{coll} = -\frac{\Delta t}{\tau} [f_i(\mathbf{x}, t) - f_i^{eq}(\mathbf{x}, t)] \quad (5.10)$$

$$f_z^{eq}(\mathbf{x}, t) = \omega_z \rho \left[1 + \frac{\mathbf{e}_z \cdot \mathbf{u}}{c_s^2} + \frac{(\mathbf{e}_z \cdot \mathbf{u})^2}{c_s^4} - \frac{\mathbf{u}^2}{2c_s^2} \right] \quad (5.11)$$

$$S_z = \left(1 - \frac{1}{2\tau}\right) \omega_z \left[\frac{\mathbf{e}_z - \mathbf{u}}{c_s^2} + \frac{(\mathbf{e}_z \cdot \mathbf{u})\mathbf{e}_z}{c_s^4} \right] \mathbf{F} \quad (5.12)$$

The LBM adopts a precise collisional operator (in this case the Bhatnagar-Gross-Kroon), discretizing the number of motions that the individual element of the model can perform (in this case a D2Q9 discretization was adopted). Each movement is then associated with a specific velocity (discrete velocity \mathbf{e}_z defined as formula 5.13) that serves to define the equilibrium state, the collision component and the external forces of the system.

$$\mathbf{e}_z = \begin{cases} (0,0), & z = 0 \\ \left(\cos\left(\frac{\pi(z-1)}{2}\right), \sin\left(\frac{\pi(z-1)}{2}\right) \right), & z \in [1,4] \\ \sqrt{2} \left(\cos\left(\frac{\pi(2z-9)}{4}\right), \sin\left(\frac{\pi(2z-9)}{4}\right) \right), & z \in [5,8] \end{cases} \quad (5.13)$$

5.1.2 POLYMER ELASTIC TENSOR

σ_p represents the component of the fluid stress tensor due to the elastic polymer, assimilated to a spring system in the Newtonian solvent. Starting from the macroscopic velocity, obtained from the LBM, σ_p was calculated by applying the method of first-order finite differences for time and second-order central finite differences for space (formulas 14-16)^{102,103}.

$$\tau_{xx}^{t+1} = \left(1 - \frac{\Delta t}{\lambda}\right) \tau_{xx} - \Delta t \left[u \frac{\partial(\tau_{xx})}{\partial x} + v \frac{\partial(\tau_{xx})}{\partial y} - 2 \frac{\partial u}{\partial x} \tau_{xx} - 2 \frac{\partial u}{\partial y} \tau_{xy} + 2 \frac{\eta_p}{\lambda} \left(\frac{\partial u}{\partial x}\right) \right], \quad (5.14)$$

$$\tau_{yy}^{t+1} = \left(1 - \frac{\Delta t}{\lambda}\right) \tau_{yy} - \Delta t \left[u \frac{\partial(\tau_{yy})}{\partial x} + v \frac{\partial(\tau_{yy})}{\partial y} - 2 \frac{\partial v}{\partial x} \tau_{xy} - 2 \frac{\partial v}{\partial y} \tau_{yy} + 2 \frac{\eta_p}{\lambda} \left(\frac{\partial v}{\partial y}\right) \right], \quad (5.15)$$

$$\tau_{xy}^{t+1} = \left(1 - \frac{\Delta t}{\lambda}\right) \tau_{xy} - \Delta t \left[u \frac{\partial(\tau_{xy})}{\partial x} + v \frac{\partial(\tau_{xy})}{\partial y} - \frac{\partial u}{\partial x} \tau_{xy} - \frac{\partial u}{\partial y} \tau_{yy} - \frac{\partial v}{\partial x} \tau_{xx} - \frac{\partial v}{\partial y} \tau_{xy} + \frac{\eta_p}{\lambda} \left(\frac{\partial v}{\partial x} + \frac{\partial u}{\partial y}\right) \right], \quad (5.16)$$

Finally, shear-thinning was fitted within the model by defining the polymer viscosity with the following power law (formula 5.17).

$$\mu_p = K |\dot{\gamma}|^{n-1} \quad (5.17)$$

$$\dot{\gamma} = \sqrt{2(\mathbf{D}:\mathbf{D})} \quad (5.18)$$

The hybrid method adopted (LBM plus finite difference) was useful to overcome numerical instabilities arising from high elasticity effects.

5.2 TESTS PERFORMED and PARAMETERS STUDIED

The model was subjected to four validation tests (Taylor-Green Vortex, Steady 2D Poiseuille, Oscillatory flow and Shear-thinning/shear-thickening). Two dimensionless numbers were used to characterise the viscoelastic properties of the fluid, the Weissenberg number (W_z) and the kinematic viscosity ratio (β) defined as follows (formulas 5.19 and 5.20)¹⁰⁰.

$$W_z = \lambda \frac{u_0}{H} \quad (5.19)$$

$$\beta = \frac{v_s}{v_{total}} \quad (5.20)$$

The first increases with the relaxation time of the system, while the latter decreases as the kinematic viscosity of the molecular polymers increases.

Chosen the parameters g_x , ξ_1 and ξ_2 , the resonance frequency (f_0) was also determined for each test as the inverse of the time passed between two peaks of the central velocity of the fluid under oscillatory force into the duct. The model passed validation tests, so W_i , β , k and n were modulated to describe viscoelastic fluids characterised by shear-thinning. These fluids have then been tested under different oscillating forces (modifying g_x , ξ_1 and ξ_2). This made possible to assess how simulated rheology affects the maximum and average flow rate of such fluids in the above mentioned geometry.

5.3 RESULTS and BIOMEDICAL PURPOSE

Tests conducted revealed an increase in mean and maximum flow rate in viscoelastic fluids characterised by shear thinning compared to Newtonian or shear-thickening ones. The flow rate was found to increase with the intensity of the applied force (g_x) and the relaxation time (W_i). The decrease in the latter, together with the increase in the viscosity of the polymeric part (β decreases), appears to result in a more rapid stabilisation of the flow at a steady state.

In addition the flow velocity peaks were found for frequencies slightly higher than the f_0 . It was also noted that this frequency decreases as the relaxation time (W_i) and flow index (n) of the fluid.

Finally, the increase of the duct height (H) decreases the resonance frequency, increasing the maximum and average flow velocity of the fluid in the stationary regime (figure 49).

The so developed model, coupled with the rheological data and interactions information gathered in this work, may be useful in deriving specific strategies for the treatment of patients with respiratory disease.

For example, the knowledge of n and k for COPD, asthma and CF with the designation of a precise zone of the respiratory tract to operate on (H value) can lead to the identification of the most suitable f_0 to treat the patient examined. In addition, knowledge of the interactions developed between components within the lung mucus of sick patients can lead to the use of targeted drugs to modify these interactions. This will indirectly influence the viscoelastic and shear thickening parameters of the mucus to improve expectoration techniques and conditions in accordance with the fluid-dynamic model.

Undoubtedly, the synergy of the information that the two projects are exchanging amplifies their effectiveness and scope in the field of combating respiratory diseases, as it provides a comprehensive view from a biochemical, rheological and fluid-dynamic perspective.

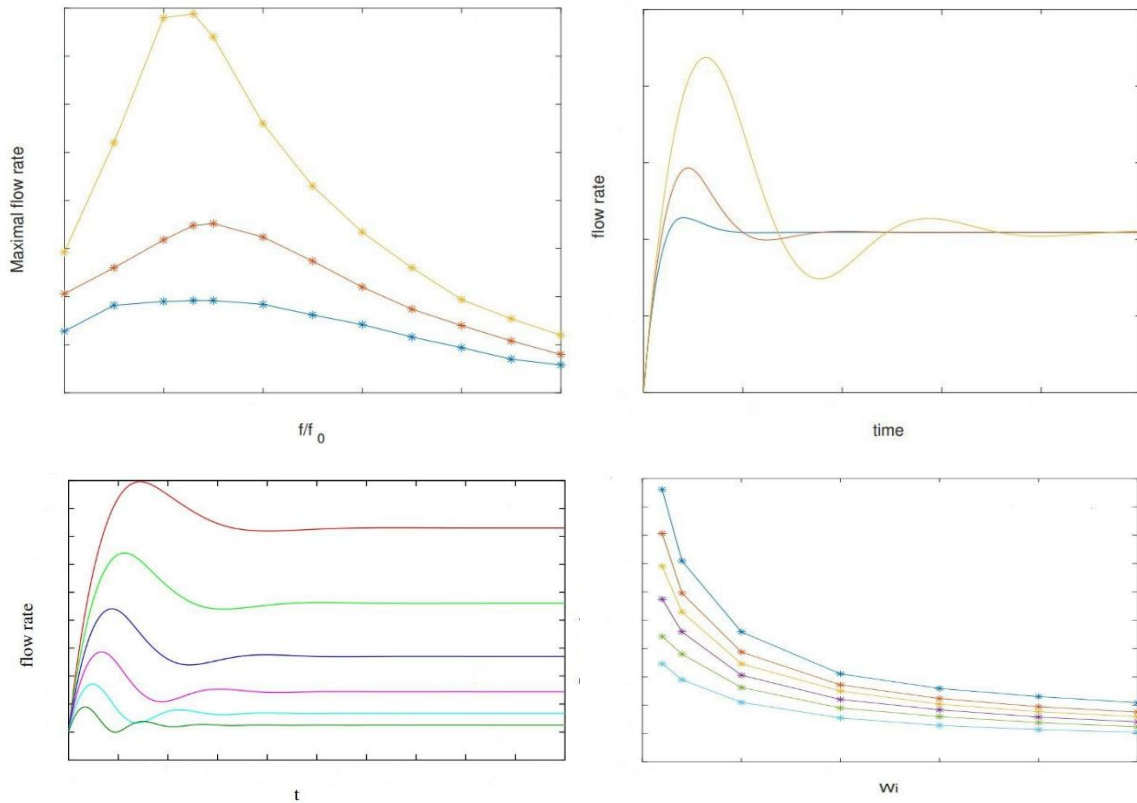


Figure 49 Simulations results of the CFD model for different viscoelastic shier-thinning fluids: 1. Changes of the maximum flow rate at increased values of W_i (in order from blue to yellow) - 2. Flow rate stabilization over time at fixed β and increasing values of W_i (in order blue, rad and yellow) - 3. Flow rate time evaluation at increasing H (in order from dark green to red) - 4. Resonance frequency at W_i increased for decreasing values of n (in order from blue to light blue).

CONCLUSIONS and FUTURE PROSPECTS

The present thesis project gives a contribution to the study of the chemical interactions between components linked to the Non-Newtonian rheological characterisation of bronchial lung mucus.

The bibliographic research carried out on healthy as well as pathologic mucus (patients suffering from COPD, CF and asthma), allowed to classify and quantify the main components of human bronchial mucus. Rheological measurements were carried out on pathological and healthy mucus samples produced by lung epithelial cells grown in the C2VN laboratory in Marseille. Based on SAOS dynamic mean measurements performed on these samples, it was shown that compared to healthy mucus, the elasticity ($G' = 40$ Pa), viscoelasticity ($\tan \delta = 0.43$) and viscoplasticity ($\tau_f = 109$ Pa) can change even by an order of magnitude during pathologies such as asthma ($G' = 900$ Pa, $\tau_f = 514$ Pa and $\tan \delta = 0.23$) or strongly vary in case of smoking habitudes ($G' = 94$ Pa, $\tau_f = 134$ Pa and $\tan \delta = 0.35$). Thanks to this model, it has also been possible to study the change in shear-thinning of a real lung mucus under pathological status. This shows that the consistency index (k) varies accordingly with the viscoplasticity (k goes from a mean value of 40 Pa in a healthy mucus to 46 Pa for the one of a smoker and 56 Pa for an asthmatic mucus), while n (shear-thinning index) did not reveal much significant variations, remaining around the value of 0.35. These results were obtained by implementing a two-level MATLAB R2022AR2022A programme to refine τ_0 , k and n values, preventing a subjective evaluation. The optimization of these parameters has been also completed by minimising the relative error between the actual data and that provided by the model using an excel spreadsheet.

The consistency of the flow curve analysis method was corroborated by the levels of the determination coefficient ($R^2 > 0.7$) found for the reduced experimental data ($\Delta\tau_1(\dot{\gamma})$) fitted by a power law (corresponding to the reduced form of the HB model).

The bibliographic research also allowed to classify the interactions between Gel Forming Mucins, macromolecules, bacteria and DNA and other molecules due to the immune system response in the mucus (disulphide, covalent, oligosaccharide side chains and hydrogen bonds, Van der Waals ionic and extra networks of high-molecular-weight interactions). A classification by chemical affinity (with respect to the actual components) of the main chemical species used since 1997 for lung mucus reconstruction was proposed. This allowed to highlight the main components responsible for the change in mucus rheology (MUC5AC, MUC5B, lipidic fraction, protein fraction and bacterial extracellular coating, AS, Casein Hydrolysis or generic aa, alginate) and to develop three DOEs to determine their respective quantitative influences and interactions on the mucus rheological properties.

Reconstructed mucus prepared in this study shown average elasticity, viscoelasticity and viscoplasticity values within the same ranges as mucus described in the literature and also as mucus analysed during the thesis period corresponding to real samples. The main results of this work show that:

- Alginate component, alone or in interaction with DNA, can increase elasticity and viscoelasticity of the fluid and preferentially binds to MUC5B mucins. This binding appears to strongly increase elasticity, viscoplasticity and shear-thinning of mucus, showing that alginate well simulates the effect of the extracellular polymeric substances secreted by bacterial populations within the mucin network.

- MUC5AC mucin, due to its structure, appears to be linked to the body's immune response to reduce the entanglement between mucus macromolecules via destructive interactions (with MUC5AB and Alginate), leading to a lowering of k , τ_0 , τ_f and G' .
- AS (Artificial surfactant), synthesised and tested for the first time on reconstructed lung mucus, increased the mobility of macromolecules such as Alginate and MUC5B, decreasing viscoplasticity and fluid shear-thinning. This shows how the lipidic components, decreased under pathological conditions such as CF and COPD, are linked to rheological transformation in the lung mucus.
- Fish sperm DNA seems to mimic very well the increase in electrostatic interactions and the formation of Neutrophilic extracellular traps with mucins and alginate, leading to an increase in elasticity, viscoplasticity and shear-thinning of the mucus. The "low molecular weight" DNA from salmon sperm was also tested and should be preferred to fish sperm DNA to mimic extra cellular DNA that is found in the mucus under pathological states. Its presence resulted in an increase of elasticity and viscoplasticity even without interacting with one of the other tested parameters.

The three DOEs allowed to develop reconstruction procedures that, coupled with an excel spreadsheet controlling the w/w % of the solutions, significantly increased the reproducibility of the rheological results (lowering by an order of magnitude the repeatability index R for individual sample). The use of a supporting spreadsheet was also useful to reduce time and material required, but finally to ensure a high degree of macroscopic homogeneity for the individual sample, preventing aging effect (observed and quantified during the analysis process).

The results achieved contribute to determining rheological properties of synthetic airway mucus, while overcoming the problems associated with the small quantity and significant variability (in composition and behaviour) of natural samples. The study of the fluid-dynamic model for the flow of mucus in lungs, developed by the IRN laboratory, then showed how the HB parameters collected in this work can be decisive in determining the resonance frequency f_0 . This opens up new scenarios in the treatment planning of respiratory diseases. Understanding the composition, the chemical interactions, the associated mucus rheology and its fluid-dynamic behaviour, it should be possible to specify chemical and/or mechanical therapeutic treatments designed not only with respect to the underlying pathologies but also specific to each patient under a given pathological state (i.e. to each mucus fluid).

The work done so far could finally be enhanced using the ideas of prospects listed below.

- Increased sampling volume of bronchial mucus (cells cultures) coupled with chemical analysis of their components could enable to establish more and more correlations between symptomatology, composition and changes in rheological characteristics for all the pathologies listed above.
- The further improvement of the CSS test range to better extract the HB parameters coupled with the fluid-dynamic model developed could ensure that each pathology can then be identified with a resonance frequency.
- In the field of reconstruction, the interpretation of the functionality and interactions of the MUC5AC mucin with the other components is of primary importance. In addition, it will be necessary to be able to find a surrogate for the protein component of the mucus, capable not only of reflecting its composition, but also its rheological influence.
- Once the contribution of the protein component is also understood, it will be possible to develop a DOE that can explain the interactions of all components in an interdependent 2 levels $2^n \times n$ optimized phenomenon model with a complete factorial design (where n is the number of components contemporary studied).

THANKSGIVING

I would first like to thank my parents, Elisabetta and Mauro, who more than 25 years ago decided to start a project that goes far beyond this thesis. A project in whose success they perhaps believe more than usual today, as I wave running this piece of paper. I run, yes, towards a tomorrow where my brother Alberto is already waiting for me. I smile embracing him as one who has struggled to return. As one who following bigger footsteps, inspired by the perseverance, tenacity, humanity and character of the bigger in front of which I stand by pare.

I would also like to thank the Politecnico di Torino, which taught me to dream big and made me realise that if you want to do it, you have to rush, know your way around with self knowledge and domain. I would therefore like to present my heartfelt appreciation to the lecturers of the Industrial Chemistry department, because if I can face the reality all around me with curious, aware, critical and proactive eyes, it is also thanks to them. Thanks to their competence, passion and method. Thank you for giving me the opportunity to test myself at a high level, to make me interface with the reality of teaching and business work in a national and international landscape. Thank you for make me believe in how much this Chemical Process Engineering can do for the future of the planet and how much this degree burdens us with responsibility towards future generations.

I would also like to thank my thesis advisor Daniele Marchisio, the M2P2 laboratory in Aix-Marseille and lecturers Isabelle Seyssiecq and Clay Magalie, for giving me the opportunity to participate in an international research project. Thank you for your care and patience, for the time invested and the effort shared.

Thank you all because if I can be proud of who I am today, it is thanks to you. I owe you a lot and I dedicate this work to you.

FIGURES

Figure 1 Free body diagram of the system of two planes moving relative to each other at constant speed and force ¹²	11
Figure 2 The three most important bronchial mucins structure and sections ¹⁹	15
Figure 3 From top to bottom left: Successive enlargements of the surface of the bronchiolar walls ⁵¹ , up to the identification of mucus and periciliary layer (PCL) ¹⁹ and observation by electronic microscope of mucins ²¹ . From top to bottom right: Molecular components of mucins ²² and pattern of interactions in gel-forming mucins (GFMs) ¹² . we distinguish 1. and 5. Van der Waals bonds 2. extra networks of high-molecular-weight 3. Disulphide bonds or covalent bonds 4. Ionic bonds 6. Oligosaccharide side chains and hydrogen bonds.	17
Figure 4 Qualitative table of the change in lung mucus mass composition for different pathologies accompanied by the tracheal sections for each pathology ¹⁰	20
Figure 5 Summary graph of mucus elastic modulus of healthy and asthma, COPD or CF patients. Denoted in grey the mean values and in red the results obtained with the most similar analysis respect the one performed at M2P2 laboratory.....	23
Figure 6 Summary graph of mucus flow point of healthy and asthma, COPD or CF patients. Denoted in grey the mean values and in red the results obtained with the most similar analysis respect the one performed at M2P2 laboratory.....	23
Figure 7 Summary graph of mucus viscoelasticity of healthy and asthma, COPD or CF patients. Denoted in grey the mean values and in red the results obtained with the most similar analysis respect the one performed at M2P2 laboratory.....	24
Figure 8 Variation of Mucins fraction in different sections of the air ways in healthy ⁴² and CF patients ⁶⁰	25
Figure 9 Rheological properties of a mucins aqueous solution (left side) compared to CF real mucus (right side) ²⁸	26
Figure 10 Left side: the comparison between rheological properties of mucins solution (squares) with a mucins-fish sperm DNA one (dots) ²⁸ . Centre: representation of possible links due to the presence of DNA within the mucins ⁴⁹ . Right side: from top to bottom DNA and actine filament obtained from molecular dynamics calculations in conjunction with synchrotron X-ray diffraction experiments ⁴⁷	27
Figure 11 Left side: rheological parameters of a mucins aqueous solution at different alginate concentration (dot) 1.0 mg/mL, (square) 0.8 mg/mL, (triangle) 0.6 mg/mL, (inverted triangle) 0.4 mg/mL and (rhombus) 0.2 mg/mL ²⁸ . Right side from top to bottom : <i>Pseudomonas aeruginosa</i> infection attached to GFMs into the bronchi and model for the interaction between alginate and the double globular comb of mucins ⁵⁵	29
Figure 12 Rheological properties comparison between reconstructed mucus with 0.5% w/w of Xantan gum (blue) and a real CF sample ²⁹	29
Figure 13 Model of normal vs CF airway mucus layer illustrating changes within the mucus network (polymer entanglement, mucin compaction, and/or changes in molecular interactions) in response to altered ionic fluxes ³⁷	30
Figure 14 From top to bottom: Schematic illustration of the proposed effects of the various environmental modifications on the supramolecular structure of the mucin network. The mesoscopic porous structure of the mucin gels is represented by the grey regions. Left side: Description of acidification effect on the structure (increase in disulphide bonds (light blue dots) and hydrophobic interactions (yellow triangles) number) and rheology (increase of elasticity and decrease in viscoelasticity) of the mucus. Right side: Description of cations increase effect on the structure (decrease of repulsion degree between sugar side chains and increasing of folded configuration of the	

mucins non-carboxylate globular part) and rheology (increase of elasticity and decrease in viscoelasticity) of the mucus ⁴³. Centre: Combined effect of increasing environment acidity and salt concentration of a non-CF and CF cultured airway epithelia (middle) ⁵⁶ and in an aqueous mucins solution (bottom) ²¹.31

Figure 15 Structure, coupling and function of the main components of the surfactant fraction of the lung mucus ⁶⁷.33

Figure 16 Structure, coupling and function of the main components of the surfactant fraction of Egg Yolk ⁷⁰.33

Figure 17 Lipids - proteins qualitative repartition in Egg Yolk (respectively grey and white) and in the mucus of people affected by the principal Bronchial pathologies (in this case red for proteins).34

Figure 18 Rheometer with the following details: 1. Coupling of the upper plate 2. Detail of the coupling for maximum efficiency of motor-upper plate coupling 3. Different types of upper plates 4. 6 Atm Pressurized motor for maximum precision and wider range of an36

Figure 19 Response of a viscoelastic sample to an oscillating step forcing function (left) at the end of SAOS analysis (middle) performed by Anton Paar MCR 302 Rheometer coupled with Rheocompass software. Detail of the geometry and operation of the conical and plate top plate under oscillation (right) ⁸⁸.38

Figure 20 Transformation of the internal structure of a viscoelastic sample at the shear stress increase.39

Figure 21 Response of a viscoelastic sample to a rotational step forcing function (left) at the end of CCS analysis (middle) performed by Anton Paar MCR 302 Rheometer coupled with Rheocompass software. Detail of the geometry and operation of the conical and plate top plate under rotation (right)⁸⁸.40

Figure 22 Response of a thixotropic sample to a tree step forcing function (left) at the end of 3ITT analysis (middle) performed by Anton Paar MCR 302 Rheometer coupled with Rheocompass software. Detail of the geometry and operation of the conical and plate top plate top plate under rotation (right) ⁸⁸.41

Figure 23 Photos of the analysis procedure. From left to right: Sample placement on the lower plate and loading of deionized water into the channel. Clamping of the moisture-controlled ambient through half covers and upper dish. Flashing of the upper dish to the analysis.43

Figure 24 Graphical output of the MATLAB R2022a programme used for data analysis. The FLOW CURVE graph shows the flow curve (black line), τ_0 entered by the driver (green dot), τ_0 approximated with the "tan method" (blue asterisk), τ_0 level refined with the second model (red dashed line) and the first approximation of the HB model for the CSS developed with τ_0 , K and n calculated in it (light blue dashed and dotted). The SAOS curve shows the elastic modulus (red line), the viscous modulus (black line), the yield stress (blue cross), the flow point (pink dot) and the τ_0 refined by the CSS analysis (green empty dot).44

Figure 25 Graphical output of the excel spreadsheet for optimising the data parameters K and n. Highlighted are the coefficient of determination (R^2) and the error minimisation option used in the solver.45

Figure 26 Increased mean values (grey dots) of elastic and viscolastic parameters (τ_y , τ_f , τ_0 and G') gained by the SAOS analysis for the bronchial cellular mucous cell of subjects with smoker (COPD) and asthma.....46

Figure 27 Different trend of increase and decrease of the mean value of shear thinning parameters (k and n) gained by the optimization of HB parameters for the bronchial cellular mucous cell of smoker subjects(COPD) and asthmatic one.....47

Figure 28 Increased variability in the results obtained when switching from the lung mucus of a healthy to a diseased subject (left) and from SAOS analysis to HB model fitting (right).47

Figure 29 Similarity of the mean value (grey dots) of the degree and level of viscoelasticity of healthy, smoker (COPD) and asthmatic cellular lungs mucus, compared to what is reported in the literature (red dots).	48
Figure 30 AZURAD Loop steps of a DOE for three factors (DNA, Alginate and Egg Yolk), two level complete factorial matrix and evaluation of effects and interactions plot for one of the four parameters considered (τ_0 , k , n , G').	50
Figure 31 SAOS test comparison for two w/w equal percentage mucins aqueous solutions performed at M2P2 laboratory (left) and reported by literature (right) ²⁸	51
Figure 32 SAOS test comparison of reconstructed mucus with (red) and without (grey) DIETHYL _{sol0.5M} (left) o with (red) and without (grey) thermal treatment at high DIETHYL _{sol0.5M} concentrations (1.18 w/w %).	53
Figure 33 R limit Comparison for the most important rheological parameters of DOE 1 (grey) and 2 (white).	56
Figure 34 Comparison of the representative parameters for which has been possible to identify a range compressive of CF asthma and COPD gained by chapter 3 (white) and the DOE 1 ones (grey dots).	57
Figure 35 Effect plot of k , τ_0 and $\tan\delta$ for the DOE 1.	57
Figure 36 Interaction plot for k , τ_0 and $\tan\delta$ for the DOE 1.	58
Figure 37 Graphs between the values reported experimentally (x-axis) and those processed by the interactional model (y-axis) for k , τ_0 and $\tan\delta$ for the DOE 1.	58
Figure 38 Comparison of the representative parameters for which has been possible to identify a range compressive of CF Asthma and COPD gained by chapter 3 (white), the DOE 1 (grey dots) and the DOE 2 ones (red dots).	59
Figure 39 Effect plot of G' , G'' and $\tan\delta$ for the DOE 2.	59
Figure 40 Effect and b_{45} (MUC5AC-Alginate), b_{25} (MUC5AC- MUCB) interaction plot of k , τ_0 , τf for the DOE 2.	60
Figure 41 b_{14} (DNA - MUC5B) and b_{15} (DNA - MUC5AC) interaction plot of G' , k , τf and τ_0 for the DOE 2.	61
Figure 42 Representative b_{23} (Alginate-AS), b_{34} (AS - MUCB) and b_{13} (DNA-AS) interaction plot of k (but also τf) for the DOE 2.	61
Figure 43 From left to right: b_{15} (DNA - MUC5AC) interaction plot of G'' for the DOE 2, effect plot of n for the DOE 1, effect plot of n for the DOE 2.	62
Figure 44 b_{24} (Alginate - MUC5B) interaction plot of G' , k , τf and τ_0 for the DOE 2.	62
Figure 45 Graphs between the values reported experimentally (x-axis) and those processed by the interactional model (y-axis) for G' , G'' , k , τ_0 , τf and $\tan\delta$ for the DOE 2.	63
Figure 46 Comparison of the representative parameters for which has been possible to identify a range compressive of CF asthma and COPD gained by chapter 3 (white dots), the DOE 2 (grey dots) and the DOE 3 ones (red dots).	64
Figure 47 Percentage increase in Elasticity (G') and viscoplasticity of reconstructed mucus at Salmon sperm DNA increase at constant mucins level (white bars), at increased level of MUC5AC (red bars) and at increased level of MUC5B (grey bars).	64
Figure 48 Geometry of CFD simulations	67
Figure 49 Simulations results of the CFD model for different viscoelastic shier-thinning fluids: 1. Changes of the maximum flow rate at increased values of Wi (in order from blue to yellow) - 2. Flow rate stabilization over time at fixed β and increasing values of Wi (in order blue, rad and yellow) - 3. Flow rate time evaluation at increasing H (in order from dark green to red) - 4. Resonance frequency at Wi increased for decreasing values of n (in order from blue to light blue).	70

TABLES

Table 1 Composition of healthy bronchial mucus.....	19
Table 2 Rheological parameters of healthy bronchial mucus.....	19
Table 3 Composition of COPD bronchial mucus	20
Table 4 Rheological parameters of COPD bronchial mucus.....	21
Table 5 Composition of CF bronchial mucus	21
Table 6 Rheological parameters of CF bronchial mucus.....	21
Table 7 Composition of Asthmatic bronchial mucus.....	22
Table 8 Rheological parameters of CF bronchial mucus.....	22
Table 9 Summary table resulting from the combination of the rheological parameter data	48
Table 10 Composition of reconstructed mucus in DOE 1	52
Table 11 Composition of reconstructed mucus in DOE 2	54
Table 12 Composition of reconstructed mucus in DOE 2	55

ANNEXES

1. Procedure for calibrating and commissioning the MCR 302 rheometer.
2. MATLAB R2022a data analysis programme.
3. Rheological analysis results of nasal asthmatic mucus.
4. Bibliographical research and comparison on the chemical composition, interactions and the rheological characteristics of components between the real and reconstructed pulmonary mucosa (both of healthy subjects and affected by respiratory pathologies).
5. Main recipes for pulmonary reconstructed mucosa without bacterial culture development.
6. DOE 1
7. DOE 2
8. DOE 3

BIBLIOGRAPHY

- (1) The Global Asthma Report 2022. *int j tuberc lung dis* **2022**, *26* (1), 1–104. <https://doi.org/10.5588/ijtld.22.1010>.
- (2) Guo, J.; Garratt, A.; Hill, A. Worldwide Rates of Diagnosis and Effective Treatment for Cystic Fibrosis. *Journal of Cystic Fibrosis* **2022**, *21* (3), 456–462. <https://doi.org/10.1016/j.jcf.2022.01.009>.
- (3) Watase, M.; Masaki, K.; Chubachi, S.; Namkoong, H.; Tanaka, H.; Lee, H.; Fukushima, T.; Otake, S.; Nakagawara, K.; Kusumoto, T.; Asakura, T.; Kamata, H.; Ishii, M.; Hasegawa, N.; Oyamada, Y.; Harada, N.; Ueda, T.; Ueda, S.; Ishiguro, T.; Arimura, K.; Saito, F.; Yoshiyama, T.; Nakano, Y.; Mutoh, Y.; Suzuki, Y.; Eda, H.; Sano, H.; Sato, Y.; Okada, Y.; Koike, R.; Kitagawa, Y.; Tokunaga, K.; Kimura, A.; Imoto, S.; Miyano, S.; Ogawa, S.; Kanai, T.; Fukunaga, K. Impact of Accumulative Smoking Exposure and Chronic Obstructive Pulmonary Disease on COVID-19 Outcomes: Report Based on Findings from the Japan COVID-19 Task Force. *International Journal of Infectious Diseases* **2023**, *128*, 121–127. <https://doi.org/10.1016/j.ijid.2022.12.019>.
- (4) Chow, Y. W.; Pietranico, R.; Mukerji, A. Studies of Oxygen Binding Energy to Hemoglobin Molecule. *Biochem Biophys Res Commun* **1975**, *66* (4), 1424–1431. [https://doi.org/10.1016/0006-291x\(75\)90518-5](https://doi.org/10.1016/0006-291x(75)90518-5).
- (5) Bucens, D.; Pain, M. C. Influence of Hematocrit, Blood Gas Tensions, and PH on Pressure-Flow Relations in the Isolated Canine Lung. *Circ Res* **1975**, *37* (5), 588–596. <https://doi.org/10.1161/01.res.37.5.588>.
- (6) Tambascio, J.; De Souza, L. T.; Lisboa, R. M.; Passarelli, R. D. C. V.; De Souza, H. C. D.; Gastaldi, A. C. The Influence of Flutter®VRP1 Components on Mucus Transport of Patients with Bronchiectasis. *Respiratory Medicine* **2011**, *105* (9), 1316–1321. <https://doi.org/10.1016/j.rmed.2011.04.017>.
- (7) Luo, M.; Ni, K.; Sun, Y.; Guo, J.; Wen, K.; Deng, L. Toward an Optimized Strategy of Using Various Airway Mucus Clearance Techniques to Treat Critically Ill COVID-19 Patients. *BIOCELL* **2022**, *46* (4), 855–871. <https://doi.org/10.32604/biocell.2022.017520>.
- (8) Thornton, D. J. From Mucins to Mucus: Toward a More Coherent Understanding of This Essential Barrier. *Proceedings of the American Thoracic Society* **2004**, *1* (1), 54–61. <https://doi.org/10.1513/pats.2306016>.
- (9) Chanez, P. Severe Asthma Is an Epithelial Disease. *European Respiratory Journal* **2005**, *25* (6), 945–946. <https://doi.org/10.1183/09031936.05.00038605>.
- (10) Fahy, J. V.; Dickey, B. F. Airway Mucus Function and Dysfunction. *N Engl J Med* **2010**, *363* (23), 2233–2247. <https://doi.org/10.1056/NEJMra0910061>.
- (11) Frisch, S.; Boese, A.; Huck, B.; Horstmann, J. C.; Ho, D.-K.; Schwarzkopf, K.; Murgia, X.; Loretz, B.; De Souza Carvalho-Wodarz, C.; Lehr, C.-M. A Pulmonary Mucus Surrogate for Investigating Antibiotic Permeation and Activity against *Pseudomonas Aeruginosa* Biofilms. *Journal of Antimicrobial Chemotherapy* **2021**, *76* (6), 1472–1479. <https://doi.org/10.1093/jac/dkab068>.
- (12) King, M. MUCUS AND ITS ROLE IN AIRWAY CLEARANCE AND CYTOPROTECTION.
- (13) Lafforgue, O. Rheology of Bronchial Mucus: Characterization and Modeling for Clearance Helping by a Medical Device. **2018**.
- (14) Fox, R. W.; Pritchard, P. J.; McDonald, A. T.; Leylegian, J. C. *Fluid Mechanics*, 8th ed., SI version.; John Wiley: Hoboken, NJ, **2012**.
- (15) Elert, G. Viscosity. In *The Physics Hypertextbook*; hypertextbook, 2021.
- (16) Batra, R. C.; Kim, C. H. Effect of Viscoplastic Flow Rules on the Initiation and Growth of Shear Bands at High Strain Rates. *Journal of the Mechanics and Physics of Solids* **1990**, *38* (6), 859–874. [https://doi.org/10.1016/0022-5096\(90\)90043-4](https://doi.org/10.1016/0022-5096(90)90043-4).
- (17) Mewis, J.; Wagner, N. J. Thixotropy. *Advances in Colloid and Interface Science* **2009**, *147–148*, 214–227. <https://doi.org/10.1016/j.cis.2008.09.005>.

- (18) Meyers, M. A.; Chawla, K. K. *Mechanical Behavior of Materials*, 2nd ed.; Cambridge University Press: Cambridge ; New York, **2009**.
- (19) Huck, B. C.; Murgia, X.; Frisch, S.; Hittinger, M.; Hidalgo, A.; Loretz, B.; Lehr, C.-M. Models Using Native Tracheobronchial Mucus in the Context of Pulmonary Drug Delivery Research: Composition, Structure and Barrier Properties. *Advanced Drug Delivery Reviews* **2022**, *183*, 114141. <https://doi.org/10.1016/j.addr.2022.114141>.
- (20) Patarin, J.; Ghiringhelli, É.; Darsy, G.; Obamba, M.; Bochu, P.; Camara, B.; Quétant, S.; Cracowski, J.-L.; Cracowski, C.; Robert De Saint Vincent, M. Rheological Analysis of Sputum from Patients with Chronic Bronchial Diseases. *Sci Rep* **2020**, *10* (1), 15685. <https://doi.org/10.1038/s41598-020-72672-6>.
- (21) Curnutt, A.; Smith, K.; Darrow, E.; Walters, K. B. Chemical and Microstructural Characterization of PH and [Ca²⁺] Dependent Sol-Gel Transitions in Mucin Biopolymer. *Sci Rep* **2020**, *10* (1), 8760. <https://doi.org/10.1038/s41598-020-65392-4>.
- (22) Kruger, A. G.; Brucks, S. D.; Yan, T.; Cárcarmo-Oyarce, G.; Wei, Y.; Wen, D. H.; Carvalho, D. R.; Hore, M. J. A.; Ribbeck, K.; Schrock, R. R.; Kiessling, L. L. Stereochemical Control Yields Mucin Mimetic Polymers. *ACS Cent. Sci.* **2021**, *7* (4), 624–630. <https://doi.org/10.1021/acscentsci.0c01569>.
- (23) Serisier, D. J.; Carroll, M. P.; Shute, J. K.; Young, S. A. Macrorheology of Cystic Fibrosis, Chronic Obstructive Pulmonary Disease & Normal Sputum. *Respir Res* **2009**, *10* (1), 63. <https://doi.org/10.1186/1465-9921-10-63>.
- (24) Patarin, J.; Ghiringhelli, E.; Camara, B.; Quétant, S.; Bosc, C.; Pison, C.; Cracowski, J.-L. CHANGE OF MUCUS RHEOLOGY IN PATIENTS WITH CYSTIC FIBROSIS, COPD AND ASTHMA DIAGNOSIS **2019**.
- (25) Kirkham, S.; Sheehan, J. K.; Knight, D.; Richardson, P. S.; Thornton, D. J. Heterogeneity of Airways Mucus : Variations in the Amounts and Glycoforms of the Major Oligomeric Mucins MUC5AC and MUC5B. **2002**.
- (26) Tunney, M. M.; Field, T. R.; Moriarty, T. F.; Patrick, S.; Doering, G.; Muhlebach, M. S.; Wolfgang, M. C.; Boucher, R.; Gilpin, D. F.; McDowell, A.; Elborn, J. S. Detection of Anaerobic Bacteria in High Numbers in Sputum from Patients with Cystic Fibrosis. *Am J Respir Crit Care Med* **2008**, *177* (9), 995–1001. <https://doi.org/10.1164/rccm.200708-1151OC>.
- (27) Piva, T. C.; Luft, C.; Antunes, K. H.; Marostica, P. J. C.; Pinto, L. A.; Donadio, M. V. F. Extracellular DNA in Sputum Is Associated with Pulmonary Function and Hospitalization in Patients with Cystic Fibrosis. *Respiratory Medicine* **2020**, *172*, 106144. <https://doi.org/10.1016/j.rmed.2020.106144>.
- (28) Nordgård, C. T.; Draget, K. I. Oligosaccharides As Modulators of Rheology in Complex Mucous Systems. *Biomacromolecules* **2011**, *12* (8), 3084–3090. <https://doi.org/10.1021/bm200727c>.
- (29) Tan, M.; Mao, Y.; Walker, T. W. Rheological Enhancement of Artificial Sputum Medium. *Applied Rheology* **2020**, *30* (1), 27–38. <https://doi.org/10.1515/arh-2020-0100>.
- (30) Huck, B. C.; Hartwig, O.; Biehl, A.; Schwarzkopf, K.; Wagner, C.; Loretz, B.; Murgia, X.; Lehr, C.-M. Macro- and Microrheological Properties of Mucus Surrogates in Comparison to Native Intestinal and Pulmonary Mucus. *Biomacromolecules* **2019**, *20* (9), 3504–3512. <https://doi.org/10.1021/acs.biomac.9b00780>.
- (31) Sriramulu, D. D.; Lünsdorf, H.; Lam, J. S.; Römling, U. Microcolony Formation: A Novel Biofilm Model of Pseudomonas Aeruginosa for the Cystic Fibrosis Lung. *Journal of Medical Microbiology* **2005**, *54* (7), 667–676. <https://doi.org/10.1099/jmm.0.45969-0>.
- (32) Aiyer, A.; Manos, J. The Use of Artificial Sputum Media to Enhance Investigation and Subsequent Treatment of Cystic Fibrosis Bacterial Infections. *Microorganisms* **2022**, *10* (7), 1269. <https://doi.org/10.3390/microorganisms10071269>.
- (33) Taylor, C.; Pearson, J.; Draget, K.; Dettmar, P.; Smidsrod, O. Rheological Characterisation of Mixed Gels of Mucin and Alginate. *Carbohydrate Polymers* **2005**, *59* (2), 189–195. <https://doi.org/10.1016/j.carbpol.2004.09.009>.
- (34) Hamilton, L. D.; Barclay, R. K.; Wilkins, M. H. F.; Brown, G. L.; Wilson, H. R.; Marvin, D. A.; Ephrussi-Taylor, H.; Simmons, N. S. Similarity of the Structure of DNA from a Variety of Sources. *The Journal of Biophysical and Biochemical Cytology* **1959**, *5* (3), 397–404.

- (35) Joo, N. S.; Evans, I. A. T.; Cho, H.-J.; Park, I.-H.; Engelhardt, J. F.; Wine, J. J. Proteomic Analysis of Pure Human Airway Gland Mucus Reveals a Large Component of Protective Proteins. *PLoS ONE* **2015**, *10* (2), e0116756. <https://doi.org/10.1371/journal.pone.0116756>.
- (36) Carpenter, J.; Wang, Y.; Gupta, R.; Li, Y.; Haridass, P.; Subramani, D. B.; Reidel, B.; Morton, L.; Ridley, C.; O'Neal, W. K.; Buisine, M.-P.; Ehre, C.; Thornton, D. J.; Kesimer, M. Assembly and Organization of the N-Terminal Region of Mucin MUC5AC: Indications for Structural and Functional Distinction from MUC5B. *Proc. Natl. Acad. Sci. U.S.A.* **2021**, *118* (39), e2104490118. <https://doi.org/10.1073/pnas.2104490118>.
- (37) Morrison, C. B.; Markovetz, M. R.; Ehre, C. Mucus, Mucins, and Cystic Fibrosis. *Pediatr Pulmonol* **2019**, *54* (S3). <https://doi.org/10.1002/ppul.24530>.
- (38) Niv, Y.; Ho, S. B.; Rokkas, T. Mucin Secretion in Cystic Fibrosis: A Systematic Review. *Dig Dis* **2021**, *39* (4), 375–381. <https://doi.org/10.1159/000512268>.
- (39) Ridley, C.; Thornton, D. J. Mucins: The Frontline Defence of the Lung. *Biochemical Society Transactions* **2018**, *46* (5), 1099–1106. <https://doi.org/10.1042/BST20170402>.
- (40) McGuire, J. F. Surfactant in the Middle Ear and Eustachian Tube: A Review. *International Journal of Pediatric Otorhinolaryngology* **2002**, *66* (1), 1–15. [https://doi.org/10.1016/S0165-5876\(02\)00203-3](https://doi.org/10.1016/S0165-5876(02)00203-3).
- (41) Chiang, W.-C.; Nilsson, M.; Jensen, P. Ø.; Høiby, N.; Nielsen, T. E.; Givskov, M.; Tolker-Nielsen, T. Extracellular DNA Shields against Aminoglycosides in *Pseudomonas Aeruginosa* Biofilms. *Antimicrob Agents Chemother* **2013**, *57* (5), 2352–2361. <https://doi.org/10.1128/AAC.00001-13>.
- (42) Okuda, K.; Chen, G.; Subramani, D. B.; Wolf, M.; Gilmore, R. C.; Kato, T.; Radicioni, G.; Kesimer, M.; Chua, M.; Dang, H.; Livraghi-Butrico, A.; Ehre, C.; Doerschuk, C. M.; Randell, S. H.; Matsui, H.; Nagase, T.; O'Neal, W. K.; Boucher, R. C. Localization of Secretory Mucins MUC5AC and MUC5B in Normal/Healthy Human Airways. *Am J Respir Crit Care Med* **2019**, *199* (6), 715–727. <https://doi.org/10.1164/rccm.201804-0734OC>.
- (43) Wagner, C. E.; Turner, B. S.; Rubinstein, M.; McKinley, G. H.; Ribbeck, K. A Rheological Study of the Association and Dynamics of MUC5AC Gels. *Biomacromolecules* **2017**, *18* (11), 3654–3664. <https://doi.org/10.1021/acs.biomac.7b00809>.
- (44) Bonser, L.; Erle, D. Airway Mucus and Asthma: The Role of MUC5AC and MUC5B. *JCM* **2017**, *6* (12), 112. <https://doi.org/10.3390/jcm6120112>.
- (45) Henke, M. O.; Renner, A.; Huber, R. M.; Seeds, M. C.; Rubin, B. K. MUC5AC and MUC5B Mucins Are Decreased in Cystic Fibrosis Airway Secretions. *Am J Respir Cell Mol Biol* **2004**, *31* (1), 86–91. <https://doi.org/10.1165/rcmb.2003-0345OC>.
- (46) Cozens, E. J.; Roohpour, N.; Gautrot, J. E. Comparative Adhesion of Chemically and Physically Crosslinked Poly(Acrylic Acid)-Based Hydrogels to Soft Tissues. *European Polymer Journal* **2021**, *146*, 110250. <https://doi.org/10.1016/j.eurpolymj.2020.110250>.
- (47) Wong, G. C. L.; Pollack, L. Electrostatics of Strongly Charged Biological Polymers: Ion-Mediated Interactions and Self-Organization in Nucleic Acids and Proteins. *Annu. Rev. Phys. Chem.* **2010**, *61* (1), 171–189. <https://doi.org/10.1146/annurev.physchem.58.032806.104436>.
- (48) Severa, L.; Nedomová, Š.; Křivánek, I.; Buchar, J. Rheological Properties of Ageing Egg Yolk. *Acta Univ. Agric. Silvic. Mendelianae Brun.* **2014**, *53* (4), 127–138. <https://doi.org/10.11118/actaun200553040127>.
- (49) Linssen, R. S.; Chai, G.; Ma, J.; Kummarapurugu, A. B.; Van Woensel, J. B. M.; Bem, R. A.; Kaler, L.; Duncan, G. A.; Zhou, L.; Rubin, B. K.; Xu, Q. Neutrophil Extracellular Traps Increase Airway Mucus Viscoelasticity and Slow Mucus Particle Transit. *Am J Respir Cell Mol Biol* **2021**, *64* (1), 69–78. <https://doi.org/10.1165/rcmb.2020-0168OC>.
- (50) Mulcahy, H.; Charron-Mazenod, L.; Lewenza, S. *Pseudomonas Aeruginosa* Produces an Extracellular Deoxyribonuclease That Is Required for Utilization of DNA as a Nutrient Source. *Environmental Microbiology* **2010**. <https://doi.org/10.1111/j.1462-2920.2010.02208.x>.

- (51) Bucki, R.; Byfield, F. J.; Janmey, P. A. Release of the Antimicrobial Peptide LL-37 from DNA/F-Actin Bundles in Cystic Fibrosis Sputum. *European Respiratory Journal* **2007**, *29* (4), 624–632. <https://doi.org/10.1183/09031936.00080806>.
- (52) Okuda, K.; Shaffer, K. M.; Ehre, C. Mucins and CFTR: Their Close Relationship. *IJMS* **2022**, *23* (18), 10232. <https://doi.org/10.3390/ijms231810232>.
- (53) Brandt, T.; Breitenstein, S.; Von Der Hardt, H.; Tummler, B. DNA Concentration and Length in Sputum of Patients with Cystic Fibrosis during Inhalation with Recombinant Human DNase. *Thorax* **1995**, *50* (8), 880–882. <https://doi.org/10.1136/thx.50.8.880>.
- (54) Lethem, M.; James, S.; Marriott, C.; Burke, J. The Origin of DNA Associated with Mucus Glycoproteins in Cystic Fibrosis Sputum. *Eur Respir J* **1990**, *3* (1), 19–23. <https://doi.org/10.1183/09031936.93.03010019>.
- (55) Menchicchi, B.; Fuenzalida, J. P.; Hensel, A.; Swamy, M. J.; David, L.; Rochas, C.; Goycoolea, F. M. Biophysical Analysis of the Molecular Interactions between Polysaccharides and Mucin. *Biomacromolecules* **2015**, *16* (3), 924–935. <https://doi.org/10.1021/bm501832y>.
- (56) Tang, X. X.; Ostedgaard, L. S.; Hoegger, M. J.; Moninger, T. O.; Karp, P. H.; McMenimen, J. D.; Choudhury, B.; Varki, A.; Stoltz, D. A.; Welsh, M. J. Acidic PH Increases Airway Surface Liquid Viscosity in Cystic Fibrosis. *Journal of Clinical Investigation* **2016**, *126* (3), 879–891. <https://doi.org/10.1172/JCI83922>.
- (57) Duggan, S. The Synthesis and Characterisation of Mucoadhesive Polymeric Systems Using Synthetic and Natural Polymers, **2015**.
- (58) Rossi, S. Influence of Mucin Type on Polymer-Mucin Rheological Interactions. *Biomaterials* **1995**, *16* (14), 1073–1079. [https://doi.org/10.1016/0142-9612\(95\)98903-R](https://doi.org/10.1016/0142-9612(95)98903-R).
- (59) Lennox, A. T.; Coburn, S. L.; Leech, J. A.; Heidrich, E. M.; Kleyman, T. R.; Wenzel, S. E.; Pilewski, J. M.; Corcoran, T. E.; Myerburg, M. M. ATP12A Promotes Mucus Dysfunction during Type 2 Airway Inflammation. *Sci Rep* **2018**, *8* (1), 2109. <https://doi.org/10.1038/s41598-018-20444-8>.
- (60) Batson, B. AIRWAY MUCIN DYNAMICS IN INFECTION AND INFLAMMATION **2019**.
- (61) Patel, M. M.; Smart, J. D.; Nevell, T. G.; Ewen, R. J.; Eaton, P. J.; Tsibouklis, J. Mucin/Poly(Acrylic Acid) Interactions: A Spectroscopic Investigation of Mucoadhesion. *Biomacromolecules* **2003**, *4* (5), 1184–1190. <https://doi.org/10.1021/bm034028p>.
- (62) Hill, D. B.; Long, R. F.; Kissner, W. J.; Atieh, E.; Garbarine, I. C.; Markovetz, M. R.; Fontana, N. C.; Christy, M.; Habibpour, M.; Tarran, R.; Forest, M. G.; Boucher, R. C.; Button, B. Pathological Mucus and Impaired Mucus Clearance in Cystic Fibrosis Patients Result from Increased Concentration, Not Altered PH. *Eur Respir J* **2018**, *52* (6), 1801297. <https://doi.org/10.1183/13993003.01297-2018>.
- (63) Leitner, V. M.; Walker, G. F.; Bernkop-Schnürch, A. Thiolated Polymers: Evidence for the Formation of Disulphide Bonds with Mucus Glycoproteins. *European Journal of Pharmaceutics and Biopharmaceutics* **2003**, *56* (2), 207–214. [https://doi.org/10.1016/S0939-6411\(03\)00061-4](https://doi.org/10.1016/S0939-6411(03)00061-4).
- (64) Dawson, M.; Wirtz, D.; Hanes, J. Enhanced Viscoelasticity of Human Cystic Fibrotic Sputum Correlates with Increasing Microheterogeneity in Particle Transport. *Journal of Biological Chemistry* **2003**, *278* (50), 50393–50401. <https://doi.org/10.1074/jbc.M309026200>.
- (65) Kočevár-Nared, J.; Kristl, J.; Šmid-Korbar, J. Comparative Rheological Investigation of Crude Gastric Mucin and Natural Gastric Mucus. *Biomaterials* **1997**, *18* (9), 677–681. [https://doi.org/10.1016/S0142-9612\(96\)00180-9](https://doi.org/10.1016/S0142-9612(96)00180-9).
- (66) Safiri, S.; Carson-Chahhoud, K.; Noori, M.; Nejadghaderi, S. A.; Sullman, M. J. M.; Ahmadian Heris, J.; Ansarin, K.; Mansournia, M. A.; Collins, G. S.; Kolahi, A.-A.; Kaufman, J. S. Burden of Chronic Obstructive Pulmonary Disease and Its Attributable Risk Factors in 204 Countries and Territories, 1990-2019: Results from the Global Burden of Disease Study 2019. *BMJ* **2022**, e069679. <https://doi.org/10.1136/bmj-2021-069679>.
- (67) Parra, E.; Pérez-Gil, J. Composition, Structure and Mechanical Properties Define Performance of Pulmonary Surfactant Membranes and Films. *Chemistry and Physics of Lipids* **2015**, *185*, 153–175. <https://doi.org/10.1016/j.chemphyslip.2014.09.002>.

- (68) Donnelly, R. F.; McCarron, P. A.; Cassidy, C. M.; Elborn, J. S.; Tunney, M. M. Delivery of Photosensitisers and Light through Mucus: Investigations into the Potential Use of Photodynamic Therapy for Treatment of *Pseudomonas Aeruginosa* Cystic Fibrosis Pulmonary Infection. *Journal of Controlled Release* **2007**, *117* (2), 217–226. <https://doi.org/10.1016/j.jconrel.2006.11.010>.
- (69) Guilmineau, F.; Krause, I.; Kulozik, U. Efficient Analysis of Egg Yolk Proteins and Their Thermal Sensitivity Using Sodium Dodecyl Sulfate Polyacrylamide Gel Electrophoresis under Reducing and Nonreducing Conditions. *J. Agric. Food Chem.* **2005**, *53* (24), 9329–9336. <https://doi.org/10.1021/jf050475f>.
- (70) Anton, M. Egg Yolk: Structures, Functionalities and Processes: Egg Yolk: Structures, Functionalities and Processes. *J. Sci. Food Agric.* **2013**, *93* (12), 2871–2880. <https://doi.org/10.1002/jsfa.6247>.
- (71) Griese, M.; Essl, R.; Schmidt, R.; Rietschel, E.; Ratjen, F.; Ballmann, M.; Paul, K. Pulmonary Surfactant, Lung Function, and Endobronchial Inflammation in Cystic Fibrosis. *Am J Respir Crit Care Med* **2004**, *170* (9), 1000–1005. <https://doi.org/10.1164/rccm.200405-575OC>.
- (72) Mander, A.; Langton-Hewer, S.; Bernhard, W.; Warner, J. O.; Postle, A. D. Altered Phospholipid Composition and Aggregate Structure of Lung Surfactant Is Associated with Impaired Lung Function in Young Children with Respiratory Infections. *Am J Respir Cell Mol Biol* **2002**, *27* (6), 714–721. <https://doi.org/10.1165/rcmb.4746>.
- (73) Seidl, E.; Kiermeier, H.; Liebisch, G.; Ballmann, M.; Hesse, S.; Paul-Buck, K.; Ratjen, F.; Rietschel, E.; Griese, M. Lavage Lipidomics Signatures in Children with Cystic Fibrosis and Protracted Bacterial Bronchitis. *Journal of Cystic Fibrosis* **2019**, *18* (6), 790–795. <https://doi.org/10.1016/j.jcf.2019.04.012>.
- (74) Diraviam Dinesh, S.; Diraviam Dinesh, S. Artificial Sputum Medium. *Protocol Exchange* **2010**. <https://doi.org/10.1038/protex.2010.212>.
- (75) Ramanathan, R.; Biniwale, M.; Sekar, K.; Hanna, N.; Golombek, S.; Bhatia, J.; Naylor, M.; Fabbri, L.; Varoli, G.; Santoro, D.; Del Buono, D.; Piccinno, A.; Dammann, C. E. Synthetic Surfactant CHF5633 Compared with Poractant Alfa in the Treatment of Neonatal Respiratory Distress Syndrome: A Multicenter, Double-Blind, Randomized, Controlled Clinical Trial. *The Journal of Pediatrics* **2020**, *225*, 90–96.e1. <https://doi.org/10.1016/j.jpeds.2020.06.024>.
- (76) Seehase, M.; Collins, J. J. P.; Kuypers, E.; Jellema, R. K.; Ophelders, D. R. M. G.; Ospina, O. L.; Perez-Gil, J.; Bianco, F.; Garzia, R.; Razzetti, R.; Kramer, B. W. New Surfactant with SP-B and C Analogs Gives Survival Benefit after Inactivation in Preterm Lambs. *PLoS ONE* **2012**, *7* (10), e47631. <https://doi.org/10.1371/journal.pone.0047631>.
- (77) *Development of Novel Synthetic Lung Surfactants for Treatment of Respiratory Distress Syndrome*; Karolinska Institutet: Stockholm, **2020**.
- (78) Markovetz, M. R.; Garbarine, I. C.; Morrison, C. B.; Kissner, W. J.; Seim, I.; Forest, M. G.; Papanikolas, M. J.; Freeman, R.; Ceppe, A.; Ghio, A.; Alexis, N. E.; Stick, S. M.; Ehre, C.; Boucher, R. C.; Esther, C. R.; Muhlebach, M. S.; Hill, D. B. Mucus and Mucus Flake Composition and Abundance Reflect Inflammatory and Infection Status in Cystic Fibrosis. *Journal of Cystic Fibrosis* **2022**, *21* (6), 959–966. <https://doi.org/10.1016/j.jcf.2022.04.008>.
- (79) Lecaille, F.; Lalmanach, G.; Andrault, P.-M. Antimicrobial Proteins and Peptides in Human Lung Diseases: A Friend and Foe Partnership with Host Proteases. *Biochimie* **2016**, *122*, 151–168. <https://doi.org/10.1016/j.biochi.2015.08.014>.
- (80) Reddy, K. V. R.; Yedery, R. D.; Aranha, C. Antimicrobial Peptides: Premises and Promises. *International Journal of Antimicrobial Agents* **2004**, *24* (6), 536–547. <https://doi.org/10.1016/j.ijantimicag.2004.09.005>.
- (81) Kiosseoglou, V. Egg Yolk Protein Gels and Emulsions. *Current Opinion in Colloid and Interface Science* **2003**.
- (82) Reid, D. W.; Carroll, V.; O'May, C.; Champion, A.; Kirov, S. M. Increased Airway Iron as a Potential Factor in the Persistence of *Pseudomonas Aeruginosa* Infection in Cystic Fibrosis. *European Respiratory Journal* **2007**, *30* (2), 286–292. <https://doi.org/10.1183/09031936.00154006>.

- (83) Lim, A. S. L.; Fenelon, M. A.; McCarthy, N. A. Physicochemical Properties and Issues Associated with Trypsin Hydrolyses of Bovine Casein-Dominant Protein Ingredients. *International Dairy Journal* **2019**, *97*, 111–119. <https://doi.org/10.1016/j.idairyj.2019.05.014>.
- (84) Fung, C.; Naughton, S.; Turnbull, L.; Tingpej, P.; Rose, B.; Arthur, J.; Hu, H.; Harmer, C.; Harbour, C.; Hassett, D. J.; Whitchurch, C. B.; Manos, J. Gene Expression of *Pseudomonas Aeruginosa* in a Mucin-Containing Synthetic Growth Medium Mimicking Cystic Fibrosis Lung Sputum. *Journal of Medical Microbiology* **2010**, *59* (9), 1089–1100. <https://doi.org/10.1099/jmm.0.019984-0>.
- (85) Barth, A. L.; Pitt, T. L. The High Amino-Acid Content of Sputum from Cystic Fibrosis Patients Promotes Growth of Auxotrophic *Pseudomonas Aeruginosa*. *Journal of Medical Microbiology* **1996**, *45* (2), 110–119. <https://doi.org/10.1099/00222615-45-2-110>.
- (86) Elkatatny, S. Evaluating the Chemical Reaction of Chelating Agents with Xanthan Gum. *Arab J Sci Eng* **2017**, *42* (4), 1427–1434. <https://doi.org/10.1007/s13369-016-2299-8>.
- (87) Anton Paar MCR. Modular Compact Rheometer Series.Pdf, **2018**.
- (88) Malvenr Instruments Limited, A Basic Introduction to Rheology.Pdf, 2016.
- (89) Lubliner, J. *Plasticity Theory*, Dover ed.; Dover books on engineering; Dover Publications: Mineola, N.Y, **2008**.
- (90) Hackley, V. A.; Ferraris, C. F. Guide to Rheological Nomenclature: Measurements in Ceramic Particulate Systems, **2001**.
- (91) Demouveau, B.; Gouyer, V.; Gottrand, F.; Narita, T.; Desseyn, J.-L. Gel-Forming Mucin Interactome Drives Mucus Viscoelasticity. *Advances in Colloid and Interface Science* **2018**, *252*, 69–82. <https://doi.org/10.1016/j.cis.2017.12.005>.
- (92) Claeys-Bruno, M. Méthodologie de la recherche Expérimentale Conf_PE_M2P2.Pptx, **2022**.
- (93) Clarissa, S. R. POLITECNICO DI TORINO, Applicazione della tecnica di Design of Experiment per l'ottimizzazione di design di veicoli ibridi, **2019**.
- (94) Natoli, C. Classical Designs: Fractional Factorial Designs, **2018**.
- (95) Duncan, G. A.; Jung, J.; Joseph, A.; Thaxton, A. L.; West, N. E.; Boyle, M. P.; Hanes, J.; Suk, J. S. Microstructural Alterations of Sputum in Cystic Fibrosis Lung Disease. *JCI Insight* **2016**, *1* (18). <https://doi.org/10.1172/jci.insight.88198>.
- (96) Voynow, J. A.; Selby, D. M.; Rose, M. C. Mucin Gene Expression (MUC1, MUC2, and MUC5/5AC) in Nasal Epithelial Cells of Cystic Fibrosis, Allergic Rhinitis, and Normal Individuals. *Lung* **1998**, *176* (5), 345–354. <https://doi.org/10.1007/PL00007616>.
- (97) Mrsny, R.; Daugherty, A.; Short, S.; Widmer, R.; Siegel, M.; Keller, G.-A. Distribution of DNA and Alginate in Purulent Cystic Fibrosis Sputum: Implications to Pulmonary Targeting Strategies. *Journal of Drug Targeting* **1996**, *4* (4), 233–243. <https://doi.org/10.3109/10611869608995625>.
- (98) Bartlett, J. W.; Frost, C. Reliability, Repeatability and Reproducibility: Analysis of Measurement Errors in Continuous Variables. *Ultrasound Obstet Gynecol* **2008**, *31* (4), 466–475. <https://doi.org/10.1002/uog.5256>.
- (99) McAlinden, C.; Khadka, J.; Pesudovs, K. Precision (Repeatability and Reproducibility) Studies and Sample-Size Calculation. *Journal of Cataract and Refractive Surgery* **2015**, *41* (12), 2598–2604. <https://doi.org/10.1016/j.jcrs.2015.06.029>.
- (100) Su, J.; Ouyang, J.; Wang, X.; Yang, B.; Zhou, W. Lattice Boltzmann Method for the Simulation of Viscoelastic Fluid Flows over a Large Range of Weissenberg Numbers. *Journal of Non-Newtonian Fluid Mechanics* **2013**, *194*, 42–59. <https://doi.org/10.1016/j.jnnfm.2012.11.006>.
- (101) Krüger, T.; Kusumaatmaja, H.; Kuzmin, A.; Shardt, O.; Silva, G.; Viggien, E. M. *The Lattice Boltzmann Method: Principles and Practice*; Graduate Texts in Physics; Springer International Publishing: Cham, **2017**. <https://doi.org/10.1007/978-3-319-44649-3>.
- (102) Tomé, M. F.; Mangiavacchi, N.; Cuminato, J. A.; Castelo, A.; McKee, S. A Finite Difference Technique for Simulating Unsteady Viscoelastic Free Surface Flows. *Journal of Non-Newtonian Fluid Mechanics* **2002**, *106* (2–3), 61–106. [https://doi.org/10.1016/S0377-0257\(02\)00064-2](https://doi.org/10.1016/S0377-0257(02)00064-2).

- (103) Zou, S.; Yuan, X.-F.; Yang, X.; Yi, W.; Xu, X. An Integrated Lattice Boltzmann and Finite Volume Method for the Simulation of Viscoelastic Fluid Flows. *Journal of Non-Newtonian Fluid Mechanics* **2014**, *211*, 99–113. <https://doi.org/10.1016/j.jnnfm.2014.07.003>.